University of Nevada, Reno

Simulation and Analysis of the Wheel Wander on Viscoelastic Pavement Structures

A thesis submitted in partial fulfillment of the
requirements for the degree of Master of Science in
Civil & Environmental Engineering

by

Xiaoshu Tan

Raj. Siddharthan, Ph.D., P.E.

Thesis Advisor

August 2013

ProQuest LLC.
789 East Eisenhower Parkway
P.O. Box 1346
Ann Arbor, MI 48106 - 1346

University of Nevada, Reno
Statewide • Worldwide

THE GRADUATE SCHOOL

We recommend that the thesis
prepared under our supervision by

XIAOSHU TAN

entitled

Simulation and Analysis of the Wheel Wander on Viscoelastic Pavement Structures

be accepted in partial fulfillment of the
requirements for the degree of

MASTER OF SCIENCE

Raj. Siddharthan, Ph.D , Advisor

Elie Hajj, Ph.D, Committee Member

Sherif Elfass, Ph.D , Committee Member

Ilya Zaliapin, Ph.D, Graduate School Representative

Marsha H. Read Ph.D., Associate Dean, Graduate School

August, 2013

ABSTRACT

Simulation and Analysis of the Wheel Wander on Viscoelastic Pavement Structures

Estimation of long-term performance (or life) is a critical pavement design concern. Though wheel wander is not routinely addressed in pavement designs, its consideration provides for a more realistic and economical design. The procedures in MEPDG and CalME to address the wheel wander recommend the use of normal distributions for transverse wheel wander. These procedures are based on dividing the wheel wander distribution into a number of segments (say five) of equal areas. Such approaches suffer from a major limitation that the selection of equal segments is arbitrary, can lead to biased results.

The study reported here covered a variety of pavement factors that significantly affect pavement performance. These factors included are: (1) pavement layer configuration (thin and thick); (2) pavement material properties (conventional and polymer-modified); (3) tire configurations (dual and wide-base); (4) pavement temperature (T = 70°F and T = 104°F); and (5) vehicle operating conditions (braking and non-braking). A major contribution of this thesis is to provide valuable design information on the relative importance of these factors on the prediction of pavement life.

A Monte-Carlo simulation scheme that addressed the role wheel wander on pavement response and performance has been developed. Since the traffic lanes are of limited width (about 12 ft.), the trial values of wheel wander was limited to ± 21 in about the centerline of the traffic lane. The proposed Monte-Carlo scheme provided cumulative distribution functions (CDFs) for all the important responses and they in turn were used in the estimation pavement performance (or life).

This study only focused on the impact of wheel wander on HMA failure modes. Required traffic-induced pavement strain database needed in the HMA distress investigations were developed using UNR's 3D-Move model. Three methods were used to evaluate the pavement performance (of life). These methods differ based on the value of the traffic-induced strains used in the performance equations. First method (Method 1) uses the maximum response strain, while the second method (Method 2) is the MEPDG approach. The Method 3 is based on the CDFs developed by the Monte-Carlo simulation scheme described in this thesis. The CDFs were divided into a number of equal segments and the strains that correspond each of the segments were used with the performance equations. As many numbers of segments as needed can be considered, however for being consistent with MEPDG approach (Method 2), it was decided to use five segments.

Since the Method 1 uses the largest pavement response, the pavement life predicted by Method 1 is always lower and this may be interpreted as being over conservative. The Method 2 (MEPDG approach), though an important step forwards realistic modeling of long-term pavement performance, its arbitrary use of fixed five locations to define the wheel wander can be biased and therefore, questionable. The Method 3 is statically-based and uses many trials for wheel wander locations to model the vehicle wander. Therefore, it takes into account in a more realistic manner the entire variation in traffic-induced strain on the transverse plane. Such an approach is considered more appealing to pavement engineers and researchers.

In summary, pavement design information presented in this thesis are in the form of datasets that the pavement engineers researchers can use to assess the sensitivity of many important factors that affect long-term pavement performance. Neither interpretation nor scrutiny

of the design information has been attempted. Instead, the thesis outlines elaborate details on a three-step approach used to develop such design guidelines.

DEDICATION

This Paper is lovingly dedicated to my respective parents who have been my constant source of inspiration. They have given me the drive and discipline to tackle any task with enthusiasm and determination. Without their love and support this project would not have been made possible.

I also dedicate this paper to my dear friend Wen, Guanxing, who has supported me throughout the process. I will always appreciate all he has done.

I dedicate this work and give special thanks to my soul mate Cui, Bicheng for being here for me throughout the entire master program.

ACKNOWLEDGMENTS

The Author is heartily thankful to Dr. Raj Siddharthan for all his support and invaluable efforts in guiding the Author throughout this thesis.

The Author would like to acknowledge Dr. Elie Hajj and Dr. Ilya Zaliapin for all their assistance support during the preparation of this thesis.

The Author also acknowledges all my colleagues who helped me along the way: Andrew, Graziella and Razor.

The Author would like to acknowledge Alvaro Ulloa Calderon, for his valuable input and assistance in this research.

The Author would also like to thank Dr Raj Sidharthan, Dr Elie Hajj, Dr Ilya Zaliapin and Dr Sherif Elfass for their comments on this thesis.

Table of Contents

LIST OF TABLES

LIST OF FIGURES

Chapter 1 – INTRODUCTION AND PAST APPROACHES

1.1 INTRODUCTION

Vehicles and their wheels do not travel along exactly the same path on a highway pavement. It is a natural phenomenon observed on public-access roadways. Various vehicle types, individual driving habits, wind effects, mechanical alignment of trailers and other factors all contribute to the randomness of wheel path, known as wheel wander (Buiter et al. 1989). In highway pavement design it is customary to assume that all vehicles load the same portion of the roadway. Although this is not an accurate assumption, it is a significantly a conservative one. Efforts should be made to model the wheel wander appropriately and account for it in pavement designs. There is considerable benefit in considering wheel wander as a design parameter in road design methods.

Field observations have shown that successive passes of vehicles along a pavement are statistically normally distributed about the pavement or lane centerline (Timm and Priest 2005). The degree of 'wander' is typically described using a standard deviation (S_d) (NCHRP 2004). For example, HoSang (HoSang 1978) found aircraft wander to be significantly different for runways (S_d = 60.866 inch), taxiways (S_d = 30.433 inch) and aircraft parking bay ($S_d \approx$ 3.937 inch). This transverse wander of aircraft wheel load significantly affects the airfield pavement life, and should be taken into account when designing aircraft pavements (Wardle et al. 2003). Typical highway pavements are not as wide as airfield pavements. They are about 12ft (3.66 m) in width and the tire edge to edge distance for typical truck is 8.5ft (2.59 m) (NCHRP 2004). Recommended S_d value for highway in design manuals is 1ft (304.8 mm) (e.g., MEPDG, CalME etc.). This means that, unlike the runway and taxiway in airfield pavements, the highways have much lower S_d.

The role of vehicle wander is strongly influenced by pavement structures (stiffness and thickness) among other factors. It is expected to be more significant for thinner pavements. This is because the load intensity at subgrade level is spread to a greater degree by thicker pavements, making the load-spreading effect of wander relatively less dramatic. About two decades ago, (Wardle and Rodway 1995) showed the effect of aircraft wander upon damage for two airfield pavements, as calculated using APSDS (Airport Pavement Structural Design System). In the case of hot mix asphalt (HMA) pavement thickness of 500 mm, taxiway wander reduces damage by 80% of that caused in the channelized, no wander case. This contrasts with HMA thickness of 1500 mm, where taxiway wander reduces damage by 30% of that caused in the channelized, no wander case.

1.2 PAST APPROACHES

Some existing highway and airfield pavement design methods consider wheel wander in their calculations, but many do not. The following routinely-used design guides take the wheel wander into consideration: MEPDG (2008), Caltrans Pavement Design (2012) and FAARFIELD (2009).

1.2.1 MEPDG (Mechanistic-Empirical Pavement Design Guide) (NCHRP 2004)

The MEPDG assumes that lateral wheel wander in highway pavement is normally distributed and the S_d of the distribution is an input. The role of wheel wander is taken into account in the computation of pavement damage. For example, in case of fatigue damage the Miner's Law is used along with as many as five pre-defined lateral location for the wheel position. The damage is computed by following relationship:

$$D = \sum_{i=1}^{T} \frac{n_i}{N_i} \qquad (1.1)$$

where: D = damage; T = total number of period i; n_i = actual traffic for period i; N_i = traffic allowed under conditions prevailing in i^{th} loading condition.

Details of the MEPDG approach are given in Fig. 1.1. Plot A shows the pavement structure with a dual wheel centered at location O. The pavement damage for example, say in terms of number of cycles to fatigue failure in HMA computed using pavement responses with no wander given by the design analysis is shown in Plot B. The maximum value from this damage will define the fatigue life, if no consideration is given for wheel wander. Plot C in this figure shows the transverse (or lateral) wander distribution, assumed to be normally distributed. The spread of the distribution is dependent on the standard deviation value S_d. The area under the normal distribution curve is divided into five quintiles of equal area, each representing twenty percent of the total distribution. For each segment or area, a representative wheel wander d_w is found by multiplying S_d by the corresponding location of the center of that segment.

It is assumed that, for the first twenty percent of the traffic (segment 1), the damage distribution will be centered at location equal to -1.28155 S_d. For this situation (Plot D), damage at location Q is D_1. Since, D_1 is zero for this case, no fatigue damage occurs at this location. The next plots (plots E through H) show damage distribution centered at d_w = -0.5244S_d, 0.0, 0.5244S_d and 1.28155S_d. Each represents the subsequent segments of twenty percent of the traffic. Damages for these cases are D_2, D_3, D_4 and D_5 respectively. According to MEPDG, the total damage at location Q can be computed as:

$$D = 0.2 \times D_1 + 0.2 \times D_2 + 0.2 \times D_3 + 0.2 \times D_4 + 0.2 \times D_5 = 0.2 \times \sum_{i=1}^{5} D_i \qquad (1.2)$$

in which, the D_i at each analysis location is determined using polynomial or linear interpolation.

An important limitation of the MEPDG analysis stems from the fact that the normal distribution that describes the lateral wheel wander is divided into five quintiles of equal area under the normal distribution plot. This means that the damage calculations are strictly dictated by these

five pre-defined locations of wheel (i.e., value of wheel wander amount, d_w). It should be noted that selection of such fixed location is quite arbitrary and the resulting damage calculation that determines the role of wheel wander is therefore, questionable. It will be clear subsequently that the pavement response variation in the lateral direction is complex and significantly varies within a short lateral distance. Therefore, it is clear that selection of wheel wander locations plays a critical role in MEPDG's damage estimation.

The above limitation can be overcome if a more realistic statically based approach is used to define the wheel wander. The approach presented in the thesis used a Monte-Carlo simulation, in which many thousands of wheel wander locations (i.e., d_w values) are used and the corresponding probability distribution functions are obtained for important pavement responses. Unlike in the case of MEPDG, the proposed approach does not use pre-defined the wheel wander locations and therefore, can more realistically account for the complex and variable nature of the pavement response.

1.2.2 CALTRANS PROCEDURES

CALTRANS (California Department of Transportation) is also implementing Mechanistic-Empirical design procedures for pavement designs. CalME is a computer program, developed by the Caltrans for analysis and design of: (a) rehabilitation using asphalt overlays, and (b) new flexible pavements. It was developed beginning in the late 1990s using research products from SHRP (1989–1993), subsequent research and development sponsored by Caltrans, and models and data from research programs around the world. When considering wheel wander，the stress and strain are calculated at as much as 10 positions for each of the axle loads similar to MEPDG procedure. The lateral wander of the wheels is assumed to follow a normal distribution with a

standard deviation. For each position, the numbers of passages are determined using the normal distribution. The limitations described relative to MEPDG approach do apply here also.

1.2.3 FAARFIELD (Pass-to-Coverage Computation for Arbitrary Gear Configurations in the FAARFIELD Program 2012; Airport Pavement Design and Evaluation 2009)

FAARFIELD (FAA Rigid and Flexible Iterative Elastic Layered Design) incorporates the effects of aircraft wander through the use of a procedure referred to as "computed pass-to-coverage (P/C) ratio". Coverages can be defined as a measure of the number of repetitions of the maximum strain (for flexible pavements) or stress (for rigid pavements) occurring at a particular location in the pavement (Ahlvin et al. 1971). The primary structural response is computed at the top of the subgrade for flexible pavements and at the bottom of the concrete slab for rigid pavements. Coverages depend on aircraft type and are a function of the tire-contact area, and the lateral distribution of the wheel wander relative to the pavement centerline. FAARFIELD establishes a pass-to-cover ratio based on strips of pavement that run parallel to the traffic flow. Each strip's pass-to-cover ratio is based on a normal distribution with S_d of 30.435 inches (773 mm) for taxiway. FAARFIELD deals only with airport pavements and cannot directly be applied to highway pavements.

FAARFIELD uses Miner's hypothesis to predict the fatigue life of a pavement structure (Kawa 2010). The method evaluates the P/C ratio using following steps: (1) Determine the rearmost wheel in each tandem group; (2) Determine the number of wheels in tandem; (3) Calculate the tandem distance for each pair of wheels in tandem; (4) Calculate the tandem factor F_{tnd} for each trailing wheel; (5) Compute the coverage-to-pass (C/P) ratio from the area under the normal traffic distribution curve between the limits of the effective tire width (where the effective tire width is defined in a subsequent section); (6) Apply the tandem factor determined in step d to the

C/P ratio determined in step; (7) $(C/P)_{final} = (C/P) \times F_{tnd}$; and (8) The P/C ratio is the inverse of the C/P ratio computed in the above steps. Once again, the main limitation of this approach is the pre-defined lateral wheel wander locations.

Chapter 2 – PAVEMENT RESPONSE MODEL 3D-MOVE

2.1 INTRODUCTION

An important first step in the study of role of wheel wander is the evaluation of pavement responses that are critical in the computation of pavement distress (or performance). Table 2.1 provides a summary of available pavement response evaluation models. The models differ because of the assumptions made in the formulation. Following are the typical assumptions that are made in the methods: (1) specification of load (e.g., circular vs. noncircular); (2) analysis procedure (e.g., finite element vs. axisymmetric); and (3) loading condition used (static vs. dynamic). This thesis used an existing computer program 3D-Move that was developed at UNR (University of Nevada, Reno) to evaluate pavement response.

3D-Move is a computer model that is based on a continuum finite-layer approach to evaluate the responses of layered medium to three-dimensional (3D) moving surface loads that move with constant speeds. It is based on the work reported by Siddharthan and his co-workers (Siddharthan et al. 1998; Siddharthan et al. 1993; Zafir et al. 1994). It is applicable to linear elastic and viscoelastic horizontal layers with finite thicknesses. The material properties of each layer are assumed to be uniform and constant within the layer (i.e., it is not a function in space or time). On the other hand, the surface load components (normal and shear) are distributed over a constant loaded area of any shape that is time invariant. Since the layered system is linear, the loads are decomposed into harmonic components using Fourier series expansion, and the total responses are computed as the summation of the individual responses from each harmonic component. A brief description of the model and the numerical problems associated with it are presented in the following sections.

2.2 3D-MOVE MODEL FORMULATION

2.2.1 Assumptions

The following assumptions were used in the development of the model:

1. The domain is composed of horizontal layers of uniform thickness, which can be of different materials.

2. Each layer can be either linear elastic or linear viscoelastic with a set of uniform material properties (e.g., shear modulus, Poisson's ratio, unit weight), which are time and space invariants.

3. Layers are modeled as single-phase.

4. The layers are finite and rest on a rigid impermeable layer.

5. The 3D surface loads are assumed to move with constant speed (i.e., no acceleration).

2.2.2 Load Idealization

The proposed approach is based on Fourier series expansion of the applied load. The applied load is modeled as a two-dimensional periodic function in x- and y-directions, as shown in Fig. 2.1. The wavelength is selected with sufficiently large "quiet zone" at the end of the applied load to allow time for the damping of the system to attenuate the response from one cycle before the beginning of the next cycle (i.e., no interference between the consecutive cycles). The surface load components (normal or shear) can be written using sum of $N \times M$ harmonics of the Fourier series as:

$$q(x,y) = \mathrm{Re}\left(\sum_{n=1}^{N} \sum_{m=1}^{M} A_{nm}\, e^{i\alpha_n x}\, e^{i\beta_m y} \right) \tag{2.1}$$

where, A_{nm} are the Fourier coefficients, which are calculated using Discrete Fourier Transform (DFT) of the sampled load values as:

$$A_{nm} = \frac{1}{N \times M} \sum_{j=1}^{N} \sum_{k=1}^{M} q(j,k)\, e^{\frac{-i2\pi(j-1)(n-1)}{N}}\, e^{\frac{-i2\pi(k-1)(m-1)}{M}} \tag{2.2}$$

$\alpha_n = \frac{2\pi(n-1)}{N \times \Delta x}$ and $\beta_m = \frac{2\pi(m-1)}{M \times \Delta y}$, where Δx and Δy are the sampling intervals in the x- and y-directions respectively.

For a moving load traveling with velocity (c) along the x-direction, Eq. 2.1 can be written as:

$$q(x,y,t) = \mathrm{Re}\left(\sum_{n=1}^{N} \sum_{m=1}^{M} A_{nm}\, e^{i\alpha_n (x-ct)}\, e^{i\beta_m y} \right) \tag{2.3}$$

2.2.3 Governing Equations

The equations of motion for a single-phase body are given by (Fung 1977):

$$\frac{\partial \sigma_{xx}}{\partial x} + \frac{\partial \tau_{xy}}{\partial y} + \frac{\partial \tau_{xz}}{\partial z} = -\rho \frac{\partial^2 u}{\partial t^2} \tag{2.4a}$$

$$\frac{\partial \tau_{xy}}{\partial x} + \frac{\partial \sigma_{yy}}{\partial y} + \frac{\partial \tau_{yz}}{\partial z} = -\rho \frac{\partial^2 v}{\partial t^2} \tag{2.4b}$$

$$\frac{\partial \tau_{xz}}{\partial x} + \frac{\partial \tau_{yz}}{\partial y} + \frac{\partial \sigma_{zz}}{\partial z} = -\rho \frac{\partial^2 w}{\partial t^2} \tag{2.4c}$$

where, σ_{xx}, σ_{yy} and σ_{zz} are the normal stresses, τ_{xy}, τ_{yz} and τ_{xz} are the shear stresses, u, v and w are the displacements in the x, y and z directions, respectively, and ρ is the mass density.

On the other hand, the stress-displacement relationships for Hookean elastic solid are given by (Fung 1977):

$$\sigma_{xx} = -\left[\lambda\left(\frac{\partial u}{\partial x}+\frac{\partial v}{\partial y}+\frac{\partial w}{\partial z}\right)+2G\frac{\partial u}{\partial x}\right] \quad (2.5a)$$

$$\sigma_{yy} = -\left[\lambda\left(\frac{\partial u}{\partial x}+\frac{\partial v}{\partial y}+\frac{\partial w}{\partial z}\right)+2G\frac{\partial v}{\partial y}\right] \quad (2.5b)$$

$$\sigma_{zz} = -\left[\lambda\left(\frac{\partial u}{\partial x}+\frac{\partial v}{\partial y}+\frac{\partial w}{\partial z}\right)+2G\frac{\partial w}{\partial z}\right] \quad (2.5c)$$

$$\tau_{xy} = -\left[G\left(\frac{\partial u}{\partial y}+\frac{\partial v}{\partial x}\right)\right] \quad (2.5d)$$

$$\tau_{yz} = -\left[G\left(\frac{\partial v}{\partial z}+\frac{\partial w}{\partial y}\right)\right] \quad (2.5e)$$

$$\tau_{xz} = -\left[G\left(\frac{\partial u}{\partial z}+\frac{\partial w}{\partial x}\right)\right] \quad (2.5f)$$

where, λ = Lamé constant $\left(\lambda = \frac{2G\nu}{1-2\nu}\right)$, G = shear modulus (or the complex shear modulus in the case of linear viscoelastic materials), and ν = Poisson's ratio. Negative sign is used in these equations because compressive stresses and strains are considered positive, which is the conventional sign convention in geomechnics.

2.2.4 Solution for a Single Harmonic

It is known that the response (output) of a time-invariant linear system to a periodic input is also periodic (Papoulis 1962). Therefore, the displacements induced in a layer in the layered

system shown in Fig. 2.2 by a single harmonic of the surface load described by Eq. 2.3 can be written as:

$$u_{nm}(x,y,z,t) = U_{nm}(z)e^{i\alpha_n x}\, e^{i\beta_m y}\, e^{-i\alpha_n ct} \tag{2.6a}$$

$$v_{nm}(x,y,z,t) = V_{nm}(z)e^{i\alpha_n x}\, e^{i\beta_m y}\, e^{-i\alpha_n ct} \tag{2.6b}$$

$$w_{nm}(x,y,z,t) = W_{nm}(z)e^{i\alpha_n x}\, e^{i\beta_m y}\, e^{-i\alpha_n ct} \tag{2.6c}$$

By substituting for U_{um}, V_{nm} and W_{nm} in Eq. 2.4, the partial differential equations are converted to a set of ordinary differential equations of the 6th order. The roots of the characteristic equation are $r_1, -r_1, r_2, -r_2, r_2$ and $-r_2$, where $r_1 = \sqrt{(\alpha_n)^2 + (\beta_m)^2 - \left(\frac{\omega}{c_1}\right)^2}$, $r_2 = \sqrt{(\alpha_n)^2 + (\beta_m)^2 - \left(\frac{\omega}{c_2}\right)^2}$, $\omega = \alpha_n c$, $c_1 = \sqrt{\frac{2G+\lambda}{\rho}}$, and $c_2 = \sqrt{\frac{G}{\rho}}$. Therefore, the solution of the ordinary differential equations is given by:

$$U_{nm}(z) = u_1 e^{r_1 z} + u_2 e^{-r_1 z} + u_3 e^{r_2 z} + u_4 e^{-r_2 z} + u_5 z e^{r_2 z} + u_6 z e^{-r_2 z} \tag{2.7a}$$

$$V_{nm}(z) = v_1 e^{r_1 z} + v_2 e^{-r_1 z} + v_3 e^{r_2 z} + v_4 e^{-r_2 z} + v_5 z e^{r_2 z} + v_6 z e^{-r_2 z} \tag{2.7b}$$

$$W_{nm}(z) = w_1 e^{r_1 z} + w_2 e^{-r_1 z} + w_3 e^{r_2 z} + w_4 e^{-r_2 z} + w_5 z e^{r_2 z} + w_6 z e^{-r_2 z} \tag{2.7c}$$

where, u_i, v_i and w_i are constants. By substituting Eqs. 2.6 and 2.7 into Eq. 2.4, it was found that only six constants are independent (Siddharthan et al. 1998). The independent constants are u_1, u_2, u_3, u_4, v_3 and v_4, while the other constants are found to be: $v_1 = u_1 \frac{\beta_m}{\alpha_n}$, $v_2 = u_2 \frac{\beta_m}{\alpha_n}$,

$$w_1 = -\frac{iu_1 r_1}{\alpha_n} \quad , \quad w_2 = \frac{iu_2 r_1}{\alpha_n} \quad , \quad w_3 = \frac{-i\alpha_n u_3 - i\beta_m v_3}{r_2} \quad , \quad w_4 = \frac{i\alpha_n u_4 + i\beta_m v_4}{r_2} \quad , \quad \text{and}$$

$u_5 = u_6 = v_5 = v_6 = w_5 = w_6 = 0$.

2.2.5 Layered System

It has been seen from the previous section that each layer has 6 unknowns (layer coefficients). For the N-layered system shown in Fig. 2.2 there are $6 \times N$ unknowns for each load harmonic. Therefore, $6 \times N$ equations are needed to solve the problem. These equations can be obtained from the boundary and interface conditions, which are defined as follows:

(a) At the surface of the layered system $(3\,\text{equations})$

$$\sigma_{zz} = q_{zz}, \qquad \tau_{xz} = q_{xz} \qquad \text{and} \qquad \tau_{yz} = q_{yz}$$

where q_{zz}, q_{xz} and q_{yz} are the surface load components defined in Eq. 2.3.

(b) At the bottom of the layered system $(3\,\text{equations})$, where rigid impermeable layer is assumed

$$u = v = w = 0$$

(c) At the interface $[(N-1) \times 6\,\text{equations}]$

$$u^+ = u^-, \qquad v^+ = v^-, \qquad w^+ = w^-$$
$$\sigma_{zz}^+ = \sigma_{zz}^-, \qquad \tau_{xz}^+ = \tau_{xz}^-, \qquad \tau_{yz}^+ = \tau_{yz}^-$$

in which + and – indicate a location just above and below the interface.

These boundary and interface conditions are to be satisfied for each load harmonic, and the complete solution is obtained by summing the responses from all harmonics.

2.3 SUMMARY AND CONCLUSIONS

The computer code 3D-Moving Load Analysis (3D-Move) utilizes a continuum based"finite-layer" approach to evaluate the response of a layered medium subjected to a moving surface load (Siddharthan et al. 1998). The pavement system is characterized through a combination of viscoelastic (for the HMA layer) and elastic (for the base and subgrade) horizontal layers with each layer characterized using a set of uniform properties that rest on a rigid impermeable layer. The finite-layer approach treats each pavement layer as a continuum and uses the Fourier transform technique to handle complex surface loadings in all three directions (vertical, longitudinal, and transverse). The 3D-Move model incorporates important pavement response factors such as the moving traffic-induced complex 3D contact stress distributions (normal and shear) of any shape, vehicle speed, viscoelastic material characterization for the pavement layers, and non-uniform interface shear stresses caused by braking and turning forces. In addition, rate-dependent material properties (viscoelastic) can be accommodated, thus pavement response as a function of vehicle speed can be studied (Ulloa 2009).

Since Fourier transform technique along with frequency-domain solutions are adopted, the approach allows for the direct use of the frequency sweep test data of HMA mixture in the analysis. In addition, many attempts that included field calibrations (e.g., Penn State University test track, MnRoad, and University of Nevada-Reno UNR Off-road Vehicle study) that compared a variety of independently-measured pavement responses (stresses, strains, and displacements) with those computed have been reported in the literature(Siddharthan et al. 1998; Siddharthan et

al. 2002a; Siddharthan 2005). These verification studies have validated the applicability and versatility of the approach.

A verification of this model using existing analytical solutions (ELSYM5) and laboratory test results has shown that the 3D-Move program is capable of simulating correctly the surface loads applied to a layered system (Siddharthan et al. 1998). In other studies, Siddharthan at al. evaluated strain histories from two different pavements, representing a thin and a thick structure subjected to loading from a moving tandem axle (Siddharthan et al. 1998; Siddharthan and Sebaaly 1999). The 3D-Move analysis was used in conjunction with the dynamic modulus (|E*|) and internal damping (ζ_{ac}), that were measured in the laboratory on the various mixes.

Chapter 3 – USE OF 3D-MOVE FOR WHEEL WANDER INVESTIGATION

3.1 DATABASE OF PAVEMENT STRAINS

The pavement strain database was generated by conducting a mechanistic analysis of two HMA pavement structures subjected to moving traffic induced loads at various speeds and under braking and non-braking conditions using 3D-Move model. The pavement responses from the 3D-Move model were scrutinized to quantify many strain components that are required as critical inputs to MEPDG's pavement performance models. The focus in this thesis is limited to HMA distresses (fatigue and rutting). Therefore, 3D-Move calculations that relate to the HMA responses only are considered. The traffic-induced load is modeled for a fully loaded 18-wheel truck having a steering axle, a driving axle and a trailer axle. The steering axle consists of a single axle configuration with a single tire, whereas the driving and trailer axles consist of a tandem axle configuration with dual tires or a wide base tire. Because of symmetry, only half of the vehicle needs to be modeled as shown in Fig. 3.1. The following presents the conditions and evaluation steps used in the response computations:

- Pavement geometry:
  - 4" HMA over 6" base
  - 8" HMA over 10" base
- Vehicle speeds:
  - 2 mph with braking
  - 60 mph without braking
- Axle analyzed:

- Driving axle

- Loaded area and contact pressure distribution:

- Circular uniform

- Non uniform (Tire configuration and contact pressure distribution from database)

- HMA mixtures:

- One aggregate source: Lockwood (andesite)

- Two asphalt binder grades: PG64-22, PG64-28NV (Polymer-modified)

- HMA layer temperatures:

- 70°F

- 104°F

- Evaluate the strain within the HMA layer at several critical depths (Al-Qadi and Wang 2009; NCHRP 2004).

- Pavement material properties: see section 3.2 below. A summary of pavement configurations and material properties are shown in Table 3.1.

3.2 CHARACTERIZATION OF PAVEMENT LAYER PROPERTIES

The dynamic modulus (|E*|) is the primary material property of HMA mixes that is used in structural pavement design and analysis. Due to the viscoelastic behavior of the HMA pavement, this property varies with temperature and frequency of loading. The dynamic modulus test is often used to develop the dynamic modulus master curve of the various HMA mixes (Al-Qadi et al. 2008). Sinusoidal (Haversine) axial compressive stresses are applied to a specimen at a given temperature and loading frequency. The applied stress and the resulting recoverable axial strain response of the specimen at different temperatures and frequencies (frequency sweep) are measured and used to calculate the complex dynamic modulus. The dynamic modulus (|E*|) is the absolute value of the complex modulus (|E*|) which is actually the summation of two

components as seen in Equation 3.1: (1) the storage or elastic modulus component (E') and (2) the loss or viscous modulus (E"):

$$E^* = \frac{\sigma}{\varepsilon} = \frac{\sigma_0 \sin\omega t}{\varepsilon_0(\sin\omega t - \emptyset)} = |E^*|\cos\varphi + i|E^*|\sin\varphi = E' + iE'' \quad (3.1)$$

where, , σ_0 = peak (amplitude) stress, ε_0 = peak (amplitude) strain, and ω = angular velocity in radian per second, and t is the time, seconds. The angle φ in Equation 3.1 is defined as the phase angle which is experimentally determined from the lag between the peak strain and the peak stress.

Mathematically, the absolute value of the complex dynamic modulus is defined as the maximum (peak) dynamic stress (σ_o) divided by the recoverable axial strain (ε_o) as shown in Equation 3.2:

$$|E^*| = \frac{\sigma_0}{\varepsilon_0} \quad (3.2)$$

To determine the dynamic viscoelastic properties of these mixtures a series of laboratory tests at various temperatures were undertaken at the UNR laboratory. The loading frequency used were f = 0.1, 0.5 1.0, 5.0, 10.0 and 25.0 Hz, and test temperature were T = 14, 40, 70, 100, and 130 °F. These laboratory results were used to develop master curves.

Master curve approach, which is widely-used in representing HMA mixture properties that vary as a function of frequency and temperature. This allows for extending the $|E^*|$ vs. frequency plot to much wider range of frequencies. Subsequently, the master curve can then be used to determine the HMA properties at any temperature. The dynamic modulus and damping properties obtained from the master curves for the PG64-22 and PG64-28NV mixture at the evaluation temperatures of T = 70°F and 104°F are shown in Tables 3a and 3b. The mixture

PG64-28NV is polymer-modified, while the mixture PG64-22 is not. Figures 3.2a and 3.2b show the dynamic modulus |E*| as a function of frequency for both the mixtures at T = 70°F and 104°F.

The internal damping for the HMA layer was measured as a function of the loading frequency in the laboratory and it was included in the 3D-Move by writing the dynamic modulus (|E*|) in its complex form (Roesset 1980) as shown in Equation 3.3:

$$E^* = E(1 + 2i\zeta_{AC}) = E' + iE'' \tag{3.3}$$

in which, ζ_{AC} is the internal damping of the HMA, and |E*|, E', and E" are experimentally determined by the dynamic modulus test as a function of loading frequency, and are subsequently used to calculate ζ_{AC} using Equation 3.4.

$$\zeta_{AC} = \frac{E'}{2E''} = \frac{\tan(\varphi)}{2} \tag{3.4}$$

It is conventional to assume a constant Poisson's ratio for HMA and it was assumed to be $\nu = 0.4$. In this research the base course and subgrade layers are treated as linear elastic materials with an elastic modulus of 35,000 psi and 15,000 psi, respectively and Poisson's ratio $\nu = 0.4$. The internal damping of the unbound layers is assumed to be 5% (Table 3.1).

3.3 LOAD DISTRIBUTION OF AN EIGHTEEN-WHEEL TRUCK

The first step of the mechanistic pavement response analysis is to estimate the load distributions on various tires of the 18-wheel tractor-semitrailer under braking and nonbreaking conditions. When a vehicle brakes, the speed decelerates and the load transfers to the front of the vehicle. Compared with a two-axle vehicle, the braking characteristics of a tractor-semitrailer are significantly more complex. When a two-axle vehicle brakes, the load transfer is barely depends

on the deceleration rate. However, when a tractor-semitrailer brakes, the load transfer is dependent on the deceleration rate and the braking force of the semitrailer.

Figure 3.3 shows the major forces acting on an eighteen-wheel tractor-semitrailer during braking on a downward sloping pavement. Since braking is the primary source of deceleration, in this investigation the aerodynamic drag and rolling resistance are neglected. In addition, since the typical highway slope is around 4%, the resulting components of truck tire loads along the slope direction is not significant and therefore, the effect of the truck going upwards or downwards can be neglected.

The 18-wheel truck has various axles: steering axle (tractor), driving axle (tractor tandem axle) and trailer axle (semitrailer tandem axle). In this investigation, steering axle and driving axle are considered without equalization, implying that an inter axle load transfer will take place between the rear and the front axle of the tandem group during the braking period of the truck (Wong 1993; Hajj et al. 2007).

When evaluating the normal load on each axle, the tractor and the semitrailer unit are considered as free bodies separately and combined. All the braking condition equations presented in this investigation are based on Hajj's work (Hajj et al. 2007) with a road slope angle equal to zero. In addition, the dimensional parameters used to describe the vehicle in this analysis are summarized here in. Axle and group spacing are chosen according to ASTM E1572-93 standards (Classifying highway vehicles from known axle count and Spacing 2004).

The vertical, horizontal, and moment equilibrium equations for the tractor, semitrailer unit, and tractor-semitrailer combination are written as a function of truck loads and truck

geometry resulting in a total of as much as eleven equilibrium equations, three characteristic equations, and fourteen unknowns.

For the tractor, the vertical and horizontal equilibrium are given by Equations 3.5 and 3.6, respectively. The moment equilibrium around the rear and front tandem axle are given by Equations 3.7 and 3.8, respectively.

$$W_s + W_{d_1} + W_{d_2} = W_1 + W_{h_2} \tag{3.5}$$

$$F_s + F_{d_1} + F_{d_2} = \frac{a}{g}W_1 + F_{h_2} \tag{3.6}$$

$$W_s\left(L_1 + \frac{c}{2}\right) + W_{d_1}c = \frac{a}{g}W_1h_1 + W_1\left(L_1 + \frac{c}{2} - l_1\right) + F_{h_1}h_3 + W_{h_1}\left(\frac{c}{2} + d_1\right) \tag{3.7}$$

$$W_s\left(L_1 - \frac{c}{2}\right) + W_{h_1}\left(\frac{c}{2} - d_1\right) = \frac{a}{g}W_1h_1 + W_1\left(L_1 + \frac{c}{2} - l_1\right) + F_{h_1}h_3 + W_{d_2} \tag{3.8}$$

For the semitrailer unit, the vertical and horizontal equilibrium are given by Equations 3.9 and 3.10, respectively. The moment equilibrium around the front support point of the semitrailer and the trailer rear axle are given by Equations 3.11 and 3.12, respectively.

$$W_{t_1} + W_{t_2} + W_{h_1} = W_2 \tag{3.9}$$

$$F_{t_1} + F_{t_2} + F_{h_1} = \frac{a}{g}W_2 \tag{3.10}$$

$$W_2 + d_2 + F_{h_1}h_3 = \frac{a}{g}W_2h_2 + W_{t_1}\left(L_2 - \frac{c'}{2} + d_1\right) + W_{t_2}\left(L_2 + \frac{c'}{2} + d_1\right) \tag{3.11}$$

$$W_{h_1}\left(L_2 + \frac{c'}{2} + d_1\right) + F_{h_1}h_3 + W_{t_1}c' = \frac{a}{g}W_2h_2 + W_2\left(L_2 + \frac{c'}{2} + d_1 - d_2\right) \tag{3.12}$$

Combined the equation for tractor and semitrailer, the vertical and horizontal equilibrium are given by Equations 3.13 and 3.14, respectively. The moment equilibrium around the steering axle is given by Equation 3.15.

$$W_s + W_{d_1} + W_{d_2} + W_{t_1} + W_{t_2} = W_2 + W_1 \tag{3.13}$$

$$F_s + F_{d_1} + F_{d_2} + F_{t_1} + F_{t_2} = \frac{a}{g}(W_1 + W_2) \tag{3.14}$$

$$W_2 l_1 + (L_1 - d_1 + d_2) = \frac{a}{g} W_1 h_1 + \frac{a}{g} W_2 W_1 + W_{d_1}\left(L_1 - \frac{c}{2}\right) + W_{d_2}\left(L_1 + \frac{c}{2}\right) +$$

$$W_{t_1}\left(L_1 + L_2 - \frac{c'}{2}\right) + W_{t_2}\left(L_1 + L_2 + \frac{c'}{2}\right) \tag{3.15}$$

where, W_{hi} and F_{hi} are the vertical and horizontal load respectively at the tractor-semitrailer articulation, "a" is the linear deceleration of the truck along the longitudinal axis, g is the deceleration due to gravity, W_1 and W_2 are the tractor and semitrailer total weights, respectively. W_s, W_{d1}, W_{d2}, W_{t1} and W_{t2}, are the normal tires loads. F_s, F_{d1}, F_{d2}, F_{t1} and F_{t2}, are the braking forces that originate from the brake system and develop on the tire road interface.

From the above equations, the normal loads on the various axles can be expressed as follows:

Tractor front axle (steering axle):

$$W_s = W_2 \frac{\left[\frac{a}{g}(h_2 d_1 + h_3 l_2) + d_1(L_2 + d_1 - d_2)\right]}{L_1(L_2 + d_1)} + W_1 \frac{\left[\frac{a}{g} h_1 + (L_1 - l_1)\right]}{L_1} +$$

$$\left(F_{t_1} + F_{t_2}\right) \frac{\frac{a}{g} h_3 L_2}{L_1(L_2 + d_1)} + \left(W_{t_1} - W_{t_2}\right) \frac{c' d_1}{2L_1(L_2 + d_1)} - (W_{d_1} - W_{d_2}) \frac{c}{2L_1} \tag{3.16}$$

Tractor rear axles (driving axles) are shown in Equation 3.17.

$$W_d = W_{d_1} + W_{d_2} = W_2 \frac{\left[\frac{a}{g}(h_2 d_1 - h_2 L_1) + h_3(L_1 + L_2)\right]}{L_1(L_2 + d_1)} - W_1 \frac{\left[\frac{a}{g}h_1 - l_1\right]}{L_1} +$$

$$\left(F_{t_1} + F_{t_2}\right)\frac{h_3(L_1 + L_2)}{L_1(L_2 + d_1)} + \left(W_{t_1} - W_{t_2}\right)\frac{c'(L_1 - d_1)}{2L_1(L_2 + d_1)} + (W_{d_1} - W_{d_2})\frac{c}{2L_1} \quad (3.17)$$

Semitrailer axles (trailer axles) are presented in Equation 3.18.

$$W_t = W_{t_1} + W_{t_2} = W_2 \frac{\left[-\frac{a}{g}(h_2 - h_3) + d_2\right]}{L_2 + d_1} - \left(F_{t_1} + F_{t_2}\right)\frac{h_3}{L_2 + d_1} + \left(W_{t_1} - W_{t_2}\right)\frac{c'(L_1 - d_1)}{2L_1(L_2 + d_1)} \quad (3.18)$$

The calculation of the normal loads on the various axles of the downward braking eighteen-wheel truck requires the following characteristic properties be specified (Hajj et al. 2007):

- Application (treadle) versus actuation (chamber) pressure at each axle: the application pressure is defined as the pressure produced at the output of the treadle valve, whereas the actuation pressure is the pressure experienced at the brake chamber. In the case where some sort of proportioning valve is used, these two pressures will differ significantly(Gillespie and Balderas 1987; Gillespie 1992).
- Brake force versus actuation pressure for the brakes on each axle: the braking force developed at the tire-road interface is determined by the actuation pressure applied to each brake and the gain of each (Gillespie and Balderas 1987; Gillespie 1992).

The braking force on individual wheels can be described by the following equation:

$$F_b = \frac{T_b}{r} = G\frac{P_{ac}}{r} \quad (3.19)$$

where, F_b = Brake force (lb); T_b = Brake torque (in-lb); r = Tire rolling radius (inch); G = Brake gain (in-lb/psi); P_{ac} = Actuation pressure (psi).

The braking system properties of a standard United States (U.S.) eighteen-wheel truck used in this investigation are taken from a National Highway Traffic Safety Administration (NHTSA) report that was conducted by Gillespie and Balderas (Gillespie and Balderas 1987). The NHTSA study considered a linear brake system (i.e., linear relationship between the application and the actuation pressure). Table 3.3 summarizes the brake system properties of the U.S. eighteen-wheel truck.

The extent to which vertical load is transferred during braking from the rear tandem tires to the front tandem tires is called the dynamic load transfer coefficient (α) as shown in Equation 3.20. In addition, the load transfer coefficient has a value of 0.0 when the loads on the front and rear tandem tires are equal (i.e. $W_{t1} = W_{t2}$; $W_{d1} = W_{d2}$) (Ulloa Calderon 2009).

$$\alpha = \frac{W_{t1} - W_{t2}}{2(F_{t1} + F_{t2})} = \frac{W_{d1} - W_{d2}}{2(F_{d1} + F_{d2})} \tag{3.20}$$

Hajj (Hajj et al. 2007) verified that the aforementioned equations against NHSTA data for the case of a level road. Based on this comparison, the author concluded that the equations of force presented in this study can be accurately used to predict the load distributions of an eighteen-wheel tractor-semitrailer vehicle on sloped and level roads.

A constant deceleration of 0.54g was used in this study. This deceleration is the rate that is required for a truck running at 40 mph to come to a complete stop in a distance of 100 feet. This deceleration rate is achieved for a treadle pressure of 80 psi (Hajj et al. 2007).

The load distributions on the various axles of the fully loaded 18-wheel tractor-trailer combination are needed under the non-braking and braking conditions. Table 3.4 summarizes the load distributions on the various axles of the 18-wheel tractor-trailer combination with and without braking. Braking forces at each tire were included as interface shear stresses with their distribution estimated by multiplying the vertical stress by a coefficient of friction, which is the ratio between the horizontal and vertical loads.

The braking phenomenon resulted in a vertical load on the steering axle (8,489 lb/tire) exceeding the tire load for the non-braking condition (6,000 lb/tire) by about 40 percent. The vertical load on the rear tire (2,161 lb/tire) of the trailer-tandem axle configuration was 33 percent lower than the corresponding tire load for the non-braking condition (4,250 lb/tire) (Table 3.3).

3.4 CONTACT STRESS DISTRIBUTION AND LOAD SHAPES

In the simulation of the actual loading conditions on pavements, an 18-wheel dual-wheel configuration was chosen for analysis of braking and non-braking conditions. The dual-wheel spacing was 14.6 inches, and the tandem axle spacing from center to center was 47.2 inches. The braking condition was analyzed at 2 mph, and the non-braking condition speed was 60 mph. For braking condition, the horizontal braking forces were included in the analysis as interface shear stresses in the longitudinal direction (i.e., traffic direction). Shear stresses induced by braking were determined by multiplying the vertical stress distribution by the coefficient of friction at every tire. More details on the calculations and assumptions have been presented above. Two tire–pavement contact stress distributions were investigated in this study: uniform circular (dual tire) and measured non-uniform stress distributions (wide-base tire). The first one is the tire–pavement contact stress distributions most used by researchers and transportation agencies and for which the contact stress distribution is assumed to be equal to the inflation pressure. For the

case of non-uniform stress distribution, the tire print is irregular in shape and the magnitude of the contact stresses varied from point to point.

Tire manufacturers introduced wide-base (or super single) tires in Europe since the early 1980s as a replacement for dual tire fitments on towed vehicles. The advantages of these tires for operators are significant; their lower assembly weight allows payload increases, and their decreased rolling resistance reduces fuel consumption.

When considering the pavement response under the wide-base tire, rather than assuming the contact pressure is uniformly distributed, the study used tire configuration and contact distribution from a database. A comprehensive database of contact stress distribution has been assembled at UNR for a wide variety of tires as a function of tire load, inflation pressure and in some cases also as a function of vehicle velocity. This database is included in 3D-Move and the user can assign the appropriate stress distribution that corresponds to the characteristics of the tire under consideration.

In 3D-Move, database of nonuniform contact stress distributions are available for eight tires (Table 3.5). GoodYear 425/65R22.5 and Michelin 495/45R22.5 are wide-base tires. Michelin 495/45R22.5, which was designed for vehicles in Europe and it is no longer on sale in Michelin official site now (Al-Qadi 2004). Therefore, this study used GoodYear 425/65R22.5 and corresponding contact stress distribution given by VRSPTA (Vehicle – Road Surface Pressure Transduced Array). This wide-base tire has been the focus in two studies (Siddharthan et al. 2002b; Al-Qadi and Wang 2009). A typical plot of VRSPTA data for GoodYear 425/65R22.5 is given in Fig. 3.4. The VRSPTA data that is available for tire pressure of 130.5 psi was selected since it is the closest data set of the target tire pressure of 125 psi. For reasonable comparison between the dual circular tires and wide-base tire, care was taken to assure

that in both cases the axle loads are the same. 3D-Move uses a linear interpolation procedure to compute the appropriate wide-base tire pressure distribution for a given tire load from the assembled database mentioned above.

3.5 PAVEMENT RESPONSE POINTS LOCATIONS

The asphalt layer was divided into sublayers as per MEPDG and responses that are required for HMA rutting evaluation were evaluated at the middle of each of the sublayers. The top portion of the asphalt layer was divided into two sublayers of 0.5 inch thickness each and the bottom portion was divided into three sublayers of 1 inch thickness. For the 6-inch and 8-inch thick asphalt layers the bottom sublayer thicknesses are 2 inches and 4 inches, respectively. Furthermore, responses were obtained at 0.5 inch below asphalt layer surface and at the bottom of the asphalt layer for top-down and bottom-up fatigue cracking analysis, respectively. In addition, Chen et al. (Chen et al. 2003) concluded that the top 2 inches of the HMA layer were critical for permanent deformation in their forensic evaluation of premature pavement failures in Texas. This location was also included as a response evaluation point. All critical depth locations are given in Table 3.6 and also depicted in diagrammatically Fig 3.5.

3.6 PROPOSED SIMULATION PROCEDURE FOR WHEEL WANDER

Figure 3.6 shows a typical truck traversing a pavement. It is clear from the previous discussions that the vehicle wander can be studied by focusing on the transverse (or lateral) movement, d_w of the vehicle about the center line of the lane. For highway pavements the variation of d_w can be represented by a normal distribution with a S_d of 1ft (see MEPDG guidelines). Accounting to AASHTO (AASHTO 2001) a typical 18-wheel truck has a tractor car width of 8ft and trailer car width of 8.5ft. For the freeway lane width of 12ft the transverse

movement, d_w should be limited to ± 1.75ft (21 inch) about the centerline of the traffic lane. It may be noted that truck swirling excessively within a lane will be often corrected by the driver and also such a situation in a two lane high way will be rare. In the Monte-Carlo simulation of the d_w values reported below, the d_w values beyond the range of ± 1.75ft were viewed as outliners and were not considered in the subsequent pavement response evaluations. It is believed such a restriction is realistic and also represents a case of conservative estimate for pavement life.

Random numbers that satisfy normal distribution can be readily generated using a function that is available under Data Analysis menu option in the Microsoft Excel. The standard deviation used was 12 inches. As representative plots, Figures 3.7a and 3.7b show the normalized distribution of d_w predicted by the Data Analysis option for trials of N = 2,000 and N = 10,000. The figures also include the limits for d_w of 21 in as noted above. Pictorially the Figures 3.6a and 3.6b show clearly the effectiveness of the random numbers generation scheme adopted here. Figure 3.8 shows the deviations in areas between the distributions. The deviations have been normalized with respect to the normal distribution. The deviations for entire distribution plots and for the regions within the acceptable limits of d_w are also presented. The case of d_w values generated within the allowable range is considered more realistic. The deviations get smaller as the number of trials increase. When N = 10,000 the deviation between the distributions for the case with limits on d_w is only 4.1%. The distribution with N = 2,000 has a deviation of 11.8%. In the interest of keeping the effort level reasonable, case of N = 10,000 was used in the subsequent pavement response calculations.

The major steps of the proposed Monte-Carlo simulation scheme for pavement response and performance may be summarized as follows:

Step1: Develop a procedure for number of trial values of wheel wander, d_w that confirms to a normal distribution about the centerline of the travel lane; Give consideration to applicable limits to d_w because of the limited width of the travel lane.

Setp2: For each the trial value of d_w, evaluate the critical pavement responses that are needed in the pavement performance (or life) estimation; Develop the corresponding cumulative distribution functions (CDFs) for each of those critical responses for all pavement cases considered in the study.

Step3: Evaluate pavement performance (or life) for each of the important HMA pavement distress modes for all pavement cases considered.

Details on the Step1 have been provided in this section, while the Steps 2 and 3 are described subsequently.

3.7 EVALUATION OF PAVEMENT RESPONSES WITH WHEEL WANDER

The next important step in the proposed approach is to evaluate the pavement responses at the critical locations identified above for each one of the trial wheel wander values of d_w. Figure 3.9a shows the variability of d_w, which occurs in the transverse direction. Say responses were computed by 3-D MOVE at many points along the middle of the sublayer, i as shown in Fig. 3.9b. 3-D MOVE responses are time histories and largest responses at any one of the responses points (mid-points) of sublayer, i irrespective of the time is the required response. The largest response can occur at one of response points, depending on the location of the contact stresses present at the pavement surface. The proposed wheel wander investigation uses the responses on the transverse plane at the instant when the largest response occurred. A sketch of this pavement response in the transverse plane is shown in Fig 3.9a. Since tire configuration under investigation

is dual tires, the response values on the transverse plane is symmetrical about the centerline of the axle.

Say it is required to find the pavement responses due to wheel wander of two d_w values about the center of axle at the locations at B and C (Fig. 3.9a). These points are located at d_b and d_c as shown. The point A represents the location of largest response, ε_A. The pavement responses ε_B and ε_c, which correspond to the wheel wander values of d_b and d_c, can now be computed using the procedure shown in Fig 3.9b. For example, the transverse distance to evaluate ε_B is d_b from A, where largest response occurs. Similarly, ε_C can be evaluated from the transverse distance d_c.

This procedure can be used to evaluate the pavement responses for every trail value of d_w generated from the approach described above. This type of Monte-Carlo simulation of pavement responses has been undertaken for all of the critical responses identified. From this simulation, cumulative distribution functions (CDFs) were also developed. As a representative case for demonstration, Figs. 3.9a and 3.9b show pavement responses on the transverse plane and the corresponding CDFs for thin pavement (4 inch HMA) for dual and wide-base tires. The responses shown are: (a) longitudinal strains, ε_{xx} near the surface (z = 0.5 inch) and at the bottom of the HMA layer (z = 4 inch) and (b) vertical strains, ε_{zz} at two locations (z =1.5inch and z = 3.5 inch). Among many pavement responses available for demonstration, these strains have been selected because ε_{xx} values are critical input to HMA fatigue cracking (top-down and bottom up) evaluation. On the other hand, ε_{zz} values are required in the HMA rutting evaluations.

The shapes of the pavement response on the transverse plane are influenced by number of loaded arrears (dual vs. single) and also depth of the response points relative to the loaded areas. Clear indication of valleys and peaks are characteristic of dual loaded areas. For example, the ε_{zz} plot shown on bottom left in Fig. 3.10a reveals the existence of dual loaded areas. On the other

hand, ε_{zz} shown in Fig 3.10b shows the case of single loaded area from the wide-base tire. The up and down variation in ε_{zz} with wide-base tire (Fig. 3.10b, bottom left) can be attributed to the non-uniform contact stress distribution used. The shapes of ε_{xx} plots at the surface (z = 0.5 inch) show a single valley, unaffected by the tire configuration. This is because the locations of the response points are very close and cumulative effects of the dual loaded areas result in a single valley.

An examination of the CDFs reveals that the shapes, in particular in the case of dual tires, are not piece-wise smooth and have clear breaks (or kinks). The breaks in CDFs are not present when the corresponding strain response is shaped like a pulse. When there are valleys and peaks in the strain responses, their CDFs show breaks. Number of breaks is same as the number of peaks. For example, the ε_{zz} responses shown on the bottom left of Fig. 3.10a has two peaks and correspondingly the CDF shown on the right has two breaks. However, the CDF of ε_{zz} at z = 1.5 inch with wide-base tire (Fig. 3.10b, bottom left) does not show any breaks. This is because the variation of the ε_{zz} at this location is not clearly prominent. Another factor that can influence the shape of CDFs is the limit imposed on d_w. It should be recalled that because of the limitation on the lane width, the range for wheel wander, d_w was ± 21 inch. This imposed limitation will restrict the wheel wander within this range and it can influence the shape of CDF.

Plots for the case of thicker pavement (8 inch HMA) are presented in Figs. 3.11a and 3.11b. As expected the strain responses are much smaller in the case of thicker pavement. Only exception is the ε_{zz} at z = 1.5 inch (Fig. 3.11b, bottom left), where the compressive component of ε_{zz} in thicker pavement is higher. This requires an explanation. The HMA layer, whether it is thin or thick acts as a single layer supported by the bottom unbound layers. The load transfers within the HMA layer the net effect of the all the pavement layers (i.e., continuum) properties.

Thinner pavement is more flexible and it can therefore, transfer loads laterally more effectively (Fig. 3.12). This may be the reason for the lower compressive component of ε_{zz} with the thinner HMA pavement. It may be concluded that the characteristics of the strain responses on the transverse plane and corresponding CDFs are similar to those seen with the thin HMA pavement.

It was noted that the Monte-Carlo simulation procedure proposed here used a total number of trials for d_w as N = 10,000. An attempt was made to verify whether this limit on N is reasonable. As representative example, the CDFs obtained two extreme cease of N = 1,000 and N = 40,000 for ε_{xx} at z = 0.5 inch with the thinner pavement and dual tire are shown in Fig. 3.13. The cases with other values of N are not shown, because the plots practically overlie on each other. The largest deviation in ε_{xx} is also shown in the figure. Figure 3.14 shows the normalized largest deviation, with respect to N = 40,000 for other values of N. It is seen that the deviations do not consistently get lower as N increased and maximum deviation is limited to about 2.8%. The case N = 10,000 gives the lowest deviation (about1%). Since the deviation are lower, it is concluded that simulations with N = 10,000, in this thesis which was use appropriate.

The pavement response strain required in the investigation of top-down and bottom-up cracking use the maximum tensile strains at the depth of z = 0.5 and at the bottom of HMA, respectively. For tandem dual tire configurations of conventional trucks with uniform contact stresses the maximum tensile strain occurs under the center of the tire and the it is given by the longitudinal strain (ε_{xx}) component. However, when wide-base tire are used with non-uniform contact stress distribution, it is not known a priori which component of strain (ε_{xx} or ε_{yy}) will be higher. The contact stress distribution along with the shape of the loaded area will dictate which component is more critical. 3D-Move analysis results need to be scrutinized to obtain the needed maximum tensile strain. Figure 3.15 shows the CDFs obtained for the wide-base tire from 3D-

Move results of ε_{xx} and ε_{yy} at z = 0.5 and 4.0 inch. It is clear that at both depths the component of strain that yields the maximum tensile strain is the longitudinal strain, ε_{xx}.

CHAPTER 4 – PAVEMENT PERFORMANCE WITH WHEEL WANDER

4.1 PAVEMENT PERFORMANCE PREDICTIONS

One of the major design concerns of pavement designers and researchers is the prediction of pavements life, which needs to be undertaken with due considerations given to all pavement distress (or performance) modes. The MEPDG procedures use a number of pavement responses induced by the traffic loads as critical inputs to the pavement prediction models. In general, the MEPDG conducts HMA pavement designs based on performance in resisting: rutting, bottom-up and top-down fatigue, thermal cracking and roughness. This study only evaluated the impact of wheel wander on rutting, top-down and bottom-up fatigue cracking of HMA. The performance models included in MEPDG were developed with attention given to every one of the distress modes. The calibrations factors given in MEPDG are known as "Nationally-Calibrated Factors". They were developed based on a large database of field performance data, which also included an extensive array of pavement sections that were a part of a large FHWA study "Long-Term Pavement Performance (LTPP)". The MEPDG calibration factors given in this document, dated 2004, are considered to be appropriate for unmodified HMA mixtures since a vast majority of the field cases considered were with unmodified HMA. Subsequently, Von Quintus et al. (Von Quintus et al. 2008) revisited the pavement performance data and recommended modified calibration factors. Their study also included performance of polymer-modified HMA mixtures. These calibration factors were used with the HMA mixture considered in the study.

4.1.1 Permanent Deformation (Rutting) (NCHRP 2004)

Rutting in flexible pavements is caused by the permanent deformation in the all pavement layers: HMA layer and unbound layers (base and subgrade). This study focused only on the rutting in the HMA layer and it was evaluated by: (1) dividing each layer into a number of sublayers with defined thicknesses (h_i), (2) computing the permanent strain in middle of each sublayer (ε_p^i), and (3) adding the resulting permanent deformation to determine the accumulated rut depth (RD) in the entire HMA layer, as expressed in equation below (MEPDG):

$$RD = \sum_{i=1}^{N_{sublayers}} \varepsilon_p^i \, h^i \tag{4.1}$$

where, RD = pavement permanent deformation; $N_{sublayers}$ = number of sublayers; ε_p^i = total plastic strain in sublayer i; h^i = thickness of sublayer i. MEPDG gives specific recommendations relative to the required number of sublayers as a function of HMA thickness. The permanent strain (ε_p^i) in each of the HMA sublayers can be calculated using traffic-induced vertical strain (ε_{zz}^i), number of axle load repetitions (N_{cy}) and temperature (T, in °F) of the HMA sublayer. The plastic strain in sublayer i is given by (Von Quintus et al. 2008) :

$$\frac{\varepsilon_p^i}{\varepsilon_{zz}^i} = k_1 \times 10^{k_{r1}} T^{1.5606} N_{cy}{}^{0.4791} \tag{4.2}$$

where, k_1 = function of total asphalt layers thickness (h_{ac}, in) and depth (depth, in) and k_{r1} = calibration factor. The recommended value for k_1 for unmodified and modified HMA mixtures is: $k_1 = (C_1 + C_2 \times \text{depth}) \times 0.328196^{\text{depth}}$; $C_1 = -0.1039 \times h^2_{ac} + 2.4868 \times h_{ac} - 17.342$; and $C_2 = 0.0172 \times h^2_{ac} - 1.7331 \times h_{ac} + 27.428$. The recommended values for k_{r1} for unmodified HMA mixtures is: $k_{r1(unmodified)} = -3.35412$. For polymer-modified HMA mixtures it is: $k_{r1(modified)} = 1.13 k_{r1(unmodified)} = -3.79016$.

It may be noted that the only load-related parameter in the above performance model is ε_{zz}^{i}, which is given by the Monte-Carlo simulation described in Chapter 3.

4.1.2 Fatigue Cracking (Bottom-up and Top-down) (NCHRP 2004)

Estimation of fatigue damage is based upon Miner's Law, which states that damage is given by the following relationship:

$$D = \sum_{i=1}^{T_N} \frac{n_i}{N_{f_i}} \tag{4.4}$$

where, D = damage; T_N = total number of periods; n_i = actual traffic for period i; N_{f_i} = cycles to failure allowed under conditions prevailing in period i.

The approach suggested in MEPDG to assess fatigue life in HMA is based on a predictive algorithm for top-down and bottom-up cracking that relates the tensile strains near the surface and the bottom of the HMA layer, respectively. Other factors such as HMA stiffness (E_{HMA}, psi), HMA thickness (inch), air void content (V_a, %), and effective binder content (V_b, % by volume) of the mixture are also required. The allowable number of axle load applications (N_{fi}) needed for the increment damage index approach to predict fatigue cracking is presented in equation below:

$$N_{f_i} = k_{f1} \times k_1' \times C \left(\frac{1}{\varepsilon_t}\right)^{3.9492} \left(\frac{1}{E}\right)^{1.281} \tag{4.5}$$

where, $C = 10^{M}$; $M = 4.84\left(\frac{V_b}{V_a+V_b} - 0.69\right)$

$$k_1' = \frac{1}{0.000398+\frac{0.003602}{1+e^{(11.02-3.49\times h_{ac})}}}, \quad \text{(Bottom} - \text{up cracking)}$$

$$k_1' = \frac{1}{0.01+\frac{12.00}{1+e^{(15.676-2.8186\times h_{ac})}}}, \quad \text{(Top} - \text{down cracking)}$$

The recommended values for k_{fl} for unmodified HMA mixtures is: $k_{fl(unmodified)} = 0.007566$. For polymer-modified HMA mixtures it is: $k_{fl(PMA)} = 0.014964$ (Von Quintus et al. 2008).

For the top-down cracking the ε_t near the surface calculated at z = 0.5 inch was used. A representative value for E_{HMA} is required to use the above equation. MEPDG recommends a procedure to estimate E_{HMA} based on vehicle speed, thickness of HMA and frequency sweep data (Figs 3.2a and b). Interpolation is necessary to get E_{HMA} value (Tables 4.1a, b and c).

4.2 EVALUATION OF PAVEMENT STRAIN FOR PERFORMANCE CALCULATIONS

Unlike in the airfield pavement designs, the role of wheel wander is not routinely taken into account in highway pavement designs (e.g., Asphalt Institute Design Guidelines). When wheel wander is not considered, the design uses the maximum pavement response in the pavement damage calculations. On the other hand, as noted in Chapter 1 MEPDG recommends a procedure where the lateral wheel wander is assumed to be normally distributed into five segments of equal areas under the normal distribution curve and damage is computed by summing the contributions from the segments. The study reported here evaluated the pavement performance (of life) using three methods. These methods differ based on the value of the traffic-induced strains used in the performance equations presented above. First method (Method 1) uses the maximum response strain, while the second method (Method 2) is the MEPDG approach. The Method 3 is based on the CDFs developed by the Monte-Carlo simulation scheme described in this thesis. The CDFs are divided into a number of equal segments (say M_{seg}) and the strains that correspond each of the segments are used with the performance equations. As many numbers of segments as needed can be considered, however for being consistent with MEPDG approach (Method 2), it was decided to use $M_{seg} = 5$. The strains (ε_1 through ε_5) obtained from a typical CDF using five segments are shown in Fig. 4.1.

An illustration of the steps adopted in using the Methods 1 through 3, is presented in Fig. 4.2. This case refers to the investigation of fatigue life for bottom-up cracking of the thin HMA pavement (4 inch thick), subjected dual tire tandem axle loading. The critical pavement response required is the longitudinal strain at the bottom of HMA layer (z = 4.0 inch) and the previous plot (Fig. 3.10a top left) has been reproduced along with the response strains used with all the methods identified (Fig. 4.2). The maximum tensile strain required with Method 1 $(\varepsilon_1)_a$ is 158μ. For the case of Method 2, which is based on MEPDG procedure, the five strain components are: $(\varepsilon_2)_a$ = 32μ; $(\varepsilon_2)_b$ = 97μ; $(\varepsilon_2)_c$ = 158μ; $(\varepsilon_2)_d$ = 130μ; and $(\varepsilon_2)_e$ = 147μ. The strain components associated with the proposed Method 3 are: $(\varepsilon_3)_a$ = 42μ; $(\varepsilon_3)_b$ = 99μ; $(\varepsilon_3)_c$ = 132μ; $(\varepsilon_3)_d$ = 145μ; and $(\varepsilon_3)_e$ = 154μ. For clarity of the figures, only the strains associated with the second segment B are clearly identified in Fig. 4.2. It may be noted the largest strain response of 158 μ is reported only by the Segment C of Method 2. Aforementioned procedure was adopted in all cases to determine the strain responses for use with the performance equations.

4.3 PAVEMENT PERFORMANCE (OR LIFE) CALCULATIONS

As pointed out earlier, the focus in this study is given to performance of HMA layer and corresponding the distress models considered are: (1) rutting; (2) top-down fatigue cracking; and (3) bottom-up fatigue cracking. It was assumed that the total rut depth of the HMA layer computed using the contributions of each of the sublayer should be limited to 0.5 inch. Asphalt Institute Design Guidelines specify this limit for rutting at the pavement surface. Through the contributions to rutting can be from all pavement layers, the rutting limit from the HMA layer of 0.5 inch was used here to evaluate the pavement life. It may be noted that use of a consistent rut depth limit in all the methods enables the direct comparison of pavement life predictions.

Equation 4.1 can be rewritten to include the rut depth limit and the use of multiple strain components as follows:

$$RD = 0.5 \text{ inch} = \sum_{i=1}^{N_{sublayers}} h^i \sum_{j=1}^{M_{seg}=5} \varepsilon_{pj}^i$$

where, ε_{pj}^i is the pavement strain in i^{th} layer computed with traffic-induced compressive vertical strain component of segment j. It should be noted in some cases traffic-induced pavement strain component can be tensile (see Fig. 3.10a, bottom left; Fig. 3.10b bottom left. Tensile vertical strains are common near the surface of the pavement. Since tensile vertical strain do not contribute to rutting and therefore, should not be used in the pavement life calculations.

Application of Miner's Law to predict fatigue cracking (top-down and bottom-up) failure (i.e., damage D = 1.0) may be rewritten to include the multiple strain components as (see Equation 4.4):

$$D = 1.0 = \frac{1}{5} \sum_{i=1}^{M_{seg}=5} \frac{(N_f)_{Cracking}}{(N_f)_i}$$

where, $(N_f)_{Cracking}$ = number of cycle needed for failure; $(N_f)_i$ = cycle to failure computed from the performance equation using traffic-induced tensile component of segment i. Similar to the case of HMA rutting, there are instance in Methods 2 and 3, where compressive strain may be present in some of the segments. In such cases, their contributions to fatigue damage are not considered.

It was noted that the number of segments (M_{seg}) used in the methods is five to be consistent with Method 2. An investigation was undertaken to explore the role of the selection of number of segments on pavement life predictions. Figure 4.3 presents number of cycles to rutting,

fatigue failure for both top-down and bottom-up modes. The following representative pavement case was considered: dual tires; pavement temperature = 70°F; Vehicle Speed = 60 mph. Results for both thin and thick pavements for segments range of 2 to 20 are given. The CDFs of required pavement strains were divided by the number of segments considered and $(N_f)_{Cracking}$ values were computed using the pavement performance Equation 4.5. The figure reveals that the selection of the segments is important and there appears to be no general relationship between $(N_f)_{Cracking}$ and number of segments. Since the routinely-used MEPDG uses five segments, for consistency reason the comparative investigation presented subsequently used also five segments with Method 3.

A comprehensive set of plots have been developed to aid with the comparison of the three methods mentioned. The pavement life results in terms of number of cycles to failure are assembled in the following order: (1) HMA rutting; (2) HMA top-down cracking; and (3) HMA bottom-up cracking. The thesis only presents the rutting results. In the following order:

Fig. 4.4: Pavement Temperature, T = 70°F; Unmodified HMA Mixture

Fig. 4.7: Pavement Temperature, T = 104°F; Unmodified HMA Mixture

Fig. 4.10: Pavement Temperature, T = 70°F; Modified HMA Mixture

Fig. 4.13: Pavement Temperature, T = 104°F; Modified HMA Mixture

The cycles to rutting failure also have been normalized with respect to Method 1 and Method 2. The normalization using Method 1 is useful to estimate the role of the consideration of wheel wander. On the other hand, the normalization using Method 2 is helpful to compare the differences between the Methods that use wheel wander (i.e., Method 2 and Method 3).

The Method 1 uses the largest pavement response, while other methods use multiple strain values from the segments as described above. Those strain values associated with the segments are lower, except for one strain value in Method 2 (see Fig. 4.2a). Therefore, the pavement life predicted by Method 1 is always lower and this may be interpreted as being overly conservative. The MEPDG approach, though an important step towards a realistic modeling of long-term pavement performance, its arbitrary use of fixed five locations to define the wheel wander can be biased and therefore, questionable. Relevant figure are for fatigue cracking (top-down and bottom-up) were also produced and are shown in Figs. 4.5; 4.6; 4.8; 4.9; 4.11; 4.12; 4.14; and 4.15.It may be noted that three noteworthy features of the proposed method (Method 3) are:

(1) The procedure developed to generate trial values for wheel wander (d_w) in the transvers direction with limits imposed on typical truck and traffic lane widths;

(2) The use of 3D-Move, which is a dynamic model that can model moving nature of load, viscoelastic material properties, nonuniform contact stress distribution and vehicle speed;

(3) The implementation of item 1 above, to obtain the representative statistical distributions (or population) of the required responses needed for the pavement performance evaluation.

These important features make the investigation of the role of wheel wander more realistic and therefore appealing to pavement engineers and researchers.

CHAPTER 5 – SUMMARY AND CONCLUSIONS

Since estimation of long-term performance (or life) is a critical pavement design concern, it has attracted considerable attention from pavement engineers and researchers. Many pavement design procedures are based on the maximum pavement response induced by the traffic (e.g., Asphalt Institute Design Procedure). Consideration of wheel wander provides for a more realistic and economical design. The procedures in MEPDG and CalME to address the wheel wander recommend the use of normal distributions for transverse wheel wander. These procedures are relatively simple and they are based on dividing the wheel wander distribution into a number of segments (say five) of equal areas. Such approaches suffer from a major limitation that the selection of equal segments is arbitrary, and can therefore, lead to biased results.

The study reported here covered a variety of pavement factors that significantly affect pavement performance. The factors included are: (1) pavement layer configuration (thin and thick); (2) pavement material properties (conventional and polymer-modified); (3) tire configurations (dual and wide-base); (4) pavement temperature (T = 70°F and T = 104°F); and (5) vehicle operating conditions (braking and non-braking). A major contribution of this thesis is to provide valuable design information on the relative importance of these factors on the prediction of pavement life.

A Monte-Carlo simulation scheme that addressed the role of wheel wander on pavement response and performance has been developed. The major steps of the proposed scheme are: (1) Step 1 – Procedure for the generation of a number of trials values of wheel wander that confirm to a normal distribution with a standard deviation of 12 inches; (2) Step 2 - Evaluation of critical responses that are needed in the estimation of long-term pavement performance (or life) for the

trial values of wheel wander developed in Step 1; and (3) Step 3 – Estimation of long term pavement performance for each of the important HMA-related distress modes. Since the traffic lanes are of limited width (about 12 ft.), the trial values of wheel wander was limited to ± 21 in about the centerline of the traffic lane. The proposed Monte-Carlo scheme provided cumulative distribution functions (CDFs) for all the important responses and they in turn were used in the estimation pavement performance (or life).

In general, the mechanistic-empirical pavement design procedures (e.g., MEPDG, CalME etc.) assess long-term pavement performance based on the following distress modes: surface rutting, top-down cracking, and bottom-up cracking. The last two distress modes are HMA failure modes, while the first distress mode has contributions from all pavement layers. This study only focused on the impact of wheel wander on HMA failure modes. An important first step is the evaluation of pavement responses that is critical in the computation of pavement distress (or performance). In the evaluation of HMA rutting the HMA layer needs to be divided into many sublayers and vertical strain responses are required at the middle of each of the sublayers (MEPDG). The critical responses that are needed for fatigue cracking evaluations are maximum tensile strains near the surface (z = 0.5 inch) and at the bottom of the HMA layer (z = 4.0 or 8.0 inch). Required pavement strain database was generated by conducting a mechanistic analysis of the two HMA pavement structures (representing a thin and a thick) using UNR's 3D-Move model. 3D-Move is a computer model that is based on a continuum finite-layer approach can evaluate the responses of layered medium to three-dimensional (3D) moving surface loads. It is applicable to linear elastic and viscoelastic horizontal layers with finite thicknesses. Since the layered system is linear or viscoelastic, the loads are decomposed into harmonic components using Fourier series expansion and the total responses are computed as the summation of the individual responses from each harmonic component.

The study reported here evaluated the pavement performance (of life) using three methods. These methods differ based on the value of the traffic-induced strains used in the performance equations. First method (Method 1) uses the maximum response strain, while the second method (Method 2) is the MEPDG approach. The Method 3 is based on the CDFs developed by the Monte-Carlo simulation scheme described in this thesis. The CDFs were divided into a number of equal segments and the strains that correspond each of the segments were used with the performance equations. As many numbers of segments as needed can be considered, however for being consistent with MEPDG approach (Method 2), it was decided to use five segments.

Since the Method 1 uses the largest pavement response, the pavement life predicted by Method 1 is always lower and this may be interpreted as being over conservative. The Method 2 (MEPDG approach), though an important step forwards realistic modeling of long-term pavement performance, its arbitrary use of fixed five locations to define the wheel wander can be biased and therefore, questionable. The Method 3 is statically-based and uses many trials of wheel locations to model the vehicle wander. Therefore, it takes into account in a more realistic manner the entire variation of the traffic-induced strain on the transverse plane. Such an approach is considered more appealing to pavement engineers and researchers.

In summary, pavement design information presented in this thesis are in the form of datasets that the pavement engineers and researchers can use to assess the sensitivity of many important factors that affect long-term pavement performance. Neither interpretation nor scrutiny of the design information has been attempted. Instead, the thesis outlines elaborate details on a three-step approach used to develop such design guidelines.

REFERENCES

1. AASHTO. 2001. Policy on Geometric Design of Highways and Streets. *American Association of State Highway and Transportation Officials, Washington, DC* 1:990.
2. Ahlvin, R. G., W. J. Turnbull, J. Sale, and A. Maxwell. 1971. Multiple-Wheel Heavy Gear Load Pavement Tests. Volume I. Basic Report: DTIC Document.
3. Airport Pavement Design and Evaluation. 2009.
4. Al-Qadi, I. 2004. Pavement damage due to different tires and vehicle configurations, VIRGINIA TECH.
5. Al-Qadi, I. L., and H. Wang. 2009. Evaluation of pavement damage due to new tire designs. *Urbana* 51:61801.
6. Al-Qadi, I. L., H. Wang, P. J. Yoo, and S. H. Dessouky. 2008. Dynamic analysis and in situ validation of perpetual pavement response to vehicular loading. *Transportation Research Record: Journal of the Transportation Research Board* 2087 (1):29-39.
7. Buiter, R., W. Cortenraad, A. Van Eck, and H. Van Rij. 1989. *Effects of transverse distribution of heavy vehicles on thickness design of full-depth asphalt pavements*.
8. Chen, D.-H., J. Bilyeu, T. Scullion, D.-F. Lin, and F. Zhou. 2003. Forensic evaluation of premature failures of Texas specific pavement study-1 sections. *Journal of performance of constructed facilities* 17 (2):67-74.
9. Classifying highway vehicles from known axle count and Spacing. 2004. American Society for Testing & Materials.
10. Fung, Y.-c. 1977. A first course in continuum mechanics. *Englewood Cliffs, NJ, Prentice-Hall, Inc., 1977. 351 p.* 1.
11. Gillespie, T. D. 1992. Fundamentals of vehicle dynamics (R-114). *SAE International, March*.
12. Gillespie, T. D., and L. Balderas. 1987. An Analytical Comparison of the Dynamic Performance of a European Heavy Vehicle and a Generic U.S. Heavy Vehicle: The University of Michigan Transportation Research Institute, 374p.
13. Hajj, E. Y., R. V. Siddharthan, P. E. Sebaaly, and D. Weitzel. 2007. Hot-Mix Asphalt Mixtures for Nevada's Intersections. *Transportation Research Record: Journal of the Transportation Research Board* 2001 (1):73-83.
14. HoSang, V. A. 1978. Field survey and analysis of aircraft distribution on airport pavements. *Transportation Research Board Special Report* (175).
15. Kawa, I., Hayhoe, G.F., and Brill, D.R. 2010. Modifications to Pass-to-Coverage Ratio Computation in the FAA's FAARFIELD Design Procedure. In *2nd International Conference on Transport Infrastructures*. São Paulo, Brazil.
16. NCHRP. 2004. Guide for Mechanistic-Empirical Design of New and Rehabilitated Structures. In *Final Report for Project 1-37A, National Cooperative Highway Research Program*: Transportation Research Board, National Research Council, Washington, D.C.
17. Papoulis, A. 1962. The Fourier Integral and its Applications McCraw Hill Book Company. *New York*.
18. Pass-to-Coverage Computation for Arbitrary Gear Configurations in the FAARFIELD Program. 2012. edited by U. S. D. o. Transportation and F. A. Administration.
19. Roesset, J. M. 1980. Stiffness and damping coefficients of foundations. Paper read at Dynamic Response of Structures@ sExperimentation, Observation, Prediction and Control.

20. Siddharthan, R., Sebaaly, P.E., El-Desouky, M., Strand, D., and Huft, D. 2005. Heavy Off-road Vehicle Tire-Pavement Interactions and Response. *Journal of Transportation Engineering* 131(3) (ASCE):239-247.
21. Siddharthan, R., Z. Zafir, and G. M. Norris. 1993. Moving load response of layered soil. I: Formulation. *Journal of Engineering Mechanics* 119 (10):2052-2071.
22. Siddharthan, R. V., N. Krishnamenon, and M. El-Mously. 2002a. Validation of a pavement response model using full-scale field tests. *International Journal of Pavement Engineering* 3 (2):85-93.
23. Siddharthan, R. V., N. Krishnamenon, M. El-Mously, and P. E. Sebaaly. 2002b. Investigation of tire contact stress distributions on pavement response. *Journal of Transportation Engineering* 128 (2):136-144.
24. Siddharthan, R. V., and P. E. Sebaaly. 1999. Investigation of asphalt concrete layer strains from wide-base tires. *Transportation Research Record: Journal of the Transportation Research Board* 1655 (1):168-174.
25. Siddharthan, R. V., J. Yao, and P. E. Sebaaly. 1998. Pavement strain from moving dynamic 3D load distribution. *Journal of Transportation Engineering* 124 (6):557-566.
26. Timm, D. H., and A. L. Priest. 2005. Wheel Wander at the NCAT Test Track. *NCAT Report*:05-02.
27. Ulloa, C. A. 2009. *Characteristics of dynamic triaxial testing of asphalt mixtures*.
28. Ulloa Calderon, A. 2009. *Characteristics of dynamic triaxial testing of asphalt mixtures*.
29. Von Quintus, H., J. Mallela, and L. Titus-Glover. 2008. Calibration Factors for Polymer-modified Asphalts Using M-e Based Design Methods ER-235: Asphalt Institute.
30. Wardle, L., G. Youdale, and B. Rodway. 2003. Current issues for mechanistic pavement design. Paper read at Proceedings of the 21st AARB and 11th REAAA Conference 18–23 May 2003, Cairns, Queensland, Australia.
31. Wardle, L. J., and B. Rodway. 1995. Development and application of an improved airport pavement design method. Paper read at The Transportation Congress. Part 1(of 2).
32. Wong, J. 1993. Theory of Ground Vehicles John Wiley & Sons Inc.
33. Zafir, Z., R. Siddharthan, and P. E. Sebaaly. 1994. Dynamic pavement-strain histories from moving traffic load. *Journal of Transportation Engineering* 120 (5):821-842.

TABLES

Table 2.1: Summary of Pavement Response Models used in Previous Studies (Al-Qadi and Wang 2009)

Source	Tire	Analysis Tool	Contact Stresses	Loading
Deacon (1969)	Single tire of dual- tire assembly	MLE*	Circular Uniform Vertical	Static
Hallin et al. (1983)	Tire width of 10, 15 and 18in.	MLE FEM**	Circular Uniform Vertical	Static
Perdomo and Nokes (1993)	16R22.5 18R22.5	MLE (CIRCLY)	Circular Non-uniform Shear stress	Static
Gillespie et al. (1993)	Single 11R22.5, 215/75R17.5 etc.	MLE (VESYSDYN)	Circular Uniform Vertical	Static
COST 334 (2001)	385/45R22.5 495/45R22.5	MLE FEM	Square Uniform Vertical	Static
AI-Qadi et al. (2002)	445/50R22.5 455/55R22.5	FEM	Square Trapezoidal Vertical	Static
Siddharthan et al. (2002)	425/65R22.5	Finite-Layer (3D-Move)	Any Shape Non-Uniform 3D Stress Distribution	Dynamic
Kim et al. (2005)	425/65R22.5	FEM	Square Uniform Trapezoidal	Static Dynamic
AI-Qadi et al. (2008a)	455R/55R22.5	FEM	Moving Load and 3D contact stress	Dynamic

* Multilayer Elastic Theory
** Finite Element Method

Table 3.1: Properties of Pavement Materials

Layer	Thickness (in)	Unit Weight (pci)	Elastic Modulus (psi)	Damping Ratio	Poisson's Ratio
HMA	4,8	0.0876	variable	variable	0.4
Base	8,10	0.0663	35,000	5.0%	0.4
Subgrade	240	0.0626	15,000	5.0%	0.4

Table 3.2(a): Dynamic Viscoelastic Properties of HMA Mixture PG64-22 Obtained from Master Curves

Test Temp. 70°F			Test Temp. 104°F		
Predicted |E*|, ksi	Freq at Selected Temp, Hz	Damping Ratio	Predicted |E*|, ksi	Freq at Selected Temp, Hz	Damping Ratio
2.195E+00	9.458E-09	1.343E+00	2.195E+00	2.424E-06	1.343E+00
2.947E+00	9.458E-08	5.854E-01	2.947E+00	2.424E-05	5.854E-01
4.636E+00	9.458E-07	3.663E-01	4.636E+00	2.424E-04	3.663E-01
8.885E+00	9.458E-06	2.709E-01	8.885E+00	2.424E-03	2.709E-01
2.074E+01	9.458E-05	2.546E-01	2.074E+01	2.424E-02	2.546E-01
5.502E+01	9.458E-04	3.014E-01	5.502E+01	2.424E-01	3.014E-01
1.458E+02	9.458E-03	3.354E-01	1.458E+02	2.424E+00	3.354E-01
3.393E+02	9.458E-02	2.742E-01	3.393E+02	2.424E+01	2.742E-01
6.479E+02	9.458E-01	1.935E-01	6.479E+02	2.424E+02	1.935E-01
1.016E+03	9.458E+00	1.405E-01	1.016E+03	2.424E+03	1.405E-01
1.361E+03	9.458E+01	1.107E-01	1.361E+03	2.424E+04	1.107E-01
1.632E+03	9.458E+02	9.432E-02	1.632E+03	2.424E+05	9.432E-02
1.822E+03	9.458E+03	8.520E-02	1.822E+03	2.424E+06	8.520E-02
1.945E+03	9.458E+04	8.005E-02	1.945E+03	2.424E+07	8.005E-02
2.021E+03	9.458E+05	7.711E-02	2.021E+03	2.424E+08	7.711E-02
2.067E+03	9.458E+06	7.542E-02	2.067E+03	2.424E+09	7.542E-02
2.094E+03	9.458E+07	7.444E-02	2.094E+03	2.424E+10	7.444E-02
2.110E+03	9.458E+08	7.387E-02	2.110E+03	2.424E+11	7.387E-02
2.119E+03	9.458E+09	7.354E-02	2.119E+03	2.424E+12	7.354E-02

Table 3.2(b): Dynamic Viscoelastic Properties of HMA Mixture PG64-28NV Obtained from Master Curves

Test Temp. 70°F				Test Temp. 104°F			
Predicted |E*|, ksi	Freq at Selected Temp, Hz	Predicted G* kPa	Damping Ratio	Predicted |E*|*, ksi	Freq at Selected Temp, Hz	Predicted G* kPa	Damping Ratio
3.072E+00	9.737E-11	7.563E+03	2.627E-01	3.072E+00	6.691E-09	7.563E+03	2.627E-01
3.153E+00	9.737E-10	7.764E+03	2.566E-01	3.153E+00	6.691E-08	7.764E+03	2.566E-01
3.303E+00	9.737E-09	8.133E+03	2.474E-01	3.303E+00	6.691E-07	8.133E+03	2.474E-01
3.584E+00	9.737E-08	8.826E+03	2.347E-01	3.584E+00	6.691E-06	8.826E+03	2.347E-01
4.129E+00	9.737E-07	1.017E+04	2.194E-01	4.129E+00	6.691E-05	1.017E+04	2.194E-01
5.243E+00	9.737E-06	1.291E+04	2.056E-01	5.243E+00	6.691E-04	1.291E+04	2.056E-01
7.706E+00	9.737E-05	1.898E+04	2.022E-01	7.706E+00	6.691E-03	1.898E+04	2.022E-01
1.375E+01	9.737E-04	3.385E+04	2.240E-01	1.375E+01	6.691E-02	3.385E+04	2.240E-01
3.008E+01	9.737E-03	7.407E+04	2.856E-01	3.008E+01	6.691E-01	7.407E+04	2.856E-01
7.561E+01	9.737E-02	1.862E+05	3.557E-01	7.561E+01	6.691E+00	1.862E+05	3.557E-01
1.903E+02	9.737E-01	4.685E+05	3.307E-01	1.903E+02	6.691E+01	4.685E+05	3.307E-01
4.174E+02	9.737E+00	1.028E+06	2.413E-01	4.174E+02	6.691E+02	1.028E+06	2.413E-01
7.465E+02	9.737E+01	1.838E+06	1.716E-01	7.465E+02	6.691E+03	1.838E+06	1.716E-01
1.100E+03	9.737E+02	2.708E+06	1.310E-01	1.100E+03	6.691E+04	2.708E+06	1.310E-01
1.398E+03	9.737E+03	3.443E+06	1.087E-01	1.398E+03	6.691E+05	3.443E+06	1.087E-01
1.613E+03	9.737E+04	3.971E+06	9.658E-02	1.613E+03	6.691E+06	3.971E+06	9.658E-02
1.751E+03	9.737E+05	4.312E+06	8.989E-02	1.751E+03	6.691E+07	4.312E+06	8.989E-02
1.835E+03	9.737E+06	4.518E+06	8.616E-02	1.835E+03	6.691E+08	4.518E+06	8.616E-02
1.884E+03	9.737E+07	4.639E+06	8.407E-02	1.884E+03	6.691E+09	4.639E+06	8.407E-02
1.912E+03	9.737E+08	4.708E+06	8.290E-02	1.912E+03	6.691E+10	4.708E+06	8.290E-02
1.928E+03	9.737E+09	4.747E+06	8.224E-02	1.928E+03	6.691E+11	4.747E+06	8.224E-02

Table 3.3: Summary of a U.S. Tractor-semitrailer Brake System Properties

Truck Unit	Axle	Torque Gain* (in-lb/psi)	Push Out Pressure (psi)
Tractor	Steering	1322.5	13.5
	Tandem Leading Driving	3280.0	5.8
	Tandem Trailing Driving	3280.0	5.8
Semi-trailer	Tandem Leading Trailer	2818.8	5.5
	Tandem Trailing Trailer	2818.8	5.5

* For a loaded truck-semitrailer

Table 3.4: Vertical Load on Various Axles of the Fully Loaded 18-Wheel Tractor-Trailer

Braking Action	Axle		Vertical Load per Tire (lb)	Horizontal Load per Tire (lb)
No Braking	Steering		6,000	0
	Driving	Front	4,250 8500*	0
		Rear	4,250 8500*	0
	Trailer	Front	4,250 8500*	0
		Rear	4,250 8500*	0
Braking (at an average deceleration rate of 17.2 ft/sec^2)	Steering		8,489	2,161
	Driving	Front	5,132 10,264*	2,968
		Rear	3,351 6,702*	2,968
	Trailer	Front	4,405 8,810*	2,561
		Rear	2,868 5,736*	2,561

* For load per wide base tire

Table 3.5 Tire Type with Configuration and Contact Distribution in 3D-Move Database

Manufacturer	Tire Type
GoodYear	10.00*20 Bias Ply Tire
	G159A,11R22.5
	385/65R22.5 G178
	295/75R22.5
	425/65R22.5
Continental	11XR22.5 Radial
GoodRich	Aircraft Tire
Michelin	495/45R22.5

Table 3.6: Locations of Response Points for MEPDG-Based Pavement Performance Calculations (NCHRP 2004)

Failure Modes			Pavement Structure	
			4"HMA+6" Base Depth from Surface (in)	8"HMA+10" Base Depth from Surface (in)
Cracking	Top-down Cracking	Surface and 0.5" Surface from HMA	0.0 0.5	0.0 0.5
	Bottom-up Cracking	Bottom of HMA	4.0	8.0
Rutting	HMA Rutting	Mid Depth of Sub-layers	0.25; 0.75; 1.5; 2.0; 2.5; 3.5; 5.0; 7.0; 9.0	0.25; 0.75; 1.5; 2.0; 2.5; 3.5; 6.0; 9.0; 11.0; 13.0; 15.0; 17.0
	Subgrade Rutting	Top and 6"deep below Subgrade Surface	10.0 16.0	18.0 24.0

Table 3.7: (a) Recommendations for Selecting Vehicle Operating Speed; (b) Estimated frequency at certain depth and (c) HMA stiffness (E_{HMA}, psi)

(a)

Type of Road Facility	Operating Speed (mph)	Estimated Frequency at Layer Mid-depth (Hz) Representative HMA Layer (4-12 in)
Interstate	60	15-40
State Primary	45	10-30
Urban Street	15	5-10
Intersection	0.5	0.1-0.5

(b)

HMA Layer Thickness	Operating Speed	Estimated Frequency at Layer Mid-depth (Hz)
4in	2	1.5
	20	13.3
	60	40
8in	2	1.0
	20	9.6
	60	27.5

(c)

Temperature	HMA Binder PG Grade	HMA Layer Thickness	Operating Speed (mph)	Estimated Frequency at Layer Mid-depth (Hz)	Stiffness |E*| (ksi)
70°F	PG64-22	4in	2	1.5	719.60
			20	13.3	1070.34
			60	40	1239.11
		8in	2	1.0	656.46
			20	9.6	1018.43
			60	27.5	1183.06
	PG64-28NV	4in	2	1.5	223.54
			20	13.3	457.17
			60	40	611.28
		8in	2	1.0	192.2
			20	9.6	415.59
			60	27.5	556.77
104°F	PG64-22	4in	2	1.5	119.83
			20	13.3	277.08
			60	40	397.53
		8in	2	1.0	101.15
			20	9.6	246.84
			60	27.5	353.43
	PG64-28NV	4in	2	1.5	41.15
			20	13.3	100.28
			60	40	156.63
		8in	2	1.0	35.9
			20	9.6	87.73
			60	27.5	134.54

FIGURES

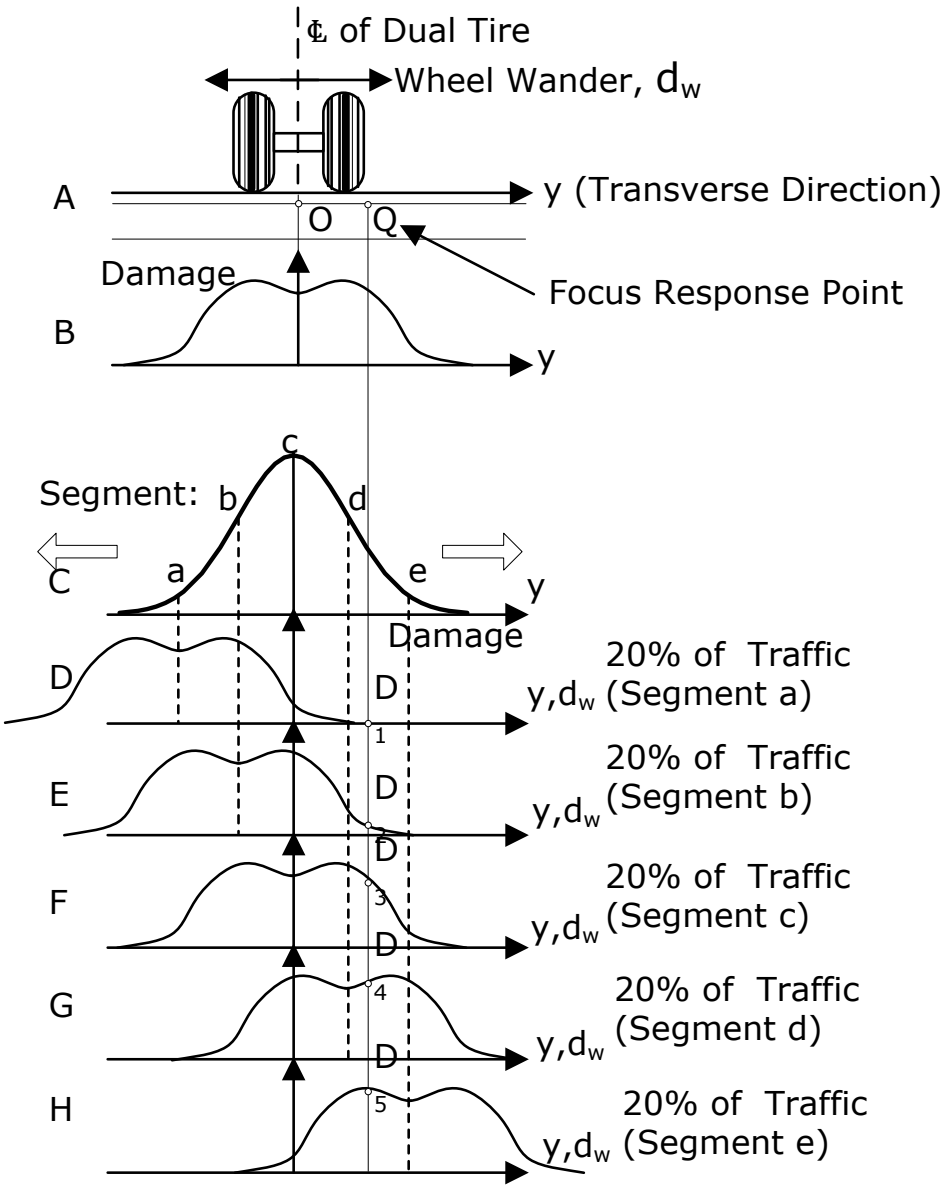

Fig. 1.1: Role of Wheel Wander: MEPDG Method (2004)

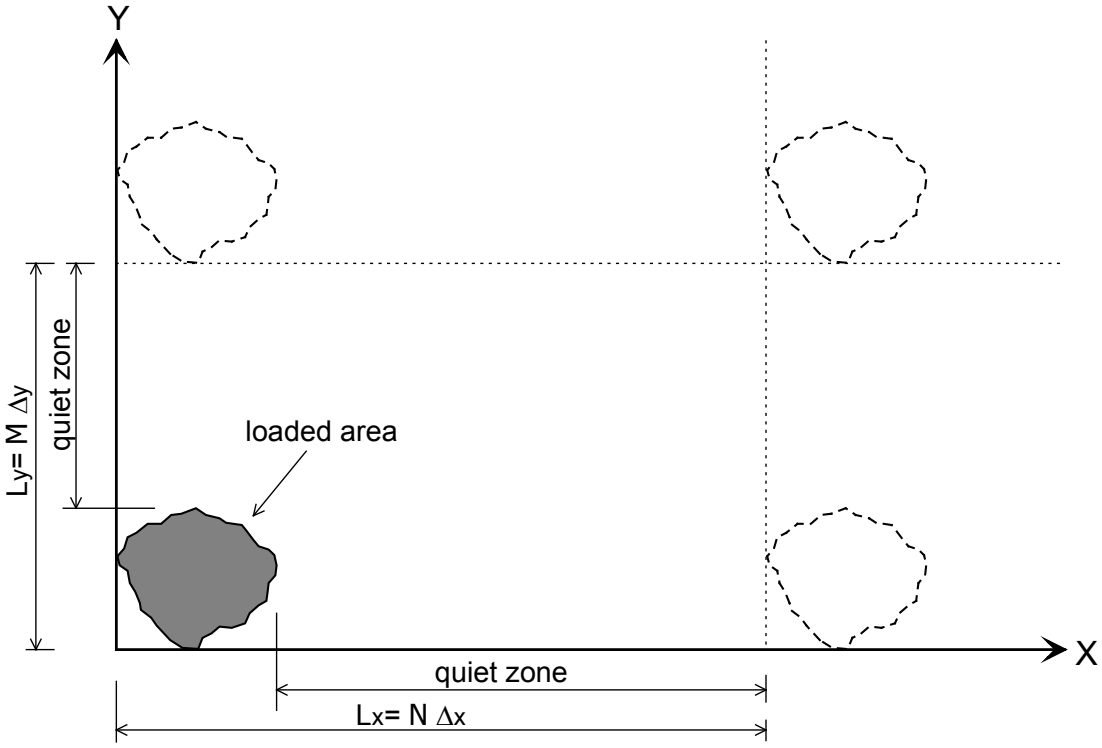

Fig. 2.1: Idealization of surface loads as a two-dimensional periodic function

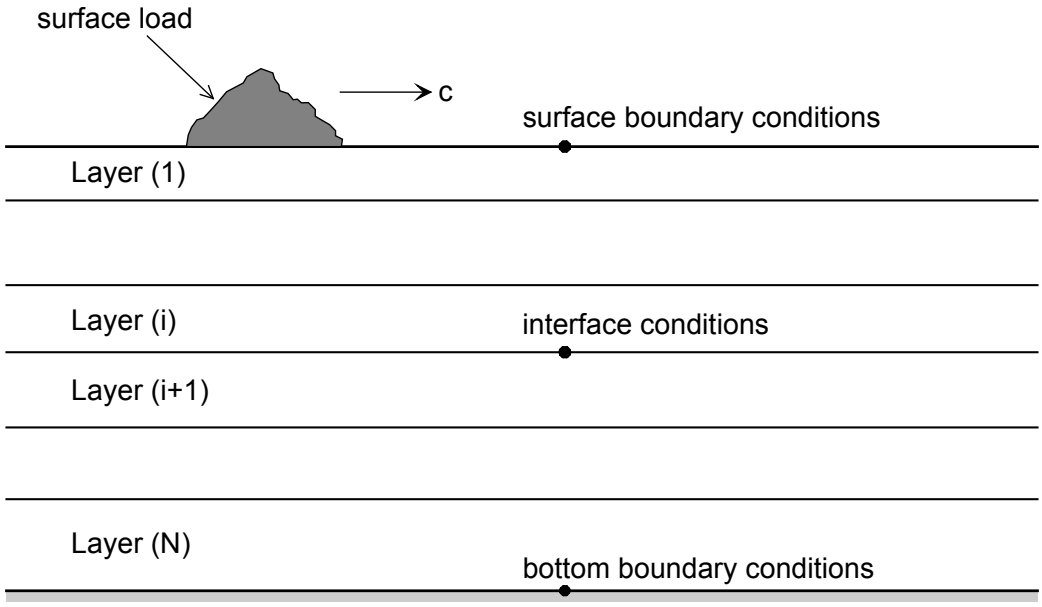

Fig. 2.2: Layout and boundary conditions of N-layered system

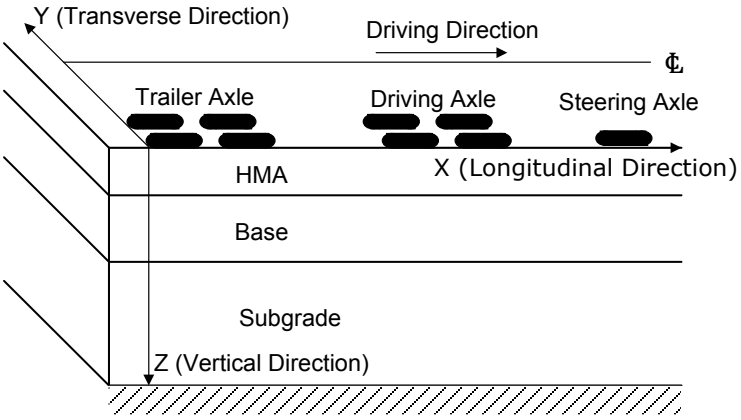

Fig. 3.1: Axle Configuration of Typical 18 Wheel Truck used in the 3D-Move Program

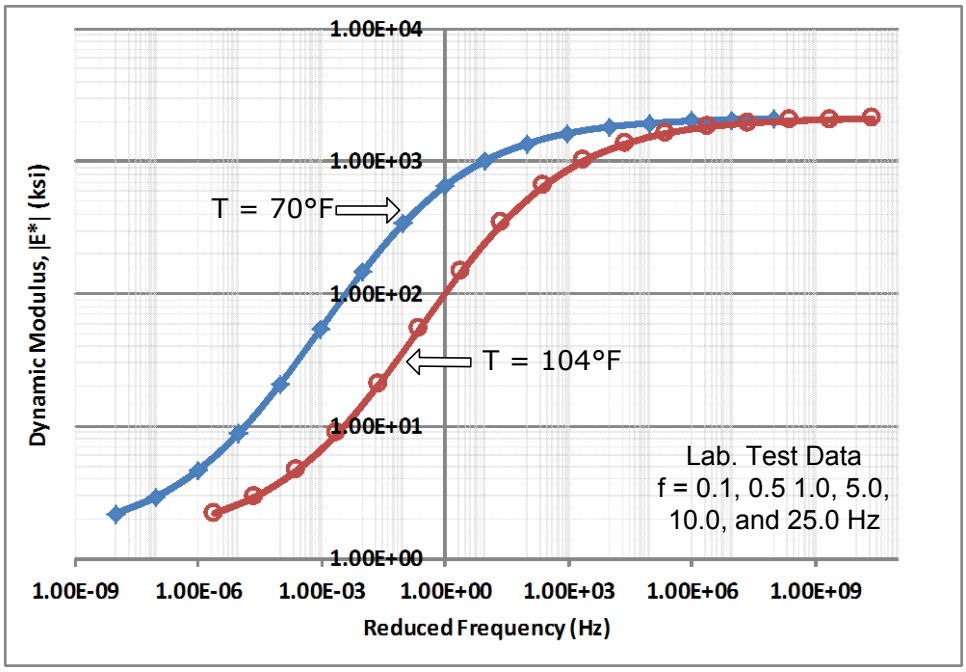

(a) PG64-22

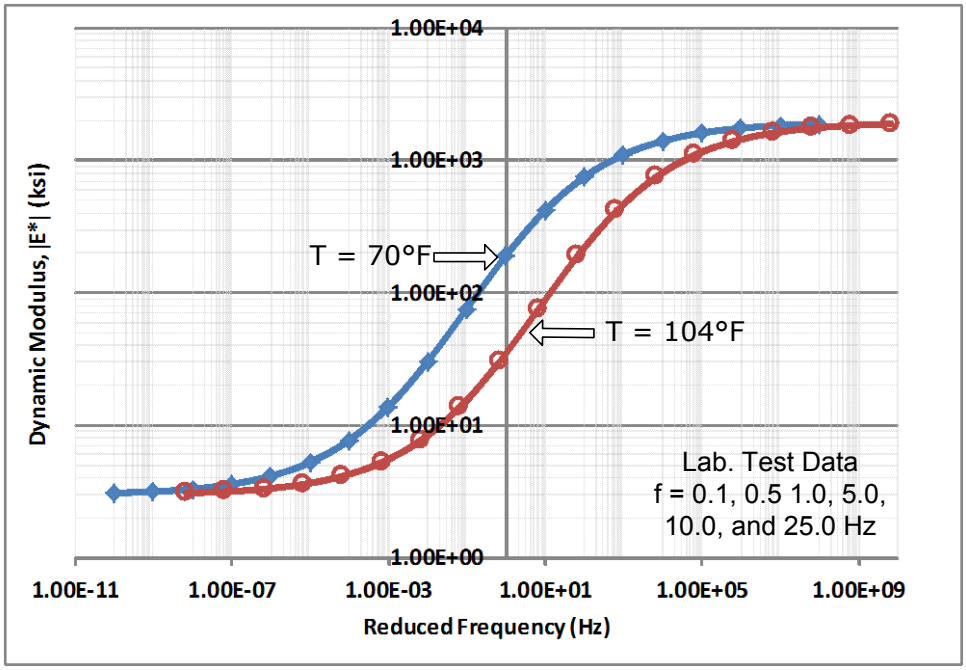

(b) PG64-28NV

Fig. 3.2: Dynamic Modulus |E*| Obtained Master Curves for T = 70°F and 104°F: (a) PG64-22 and (b) PG64-28NV (Polymer-modified)

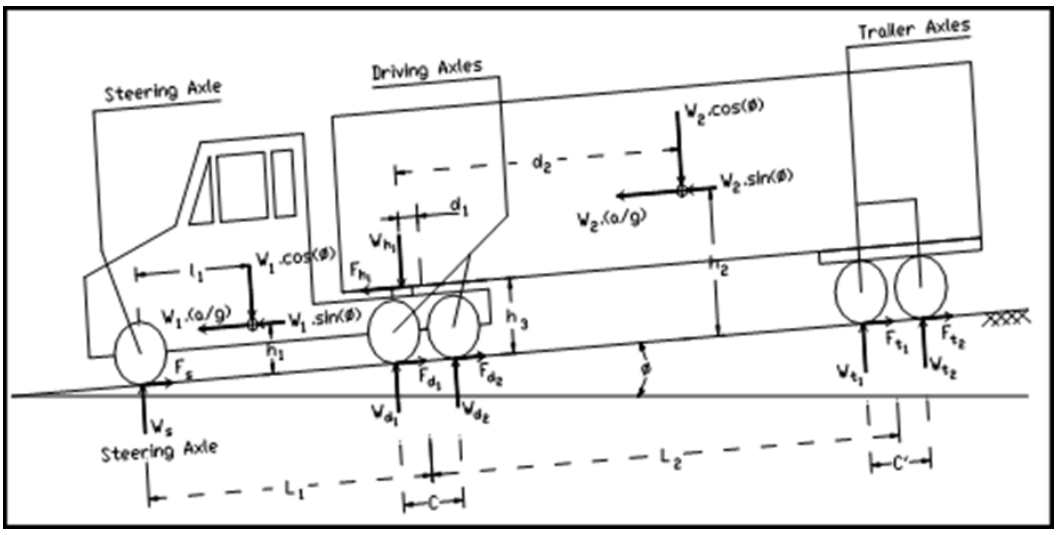

Fig.3.3: Forces Acting on a Tractor-Semitrailer During Braking on a Downward Slope (Hajj et al. 2007)

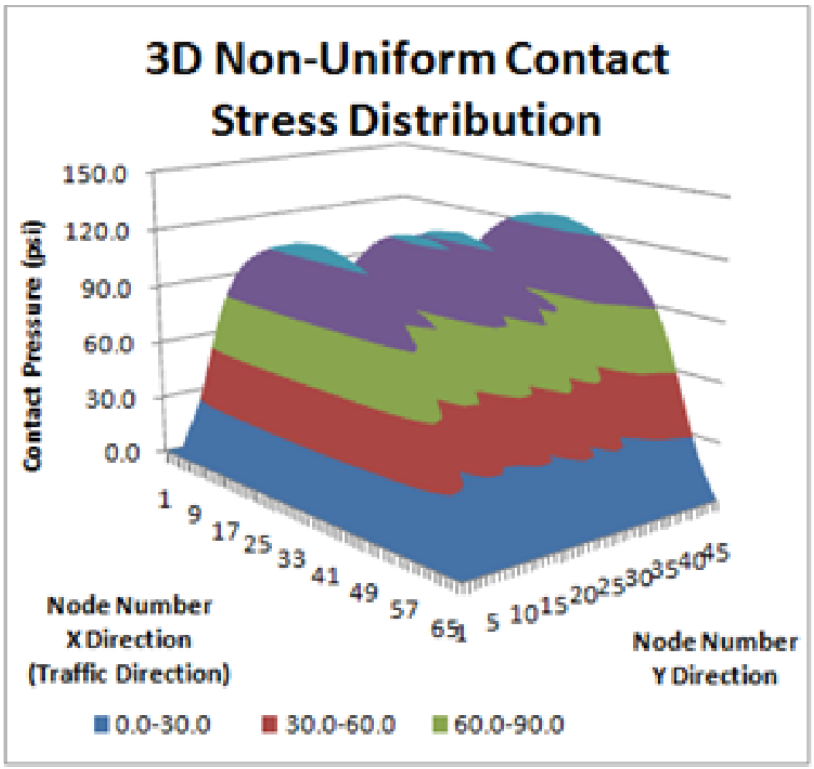

Fig. 3.4: Tire Contact Stress Distribution for GoodYear 425/65R22.5 (Tire Pressure = 130.5 psi; Tire Load 8093 lb; Vehicle Speed = 40 mph

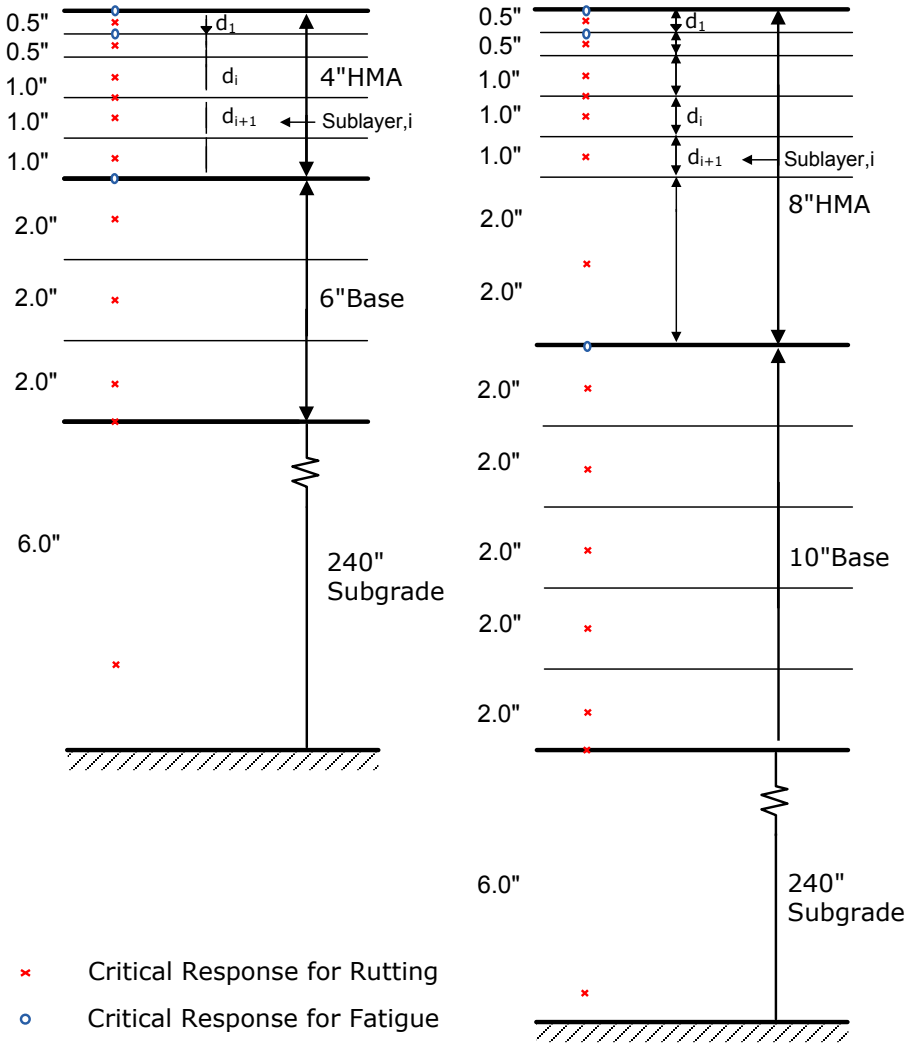

Fig. 3.5: Locations of Response Points for Pavement Performance Calculations

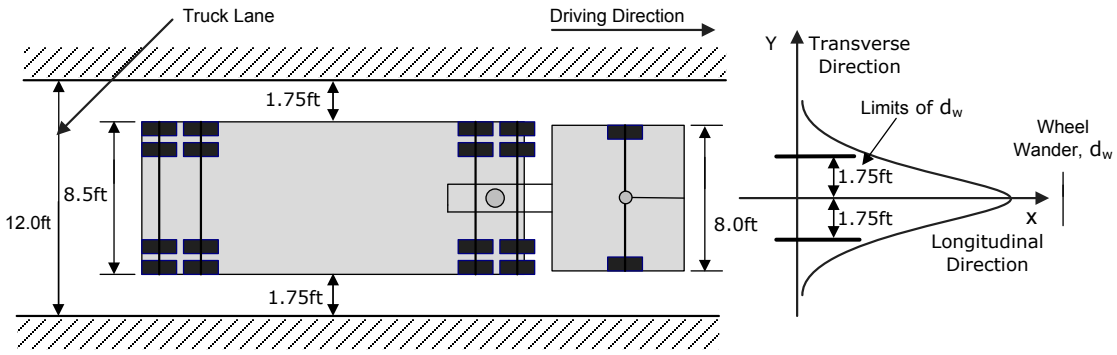

Fig. 3.6: Top View of Typical 18 Wheel Truck on Highw

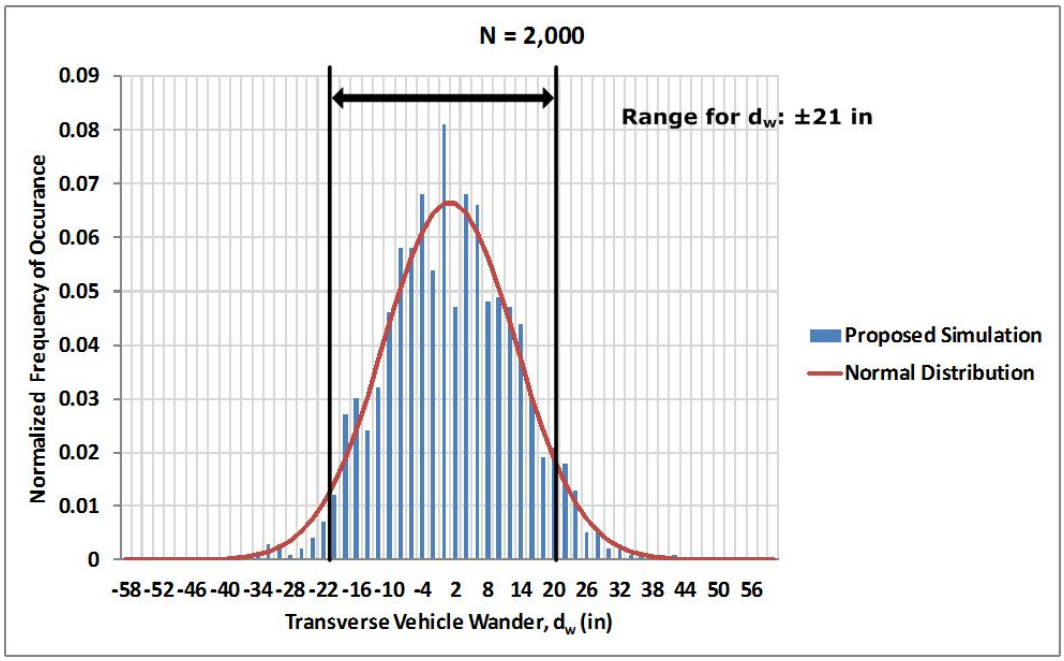

(a)

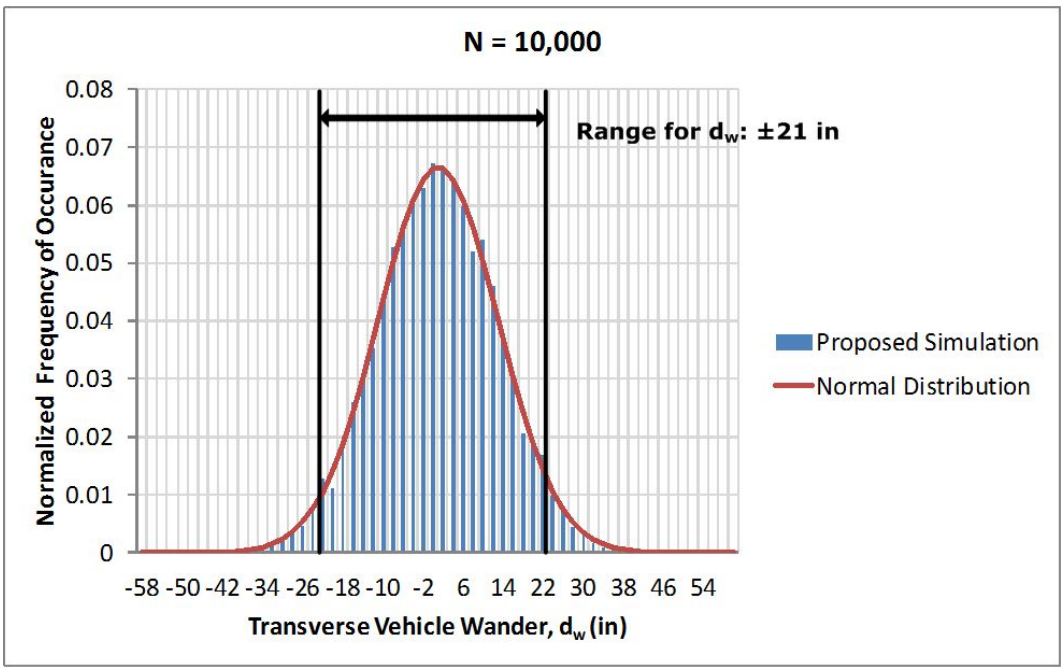

(b)

Fig. 3.7: Normalized Distribution of Wheel Wander with Number of Trails: (a) N=2000 and (b) N=10,000

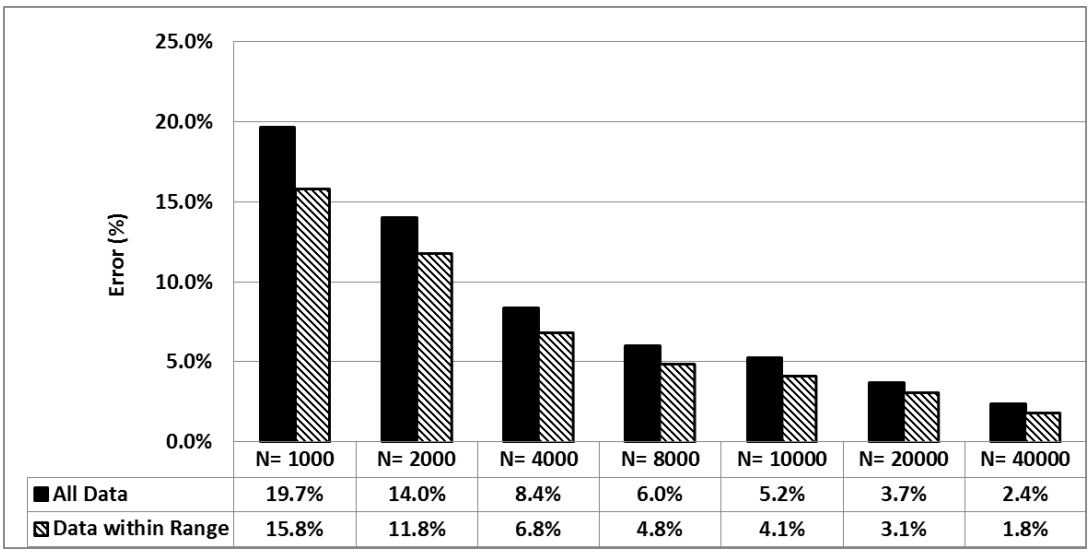

	N= 1000	N= 2000	N= 4000	N= 8000	N= 10000	N= 20000	N= 40000
All Data	19.7%	14.0%	8.4%	6.0%	5.2%	3.7%	2.4%
Data within Range	15.8%	11.8%	6.8%	4.8%	4.1%	3.1%	1.8%

Fig. 3.8: Difference between the Proposed Simulation and Normal Distribution

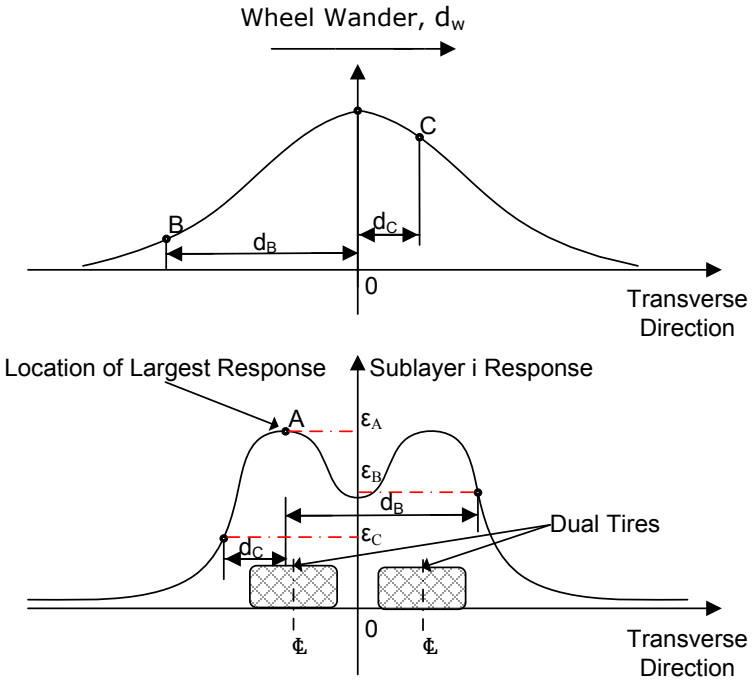

(a)

ε_C =Response at A with Center of wheel at C
ε_D =Response at A with Center of wheel at D

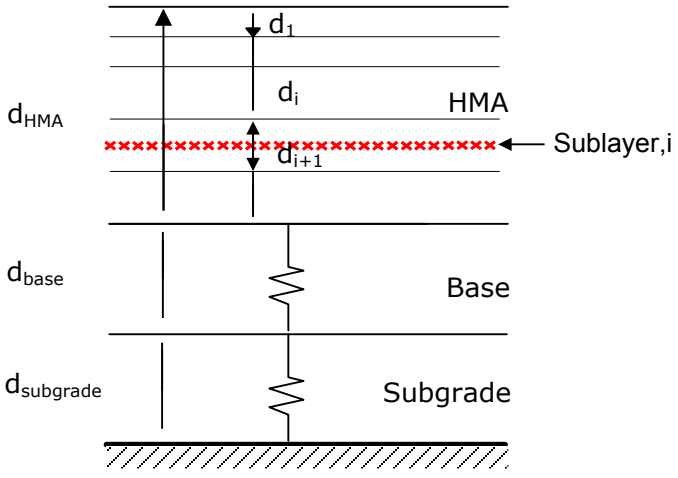

(b)

Fig. 3.9: Estimation of Pavement Response from Wheel Wander: (a) Pavement Surface Loading with Wheel Wander (b) Pavement Layer System

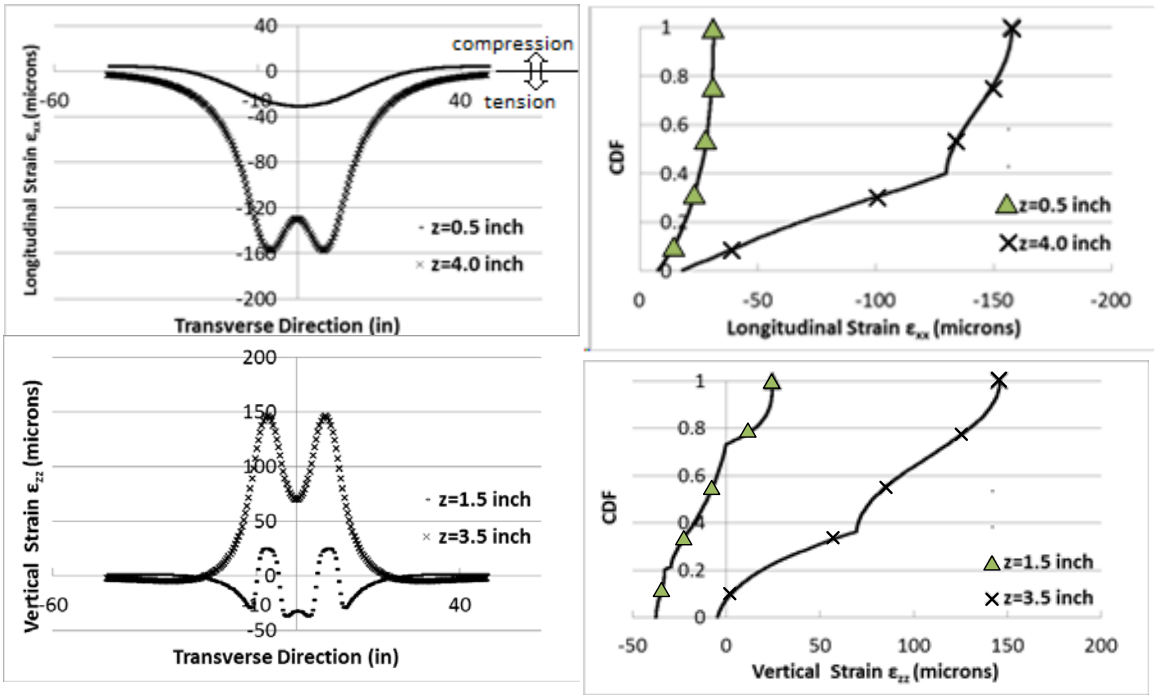

(a)

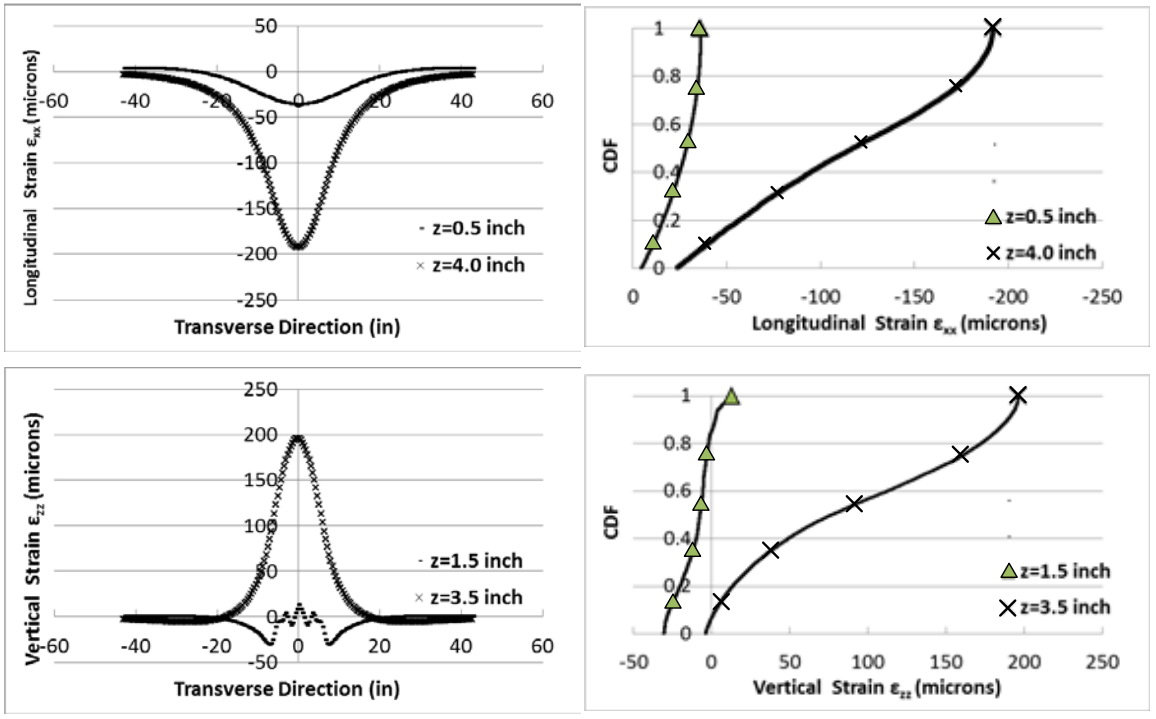

(b)

Fig.3.10: Thin Pavement (4 inch HMA Layer) Responses under: (a) Dual Tire (b) Wide-base Tire, and Corresponding Cumulative Distribution Functions (CDF)

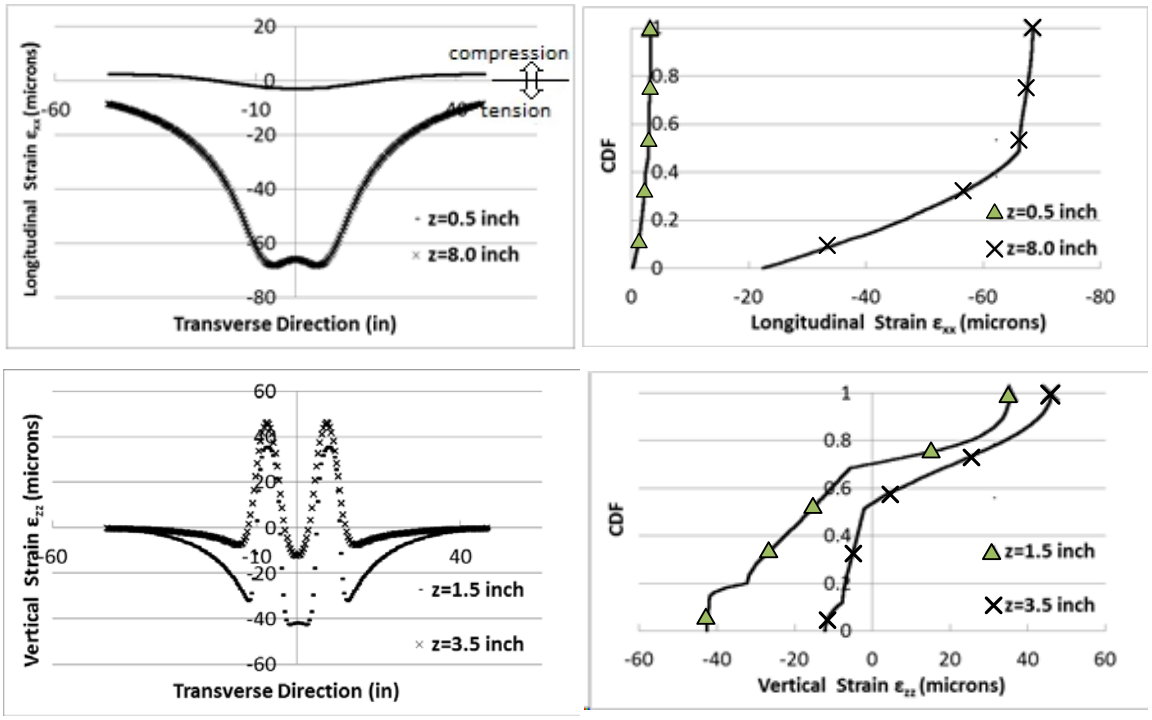

(a)

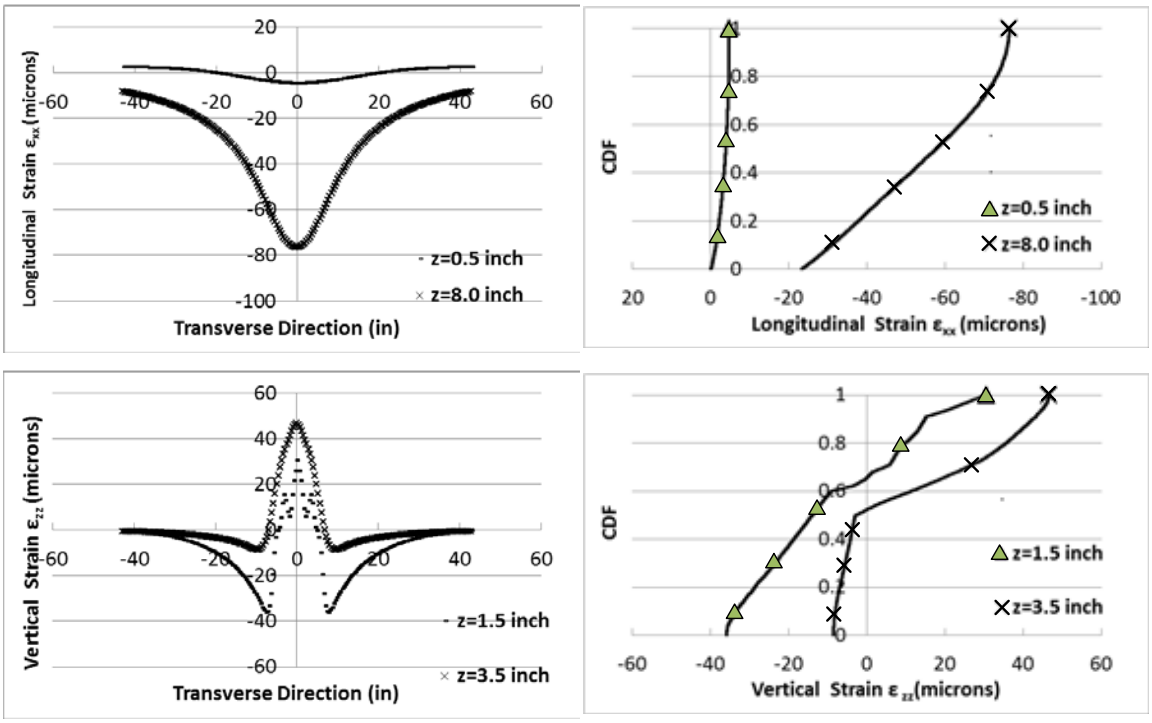

(b)

Fig.3.11: Thick Pavement (8 inch HMA Layer) Responses under: (a) Dual Tire (b) Wide-base Tire, and Corresponding Cumulative Distribution Function (CDF)

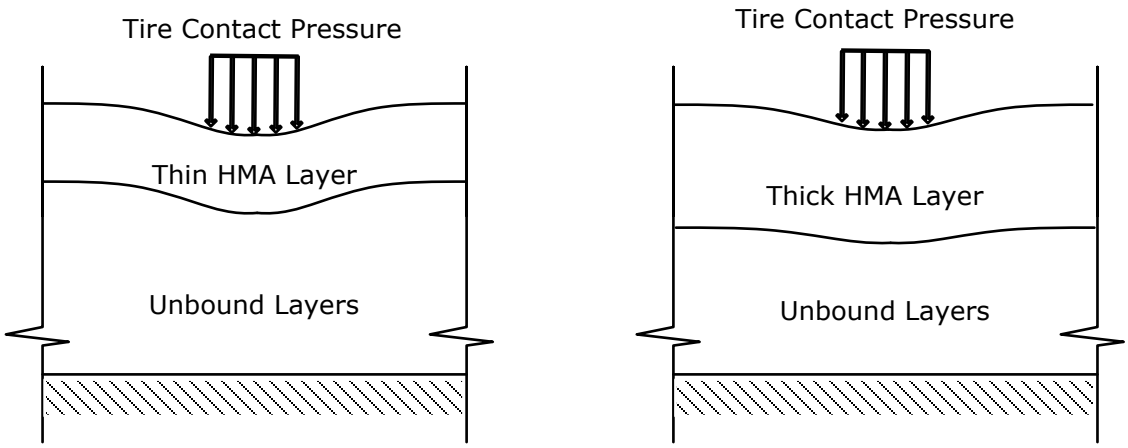

Fig. 3.12: Load Transfer in Thin and Thick Pavements

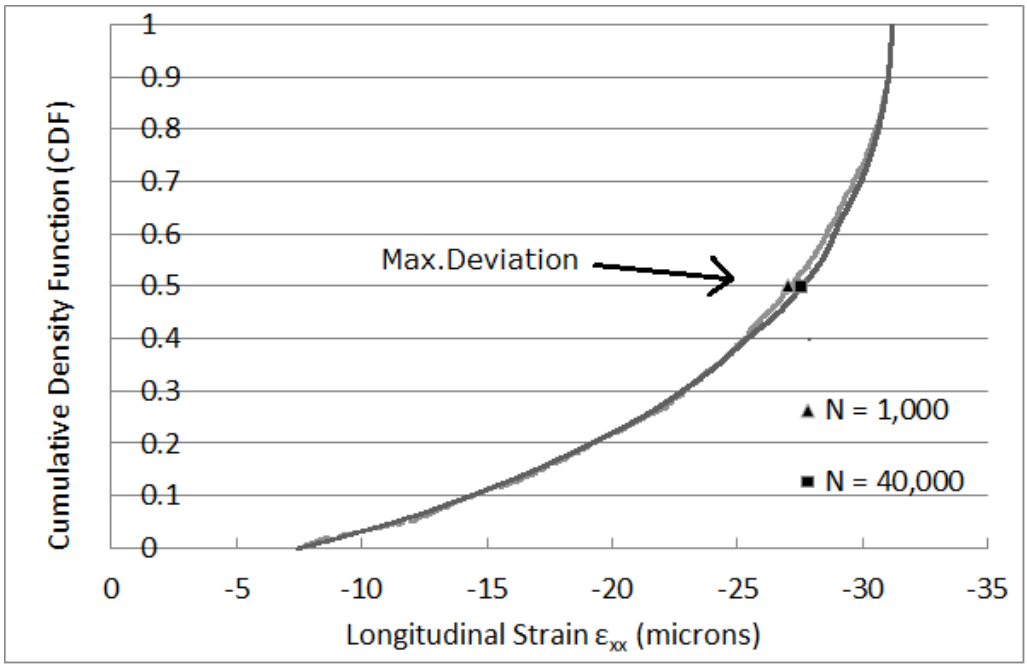

Fig.3.13: Difference in CDF of Longitudinal Strain ε_{xx} at a Depth of 0.5 inch for thin Pavement with Dual Tires (N=Number of Trials)

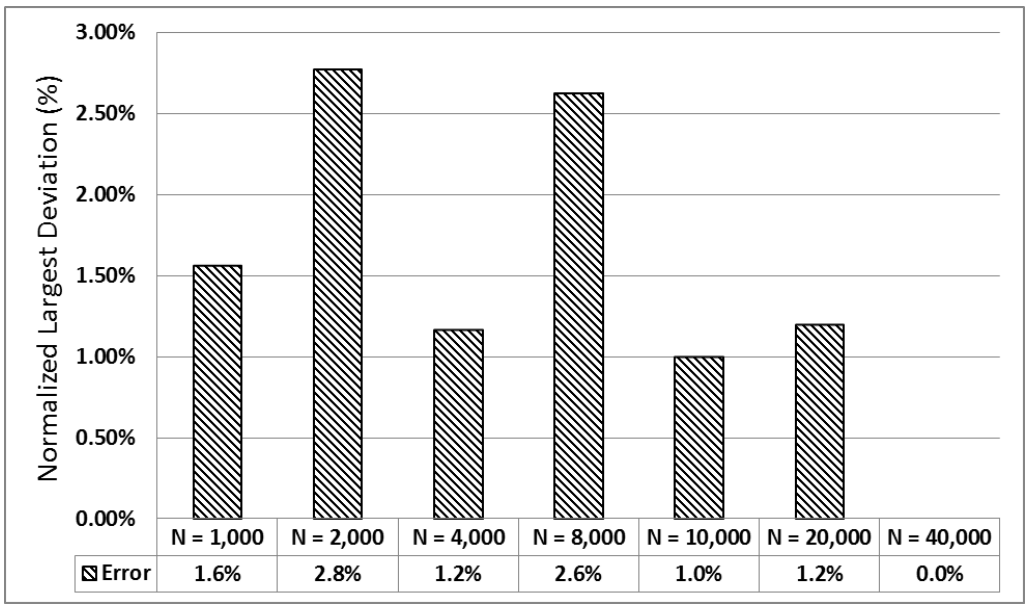

Fig.3.14: Normalized Deviation of Longitudinal Strain ε_{xx} with Number of Trails (N=Number of Trials)

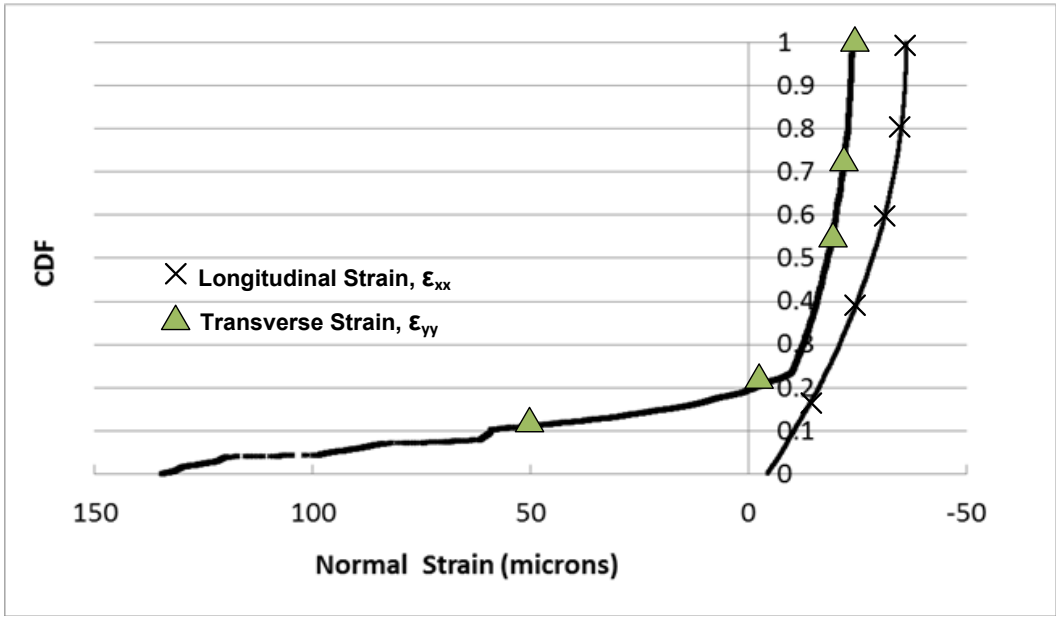

(a) z = 0.5inch

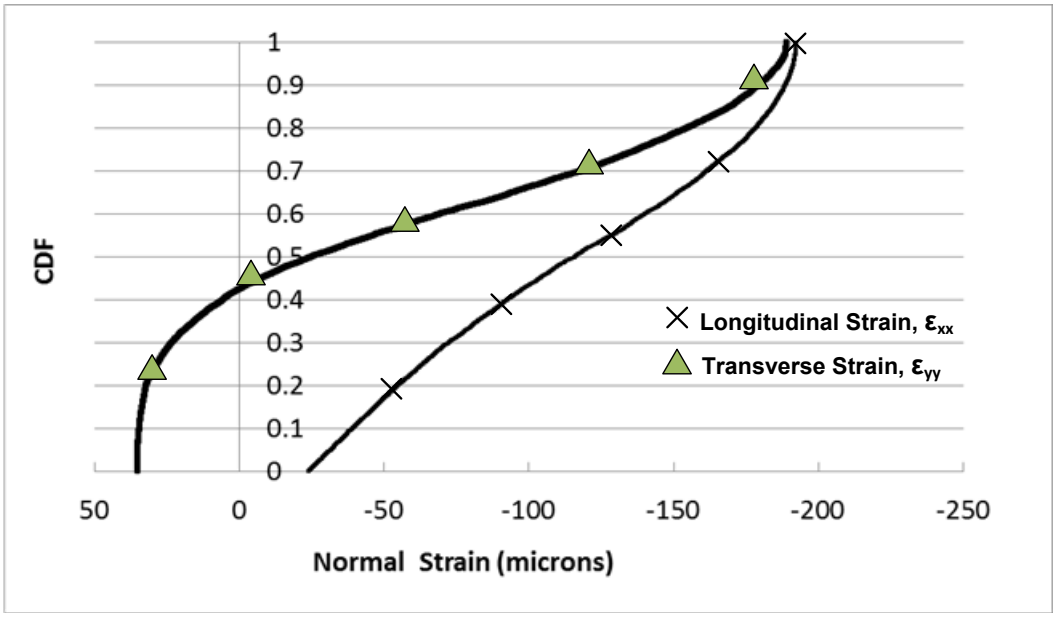

(b) z = 4.0inch

Fig. 3.15: CDFs of Normal Strains ε_{xx} and ε_{yy} for Wide-base Tire (GoodYear 425/65R22.5) with Conventional HMA Mixtures (PG64-22) at Two Depths (z = 0.5 and 4.0 inch)

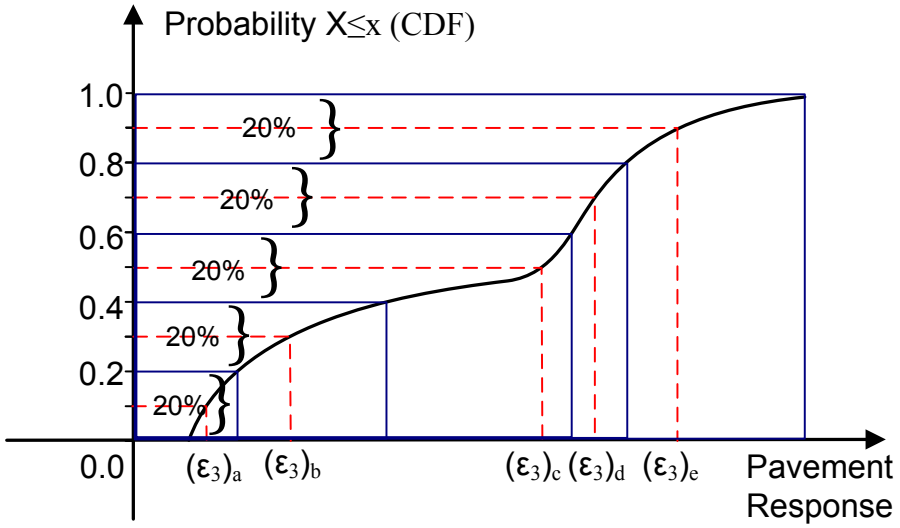

Fig.4.1: Division of CDF into Number of Equal Segments (Method 3)

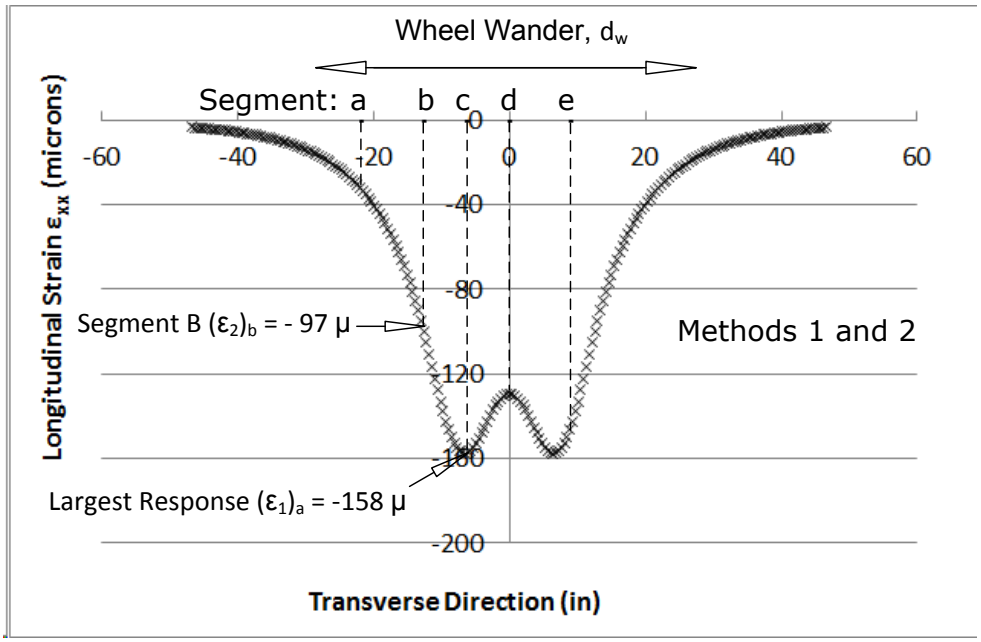

(a)

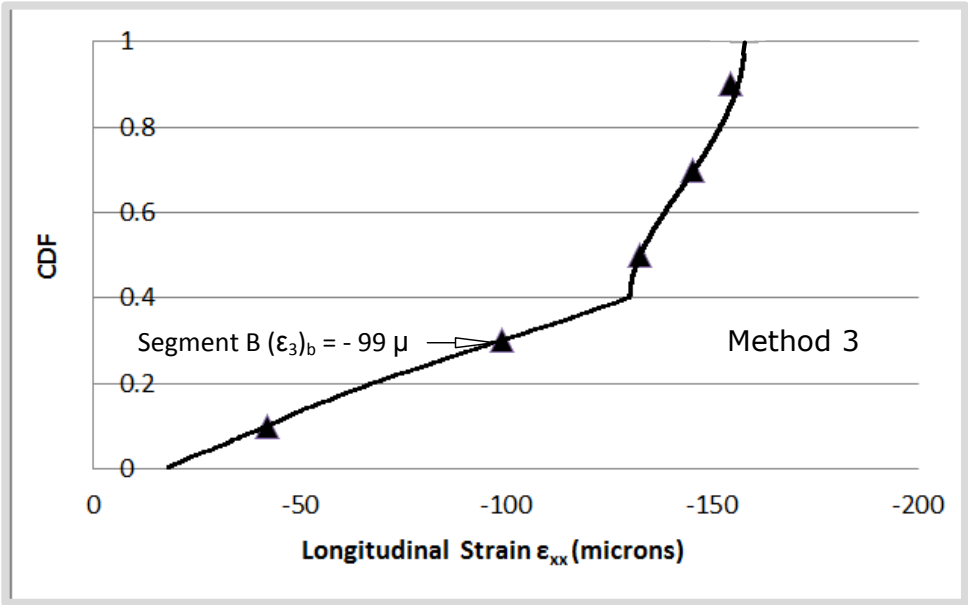

(b)

Fig. 4.2: Illustration of Various Methods used to Obtain Pavement Strain Response: (a) Methods 1 and 2; (b) Method 3

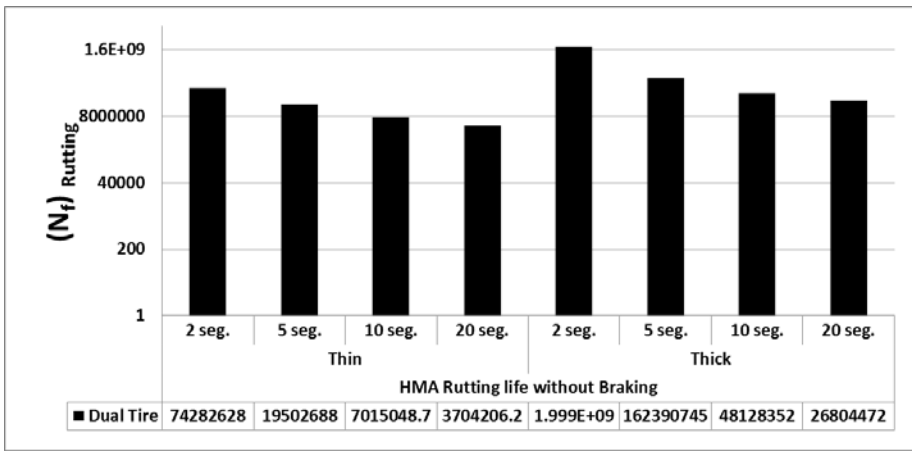

(a)

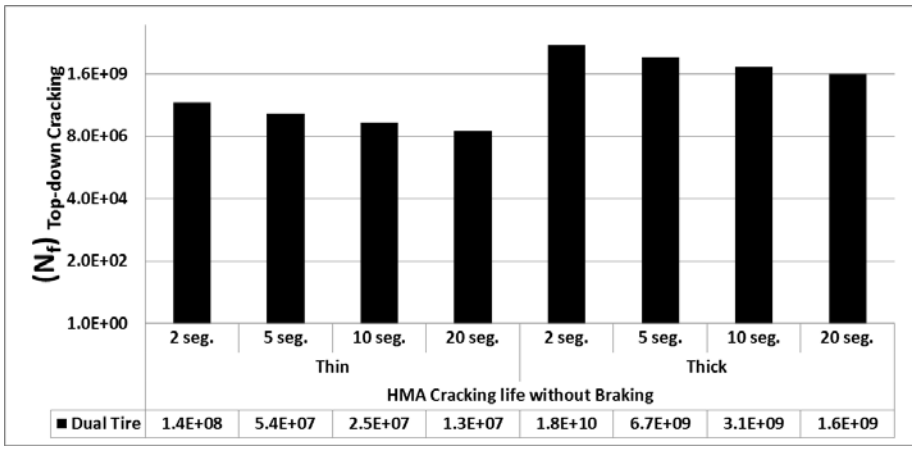

(b)

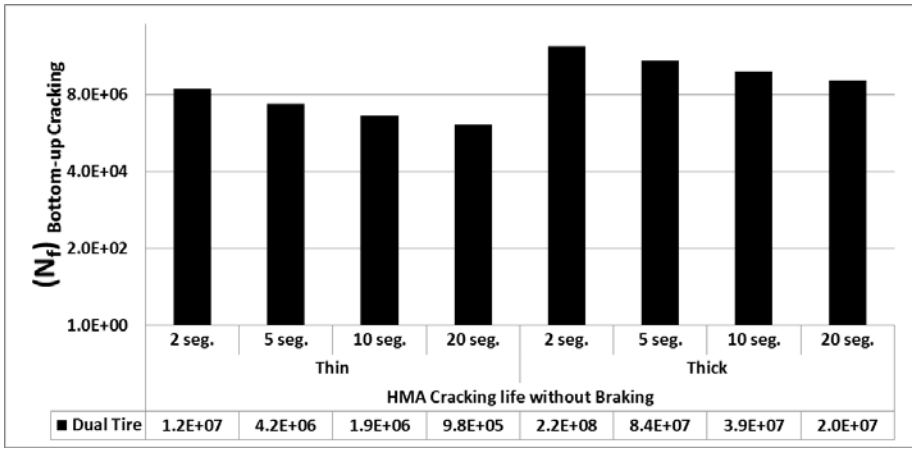

(c)

Fig. 4.3: Role of the Selection of Number of Segments on Pavement Life: (a) Rutting; (b) Top-down Cracking and (c) Bottom-up Cracking

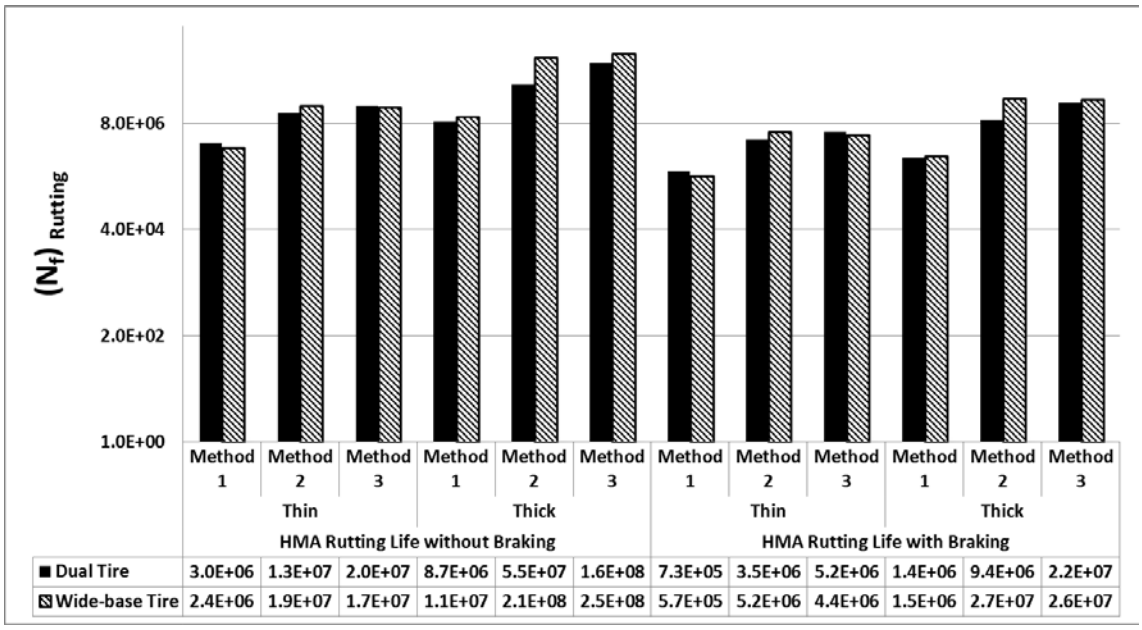

	Method 1	Method 2	Method 3	Method 1	Method 2	Method 3	Method 1	Method 2	Method 3	Method 1	Method 2	Method 3
	Thin			Thick			Thin			Thick		
	HMA Rutting Life without Braking						HMA Rutting Life with Braking					
Dual Tire	3.0E+06	1.3E+07	2.0E+07	8.7E+06	5.5E+07	1.6E+08	7.3E+05	3.5E+06	5.2E+06	1.4E+06	9.4E+06	2.2E+07
Wide-base Tire	2.4E+06	1.9E+07	1.7E+07	1.1E+07	2.1E+08	2.5E+08	5.7E+05	5.2E+06	4.4E+06	1.5E+06	2.7E+07	2.6E+07

(a)

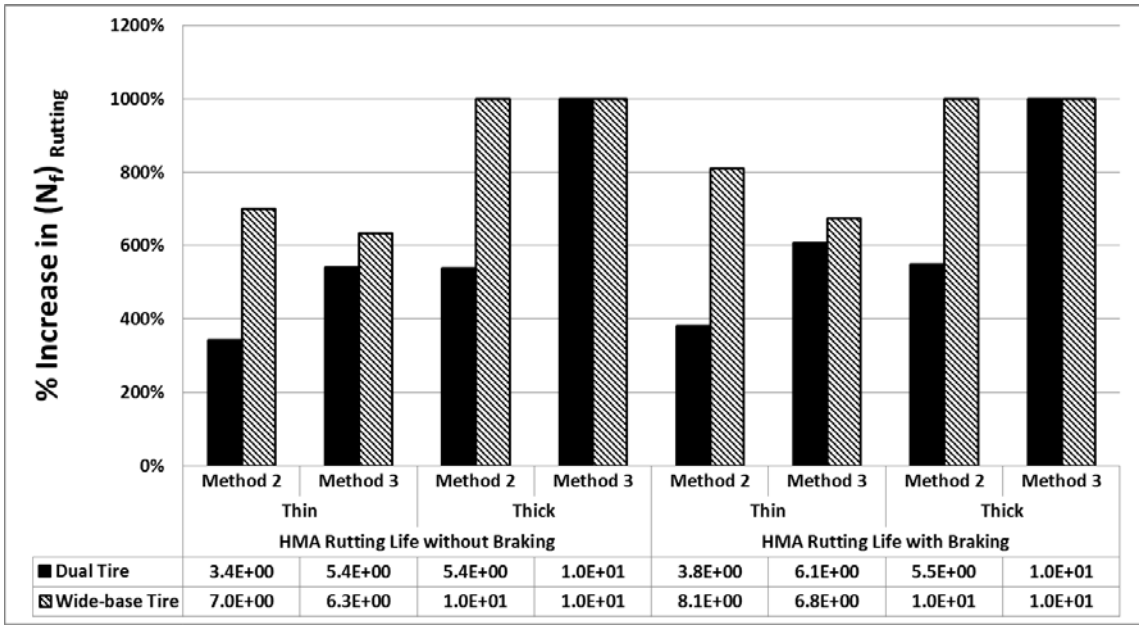

	Method 2	Method 3	Method 2	Method 3	Method 2	Method 3	Method 2	Method 3
	Thin		Thick		Thin		Thick	
	HMA Rutting Life without Braking				HMA Rutting Life with Braking			
Dual Tire	3.4E+00	5.4E+00	5.4E+00	1.0E+01	3.8E+00	6.1E+00	5.5E+00	1.0E+01
Wide-base Tire	7.0E+00	6.3E+00	1.0E+01	1.0E+01	8.1E+00	6.8E+00	1.0E+01	1.0E+01

(b)

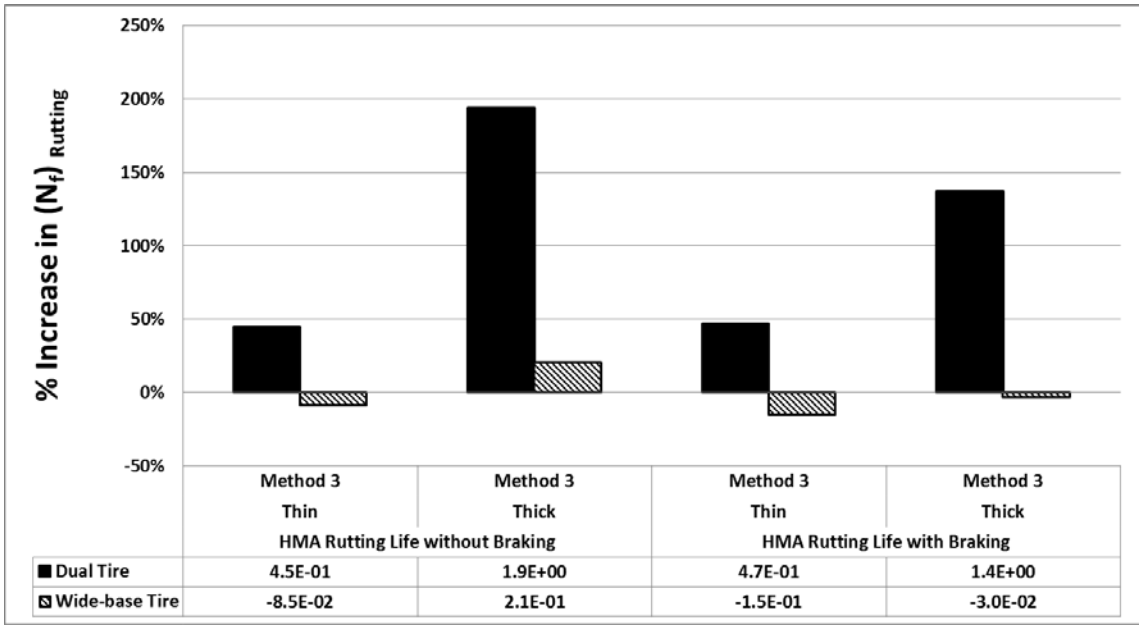

(c)

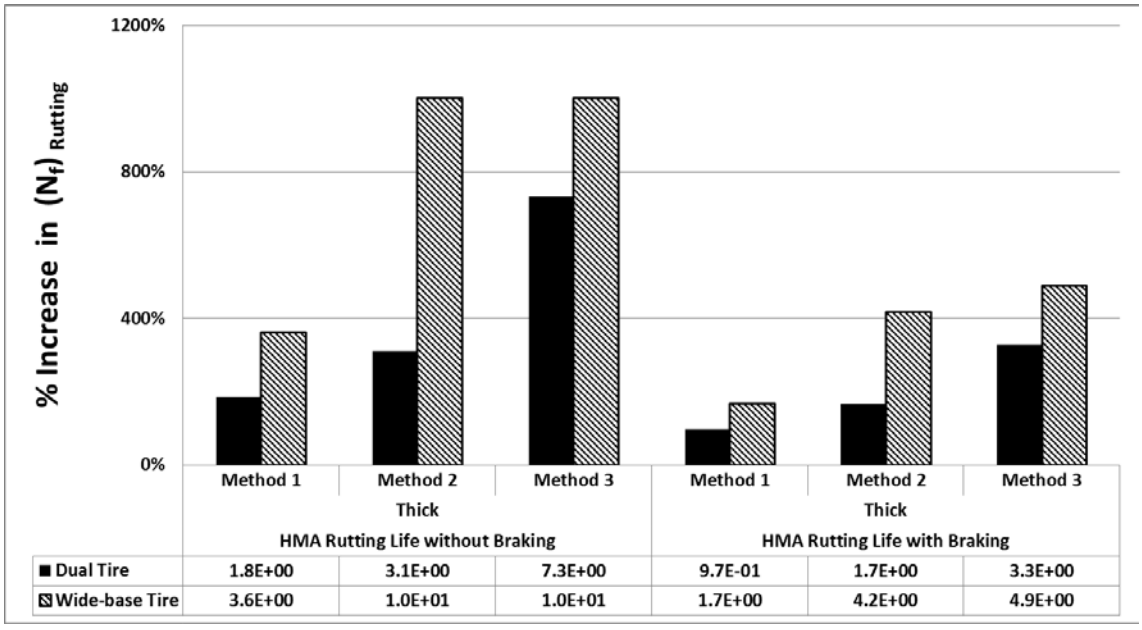

(d)

Fig. 4.4: PG64-22, 70°F, HMA Rutting Failure Cycle for 0.5 Inches Rut Depth: (a) Predicted (b) Percentage of Increase of Predictions Using Method 2 and Method 3 Based on Method 1 (c) Percentage of Increase of Predictions Using Method 3 Based on Method 2 (d) Percentage of Increase of Predictions Using Thick Pavement Based on Thin Pavement

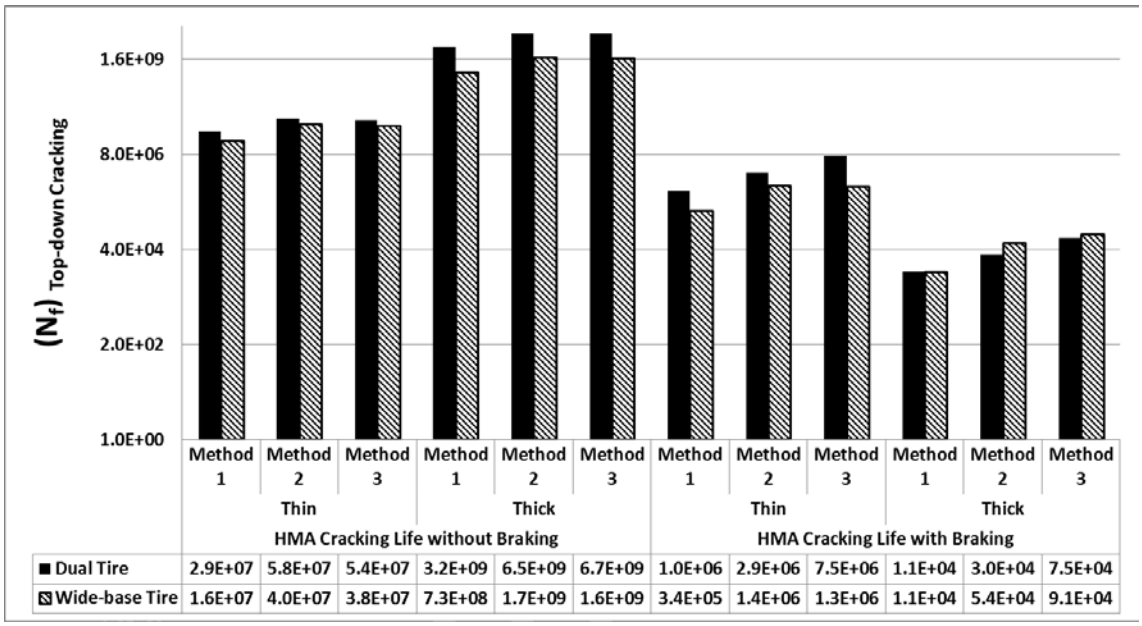

	Method 1	Method 2	Method 3	Method 1	Method 2	Method 3	Method 1	Method 2	Method 3	Method 1	Method 2	Method 3
	Thin			Thick			Thin			Thick		
	HMA Cracking Life without Braking						HMA Cracking Life with Braking					
Dual Tire	2.9E+07	5.8E+07	5.4E+07	3.2E+09	6.5E+09	6.7E+09	1.0E+06	2.9E+06	7.5E+06	1.1E+04	3.0E+04	7.5E+04
Wide-base Tire	1.6E+07	4.0E+07	3.8E+07	7.3E+08	1.7E+09	1.6E+09	3.4E+05	1.4E+06	1.3E+06	1.1E+04	5.4E+04	9.1E+04

(a)

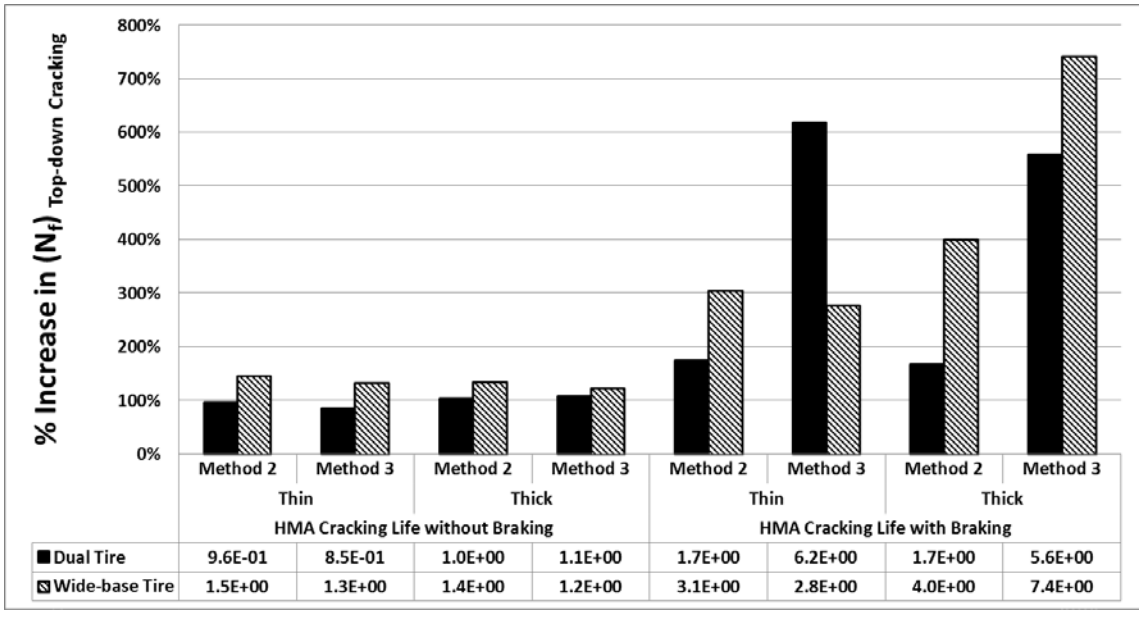

	Method 2	Method 3	Method 2	Method 3	Method 2	Method 3	Method 2	Method 3
	Thin		Thick		Thin		Thick	
	HMA Cracking Life without Braking				HMA Cracking Life with Braking			
Dual Tire	9.6E-01	8.5E-01	1.0E+00	1.1E+00	1.7E+00	6.2E+00	1.7E+00	5.6E+00
Wide-base Tire	1.5E+00	1.3E+00	1.4E+00	1.2E+00	3.1E+00	2.8E+00	4.0E+00	7.4E+00

(b)

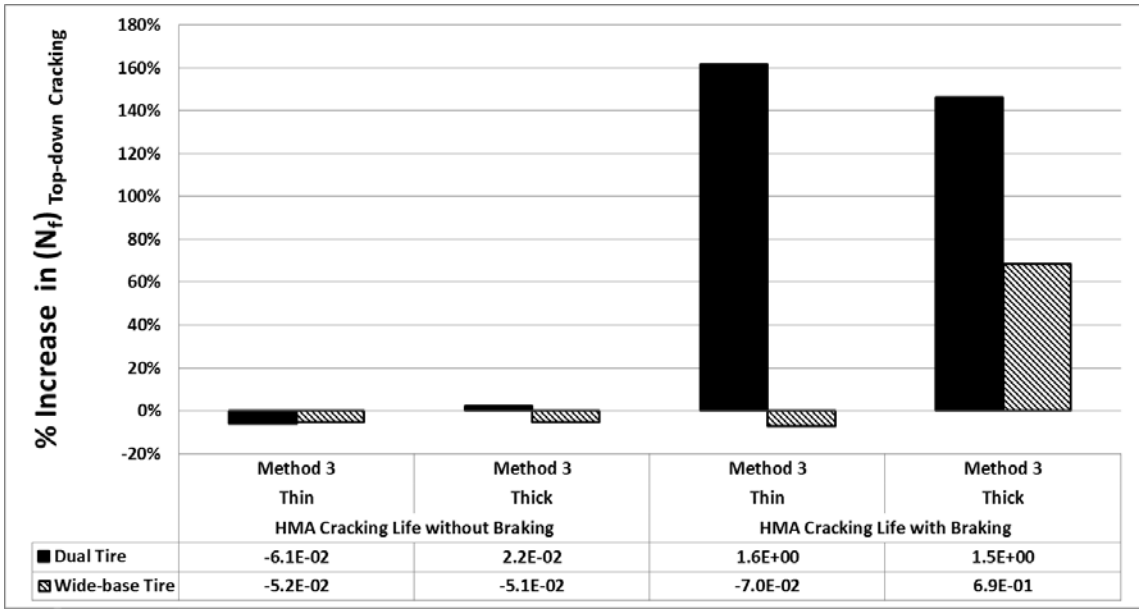

(c)

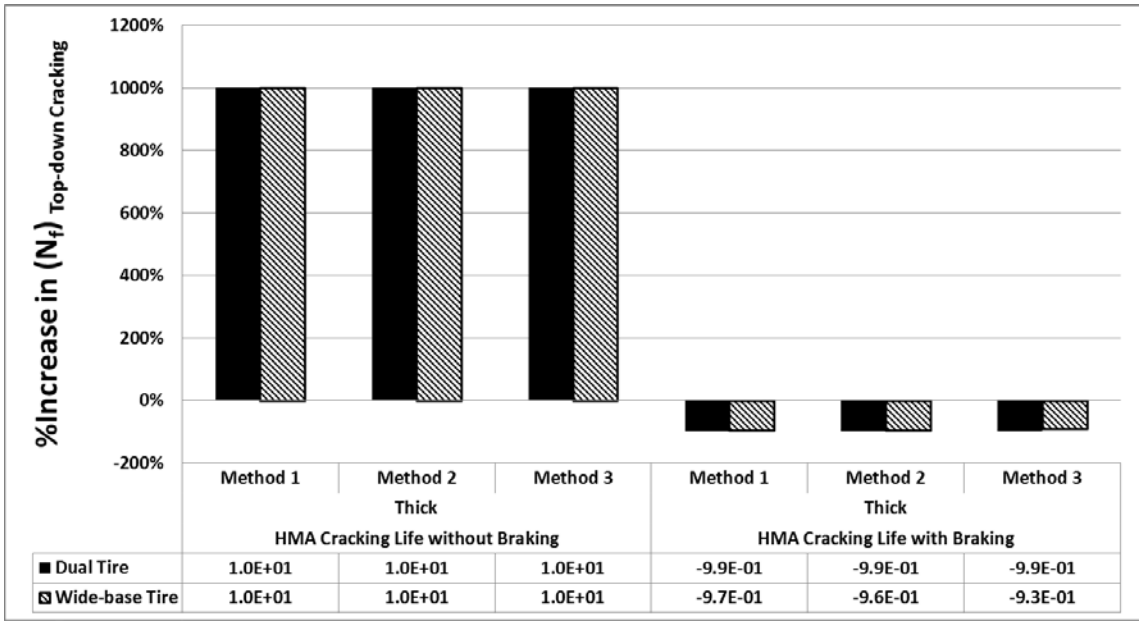

(d)

Fig. 4.5: PG64-22, 70°F, HMA top-down cracking life: (a) Predicted (b) Percentage of Increase of Predictions Using Method 2 and Method 3 Based on Method 1 (c) Percentage of Increase of Predictions Using Method 3 Based on Method 2 (d) Percentage of Increase of Predictions Using Thick Pavement Based on Thin Pavement

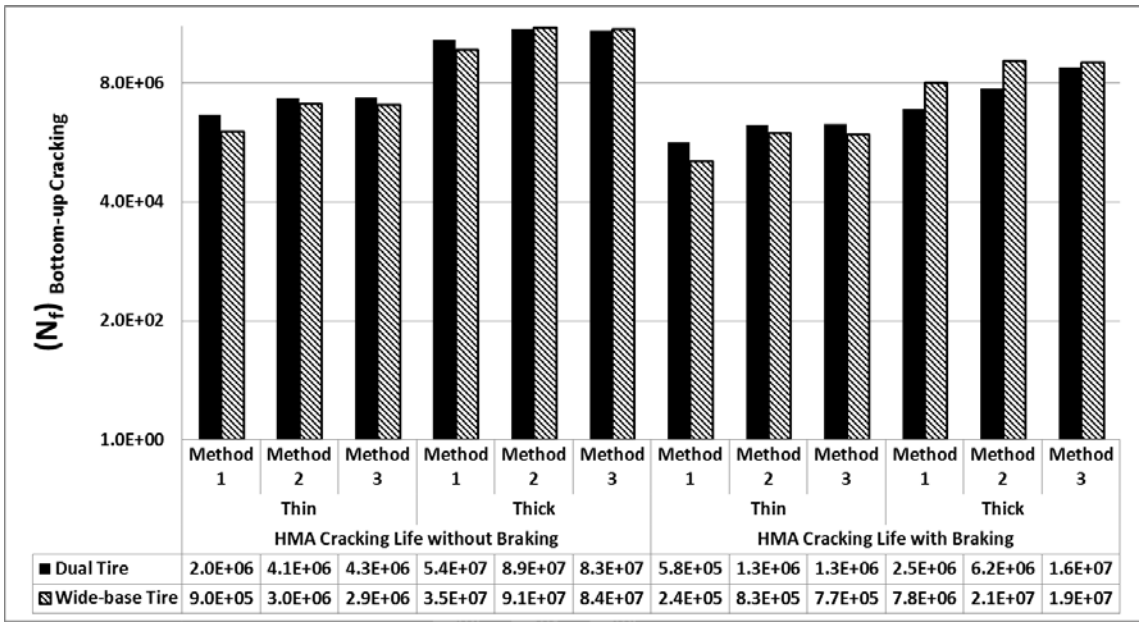

	Thin, HMA Cracking Life without Braking			Thick, HMA Cracking Life without Braking			Thin, HMA Cracking Life with Braking			Thick, HMA Cracking Life with Braking		
	Method 1	Method 2	Method 3	Method 1	Method 2	Method 3	Method 1	Method 2	Method 3	Method 1	Method 2	Method 3
Dual Tire	2.0E+06	4.1E+06	4.3E+06	5.4E+07	8.9E+07	8.3E+07	5.8E+05	1.3E+06	1.3E+06	2.5E+06	6.2E+06	1.6E+07
Wide-base Tire	9.0E+05	3.0E+06	2.9E+06	3.5E+07	9.1E+07	8.4E+07	2.4E+05	8.3E+05	7.7E+05	7.8E+06	2.1E+07	1.9E+07

(a)

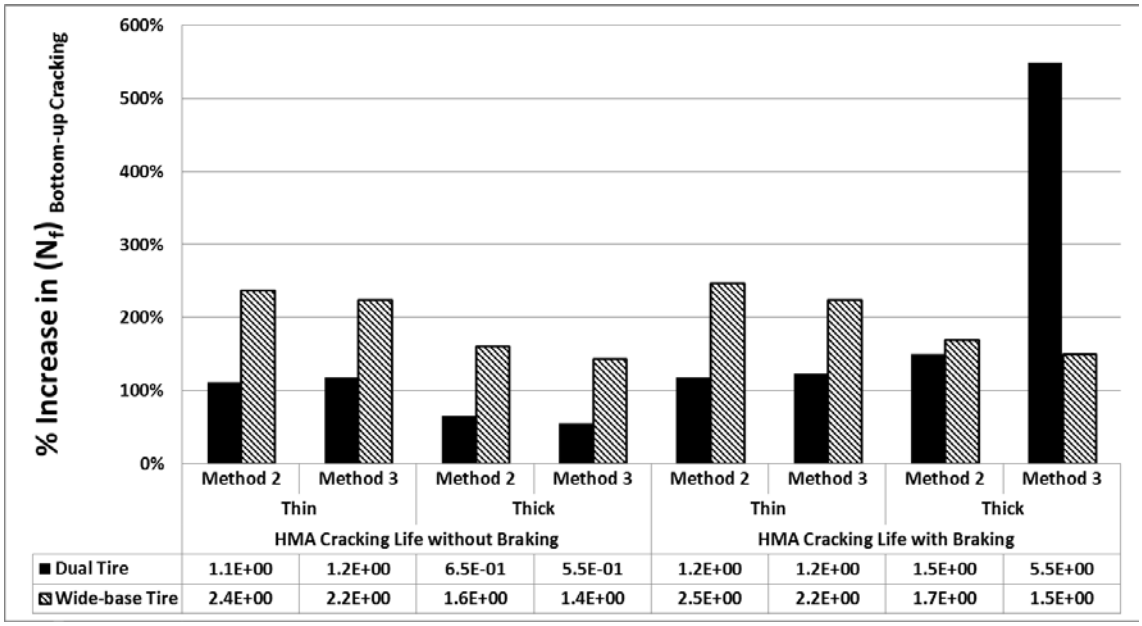

	Thin, HMA Cracking Life without Braking		Thick, HMA Cracking Life without Braking		Thin, HMA Cracking Life with Braking		Thick, HMA Cracking Life with Braking	
	Method 2	Method 3	Method 2	Method 3	Method 2	Method 3	Method 2	Method 3
Dual Tire	1.1E+00	1.2E+00	6.5E-01	5.5E-01	1.2E+00	1.2E+00	1.5E+00	5.5E+00
Wide-base Tire	2.4E+00	2.2E+00	1.6E+00	1.4E+00	2.5E+00	2.2E+00	1.7E+00	1.5E+00

(b)

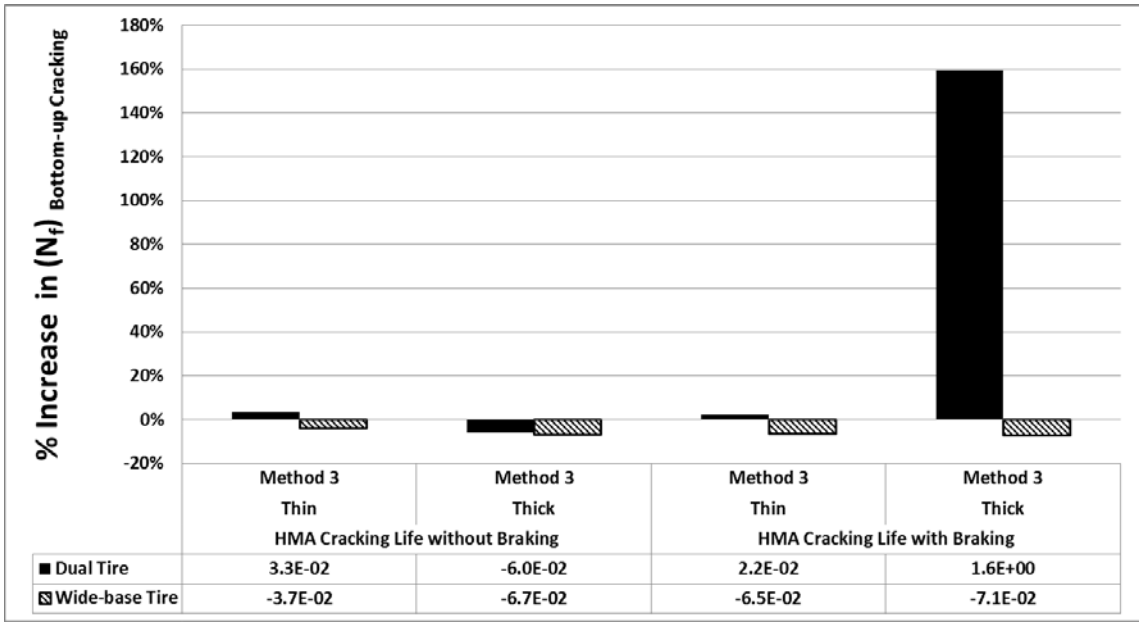

(c)

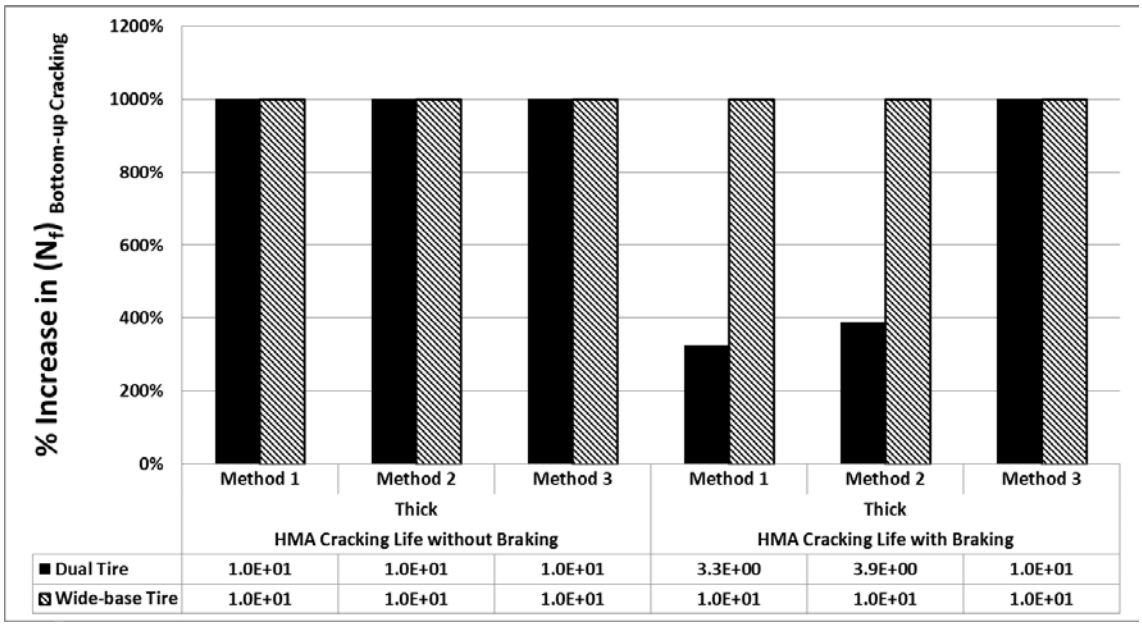

(d)

Fig. 4.6: PG64-22, 70°F, HMA bottom-up cracking life: (a) Predicted (b) Percentage of Increase of Predictions Using Method 2 and Method 3 Based on Method 1 (c) Percentage of Increase of Predictions Using Method 3 Based on Method 2 (d) Percentage of Increase of Predictions Using Thick Pavement Based on Thin Pavement

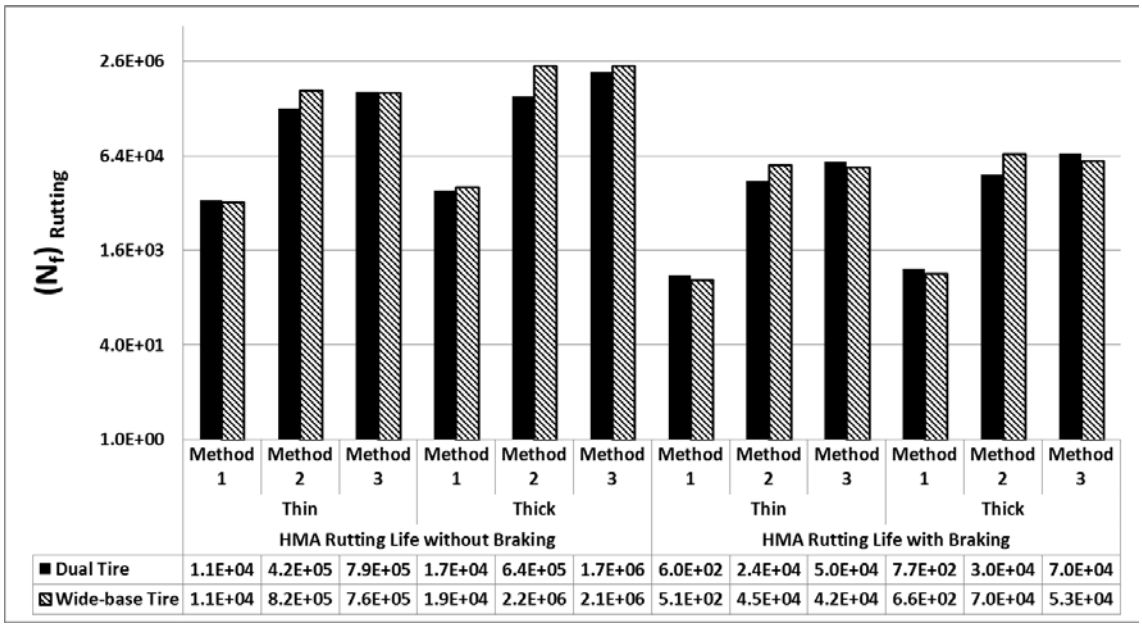

	Method 1	Method 2	Method 3	Method 1	Method 2	Method 3	Method 1	Method 2	Method 3	Method 1	Method 2	Method 3
	Thin			Thick			Thin			Thick		
	HMA Rutting Life without Braking						HMA Rutting Life with Braking					
Dual Tire	1.1E+04	4.2E+05	7.9E+05	1.7E+04	6.4E+05	1.7E+06	6.0E+02	2.4E+04	5.0E+04	7.7E+02	3.0E+04	7.0E+04
Wide-base Tire	1.1E+04	8.2E+05	7.6E+05	1.9E+04	2.2E+06	2.1E+06	5.1E+02	4.5E+04	4.2E+04	6.6E+02	7.0E+04	5.3E+04

(a)

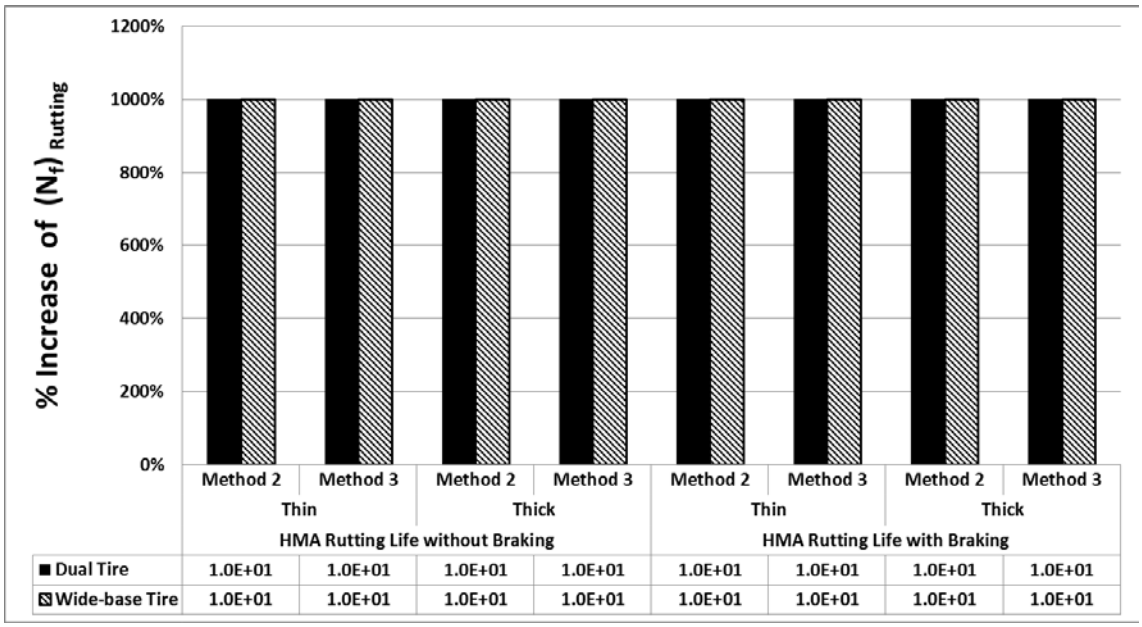

	Method 2	Method 3	Method 2	Method 3	Method 2	Method 3	Method 2	Method 3
	Thin		Thick		Thin		Thick	
	HMA Rutting Life without Braking				HMA Rutting Life with Braking			
Dual Tire	1.0E+01	1.0E+01	1.0E+01	1.0E+01	1.0E+01	1.0E+01	1.0E+01	1.0E+01
Wide-base Tire	1.0E+01	1.0E+01	1.0E+01	1.0E+01	1.0E+01	1.0E+01	1.0E+01	1.0E+01

(b)

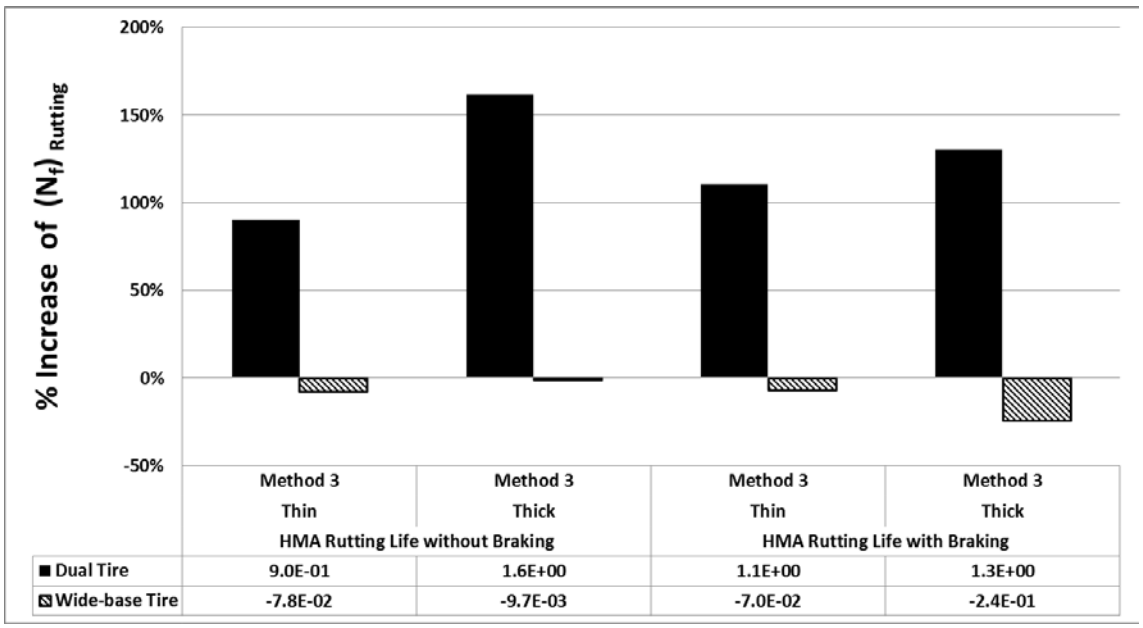

(c)

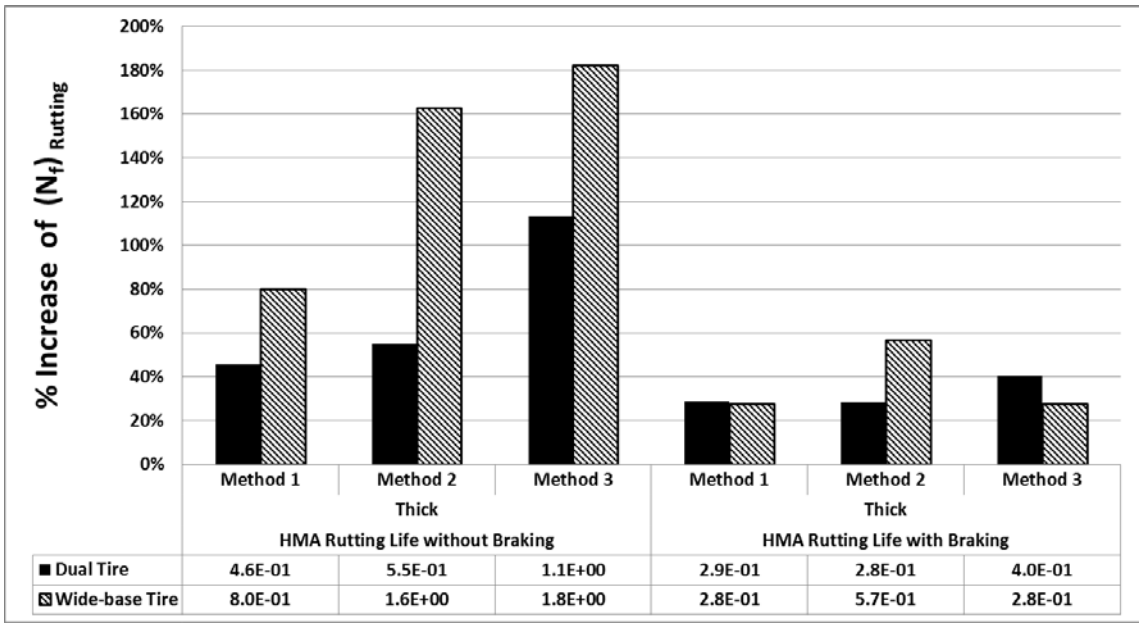

(d)

Fig. 4.7: PG64-22, 104°F, HMA Rutting Failure Cycle for 0.5 Inches Rut Depth: (a) Predicted (b) Percentage of Increase of Predictions Using Method 2 and Method 3 Based on Method 1 (c) Percentage of Increase of Predictions Using Method 3 Based on Method 2 (d) Percentage of Increase of Predictions Using Thick Pavement Based on Thin Pavement

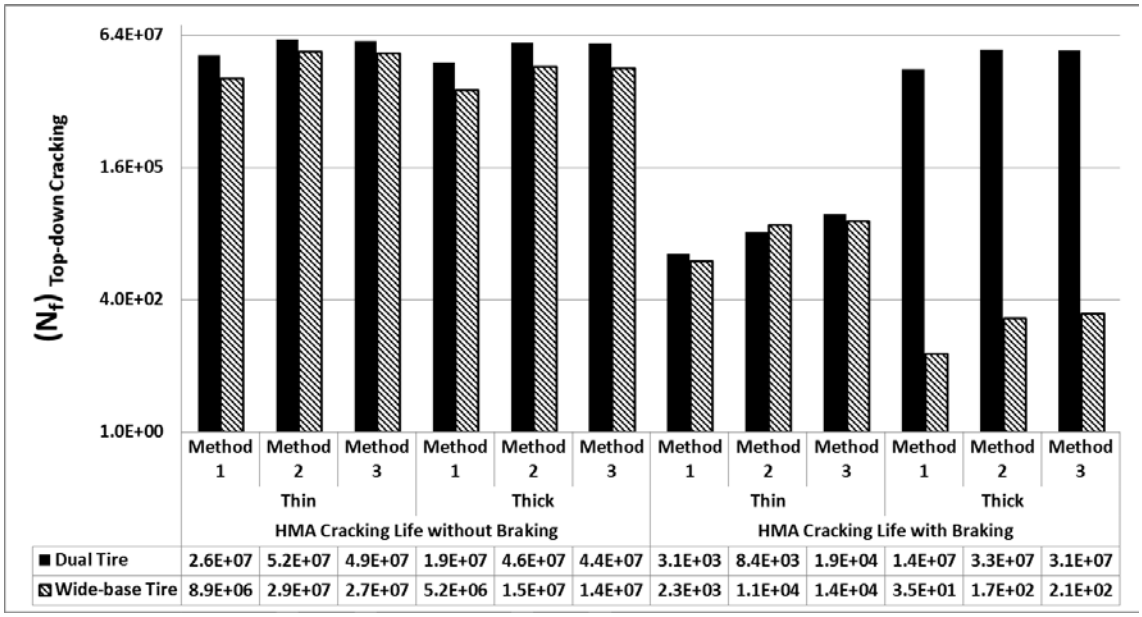

	Thin			Thick			Thin			Thick		
	Method 1	Method 2	Method 3	Method 1	Method 2	Method 3	Method 1	Method 2	Method 3	Method 1	Method 2	Method 3
	HMA Cracking Life without Braking						HMA Cracking Life with Braking					
Dual Tire	2.6E+07	5.2E+07	4.9E+07	1.9E+07	4.6E+07	4.4E+07	3.1E+03	8.4E+03	1.9E+04	1.4E+07	3.3E+07	3.1E+07
Wide-base Tire	8.9E+06	2.9E+07	2.7E+07	5.2E+06	1.5E+07	1.4E+07	2.3E+03	1.1E+04	1.4E+04	3.5E+01	1.7E+02	2.1E+02

(a)

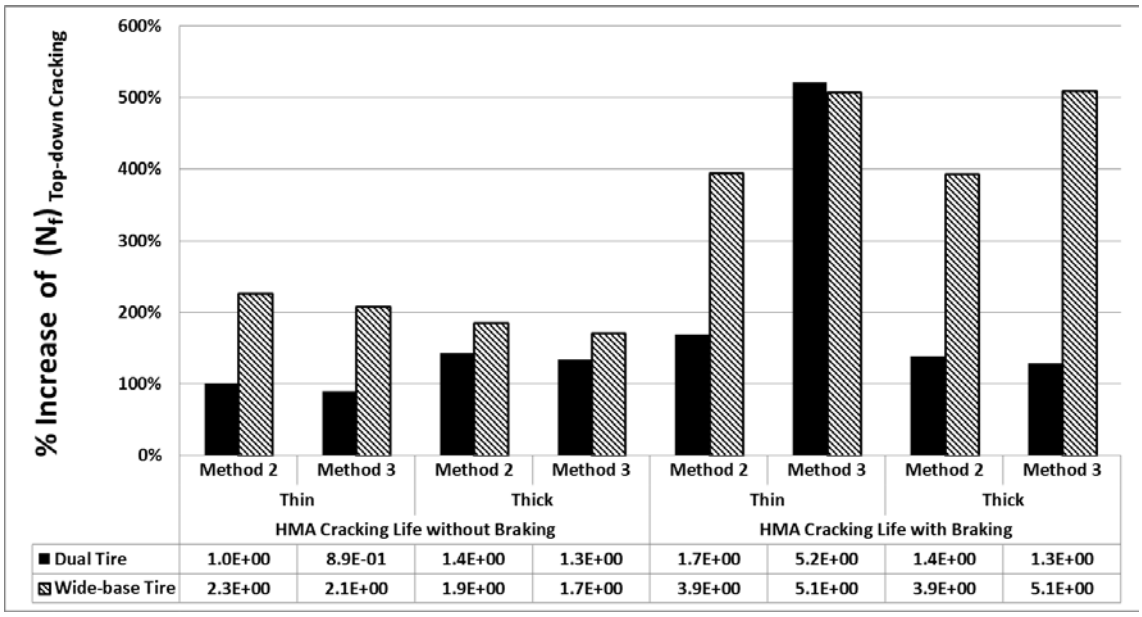

	Thin		Thick		Thin		Thick	
	Method 2	Method 3	Method 2	Method 3	Method 2	Method 3	Method 2	Method 3
	HMA Cracking Life without Braking				HMA Cracking Life with Braking			
Dual Tire	1.0E+00	8.9E-01	1.4E+00	1.3E+00	1.7E+00	5.2E+00	1.4E+00	1.3E+00
Wide-base Tire	2.3E+00	2.1E+00	1.9E+00	1.7E+00	3.9E+00	5.1E+00	3.9E+00	5.1E+00

(b)

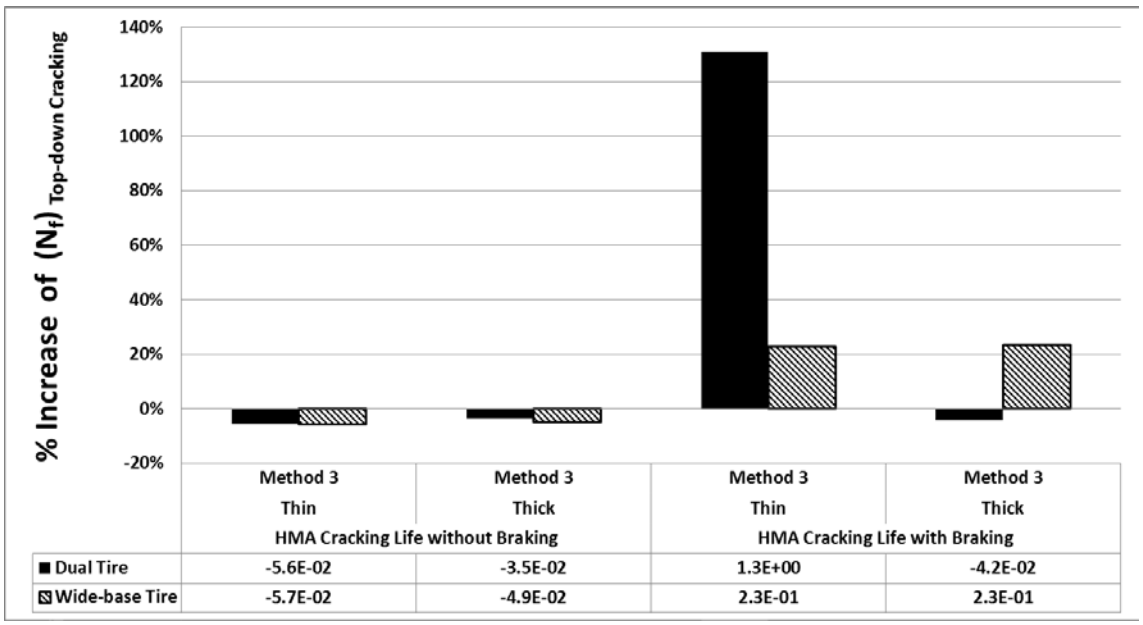

(c)

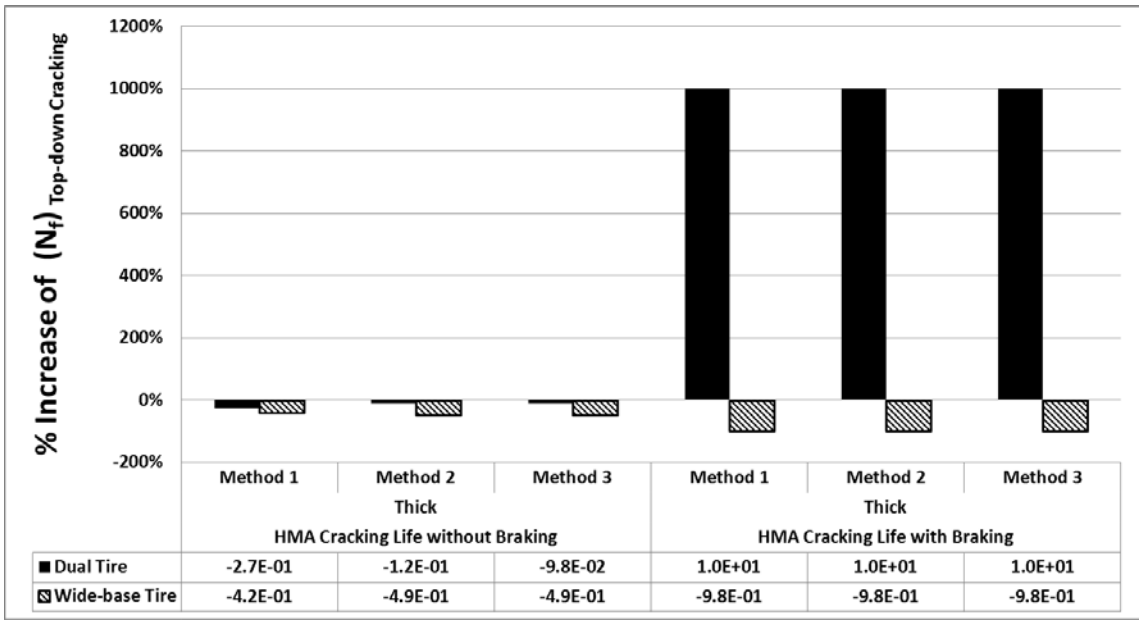

(d)

Fig. 4.8: PG64-22, 104°F, HMA top-down cracking life: (a) Predicted (b) Percentage of Increase of Predictions Using Method 2 and Method 3 Based on Method 1 (c) Percentage of Increase of Predictions Using Method 3 Based on Method 2 (d) Percentage of Increase of Predictions Using Thick Pavement Based on Thin Pavement

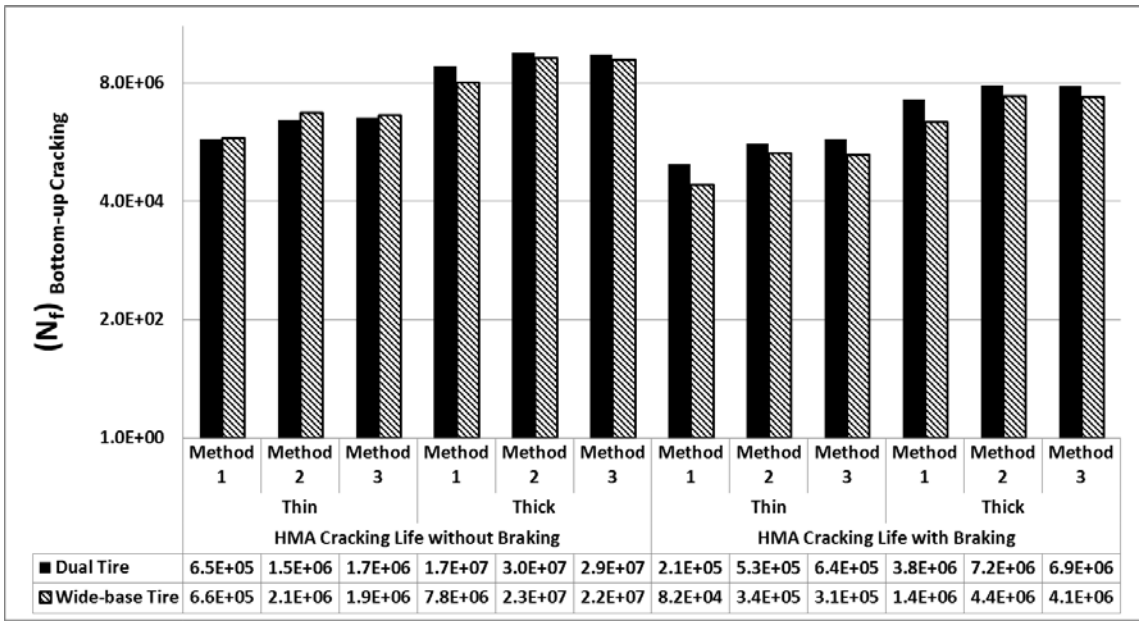

	Thin			Thick			Thin			Thick		
	Method 1	Method 2	Method 3	Method 1	Method 2	Method 3	Method 1	Method 2	Method 3	Method 1	Method 2	Method 3
	HMA Cracking Life without Braking						HMA Cracking Life with Braking					
Dual Tire	6.5E+05	1.5E+06	1.7E+06	1.7E+07	3.0E+07	2.9E+07	2.1E+05	5.3E+05	6.4E+05	3.8E+06	7.2E+06	6.9E+06
Wide-base Tire	6.6E+05	2.1E+06	1.9E+06	7.8E+06	2.3E+07	2.2E+07	8.2E+04	3.4E+05	3.1E+05	1.4E+06	4.4E+06	4.1E+06

(a)

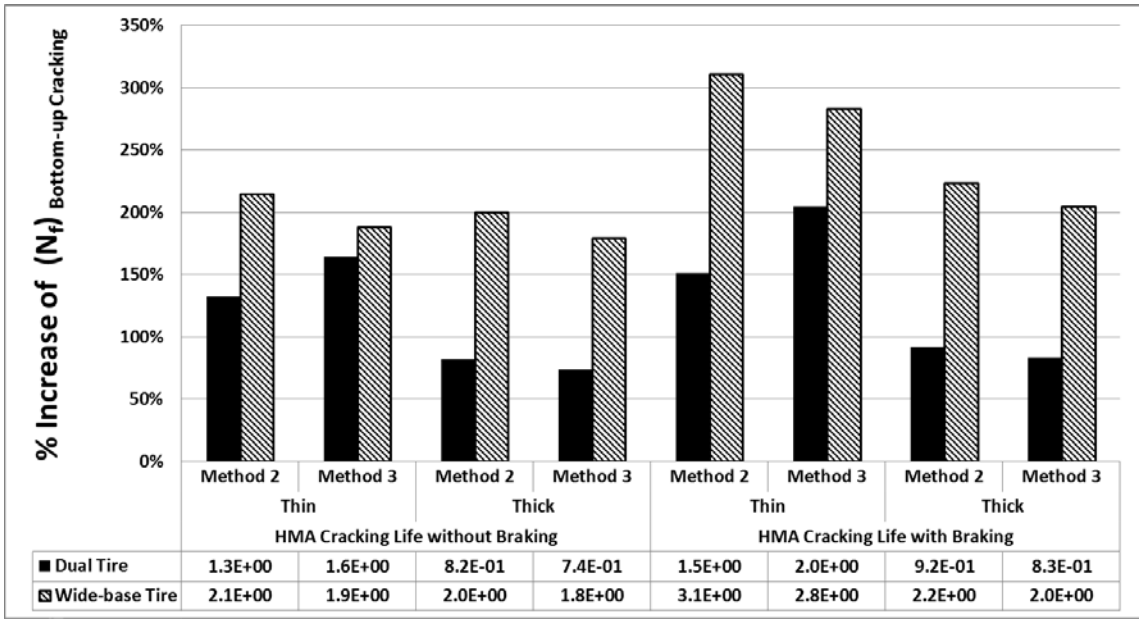

	Thin		Thick		Thin		Thick	
	Method 2	Method 3	Method 2	Method 3	Method 2	Method 3	Method 2	Method 3
	HMA Cracking Life without Braking				HMA Cracking Life with Braking			
Dual Tire	1.3E+00	1.6E+00	8.2E-01	7.4E-01	1.5E+00	2.0E+00	9.2E-01	8.3E-01
Wide-base Tire	2.1E+00	1.9E+00	2.0E+00	1.8E+00	3.1E+00	2.8E+00	2.2E+00	2.0E+00

(b)

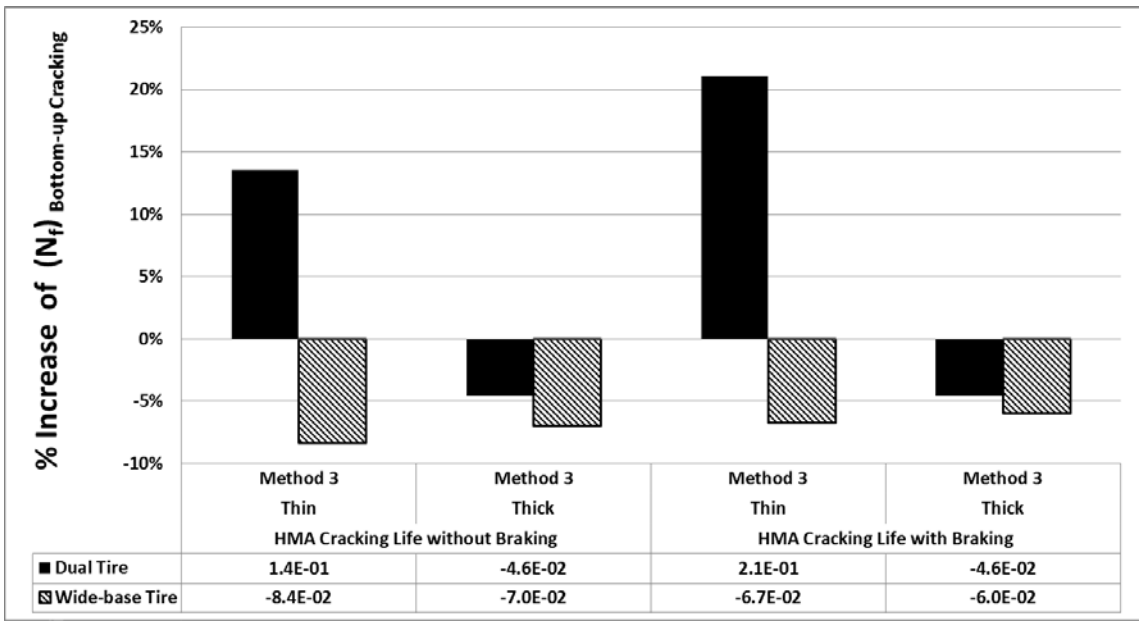

(c)

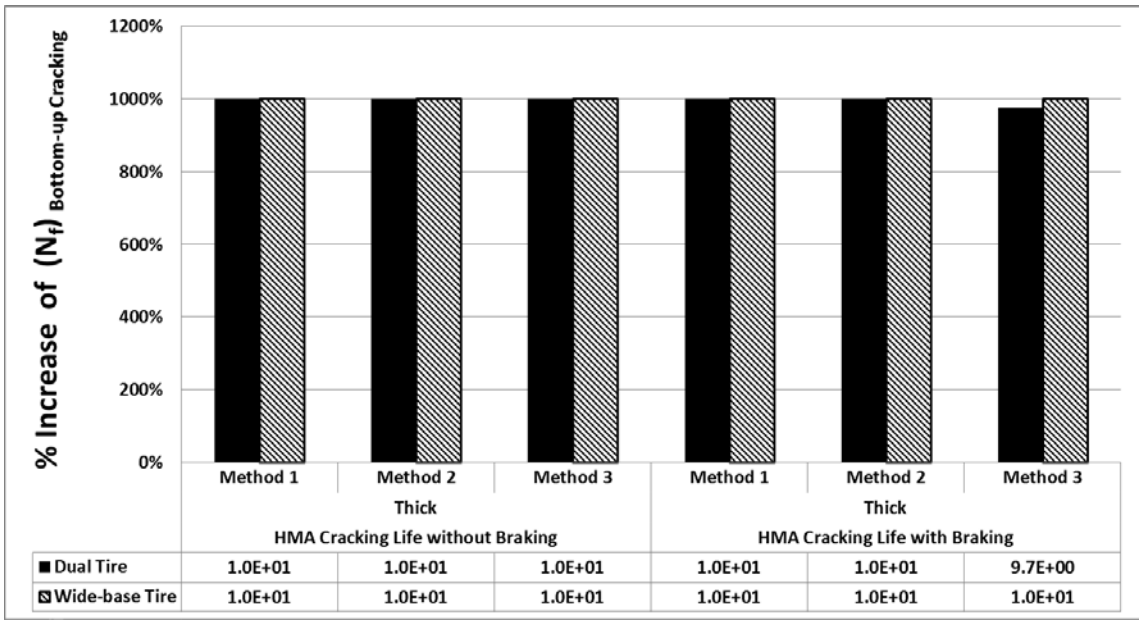

(d)

Fig. 4.9: PG64-22, 104°F, HMA bottom-up cracking life: (a) Predicted (b) Percentage of Increase of Predictions Using Method 2 and Method 3 Based on Method 1 (c) Percentage of Increase of Predictions Using Method 3 Based on Method 2 (d) Percentage of Increase of Predictions Using Thick Pavement Based on Thin Pavement

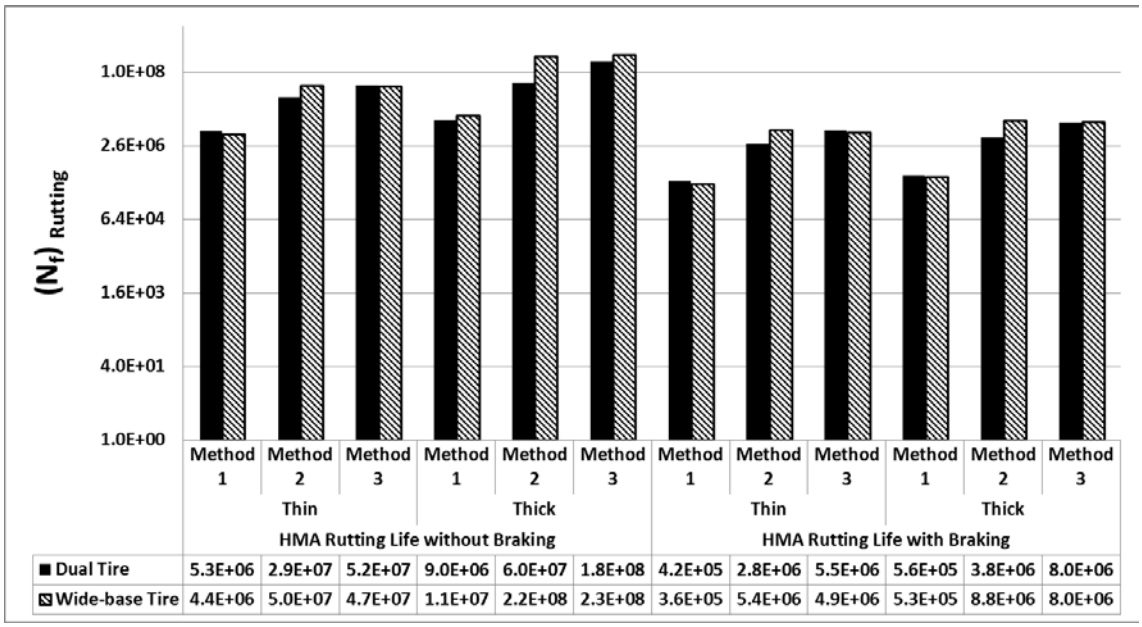

	Method 1	Method 2	Method 3	Method 1	Method 2	Method 3	Method 1	Method 2	Method 3	Method 1	Method 2	Method 3
	Thin			Thick			Thin			Thick		
	HMA Rutting Life without Braking						HMA Rutting Life with Braking					
Dual Tire	5.3E+06	2.9E+07	5.2E+07	9.0E+06	6.0E+07	1.8E+08	4.2E+05	2.8E+06	5.5E+06	5.6E+05	3.8E+06	8.0E+06
Wide-base Tire	4.4E+06	5.0E+07	4.7E+07	1.1E+07	2.2E+08	2.3E+08	3.6E+05	5.4E+06	4.9E+06	5.3E+05	8.8E+06	8.0E+06

(a)

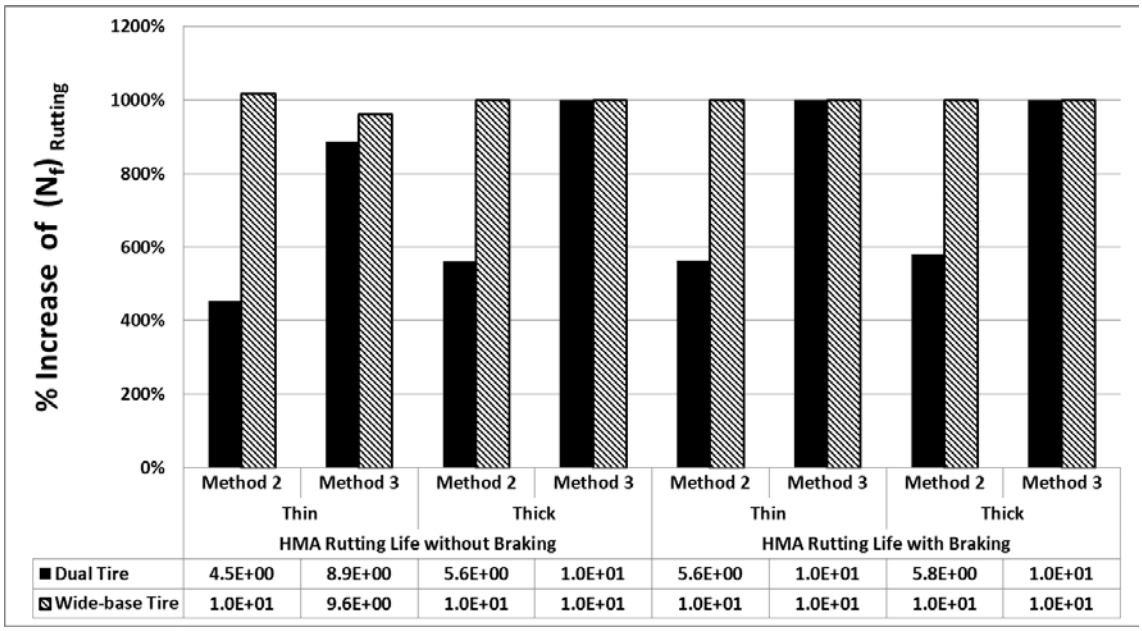

	Method 2	Method 3	Method 2	Method 3	Method 2	Method 3	Method 2	Method 3
	Thin		Thick		Thin		Thick	
	HMA Rutting Life without Braking				HMA Rutting Life with Braking			
Dual Tire	4.5E+00	8.9E+00	5.6E+00	1.0E+01	5.6E+00	1.0E+01	5.8E+00	1.0E+01
Wide-base Tire	1.0E+01	9.6E+00	1.0E+01	1.0E+01	1.0E+01	1.0E+01	1.0E+01	1.0E+01

(b)

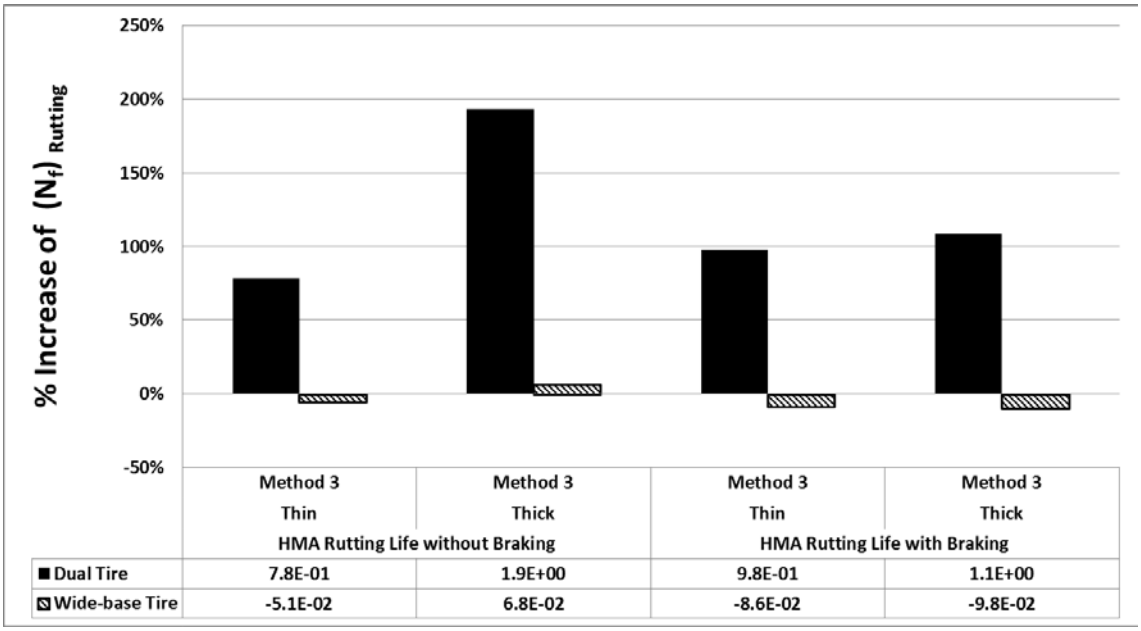

(c)

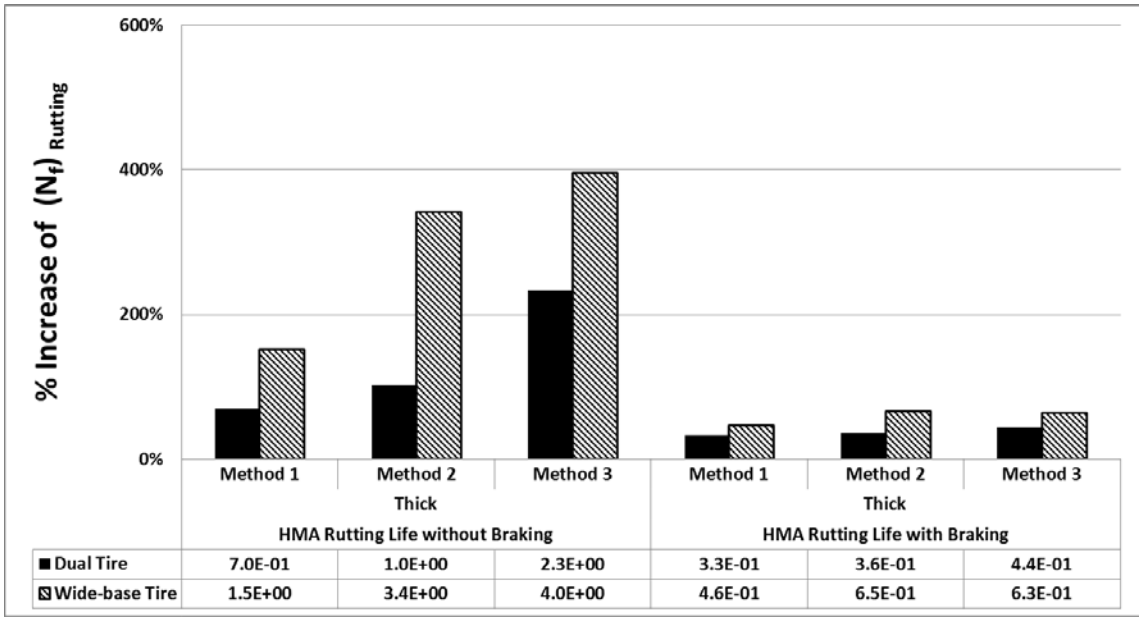

(d)

Fig. 4.10: PG64-28NV, 70°F, HMA Rutting Failure Cycle for 0.5 Inches Rut Depth: (a) Predicted (b) Percentage of Increase of Predictions Using Method 2 and Method 3 Based on Method 1 (c) Percentage of Increase of Predictions Using Method 3 Based on Method 2 (d) Percentage of Increase of Predictions Using Thick Pavement Based on Thin Pavement

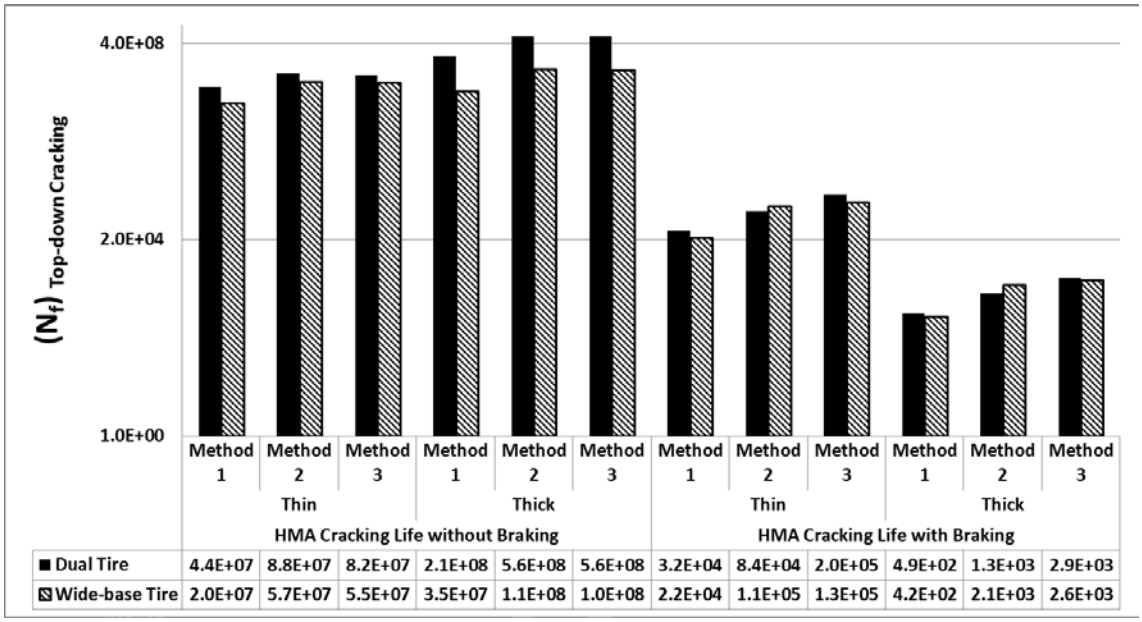

	Thin			Thick			Thin			Thick		
	Method 1	Method 2	Method 3	Method 1	Method 2	Method 3	Method 1	Method 2	Method 3	Method 1	Method 2	Method 3
	HMA Cracking Life without Braking						HMA Cracking Life with Braking					
Dual Tire	4.4E+07	8.8E+07	8.2E+07	2.1E+08	5.6E+08	5.6E+08	3.2E+04	8.4E+04	2.0E+05	4.9E+02	1.3E+03	2.9E+03
Wide-base Tire	2.0E+07	5.7E+07	5.5E+07	3.5E+07	1.1E+08	1.0E+08	2.2E+04	1.1E+05	1.3E+05	4.2E+02	2.1E+03	2.6E+03

(a)

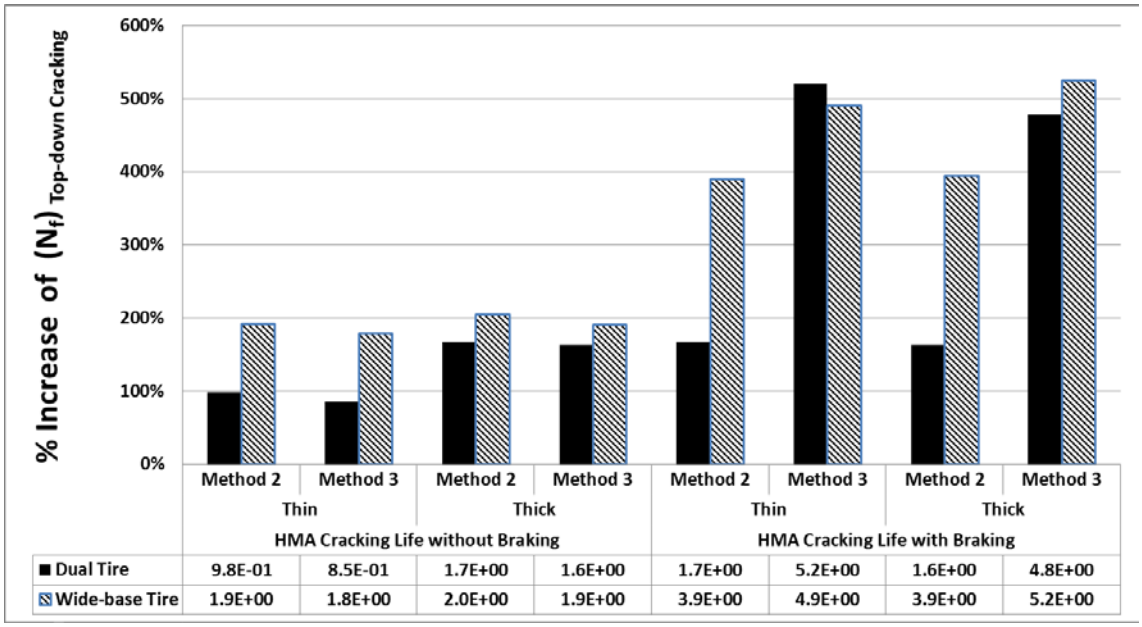

	Thin		Thick		Thin		Thick	
	Method 2	Method 3	Method 2	Method 3	Method 2	Method 3	Method 2	Method 3
	HMA Cracking Life without Braking				HMA Cracking Life with Braking			
Dual Tire	9.8E-01	8.5E-01	1.7E+00	1.6E+00	1.7E+00	5.2E+00	1.6E+00	4.8E+00
Wide-base Tire	1.9E+00	1.8E+00	2.0E+00	1.9E+00	3.9E+00	4.9E+00	3.9E+00	5.2E+00

(b)

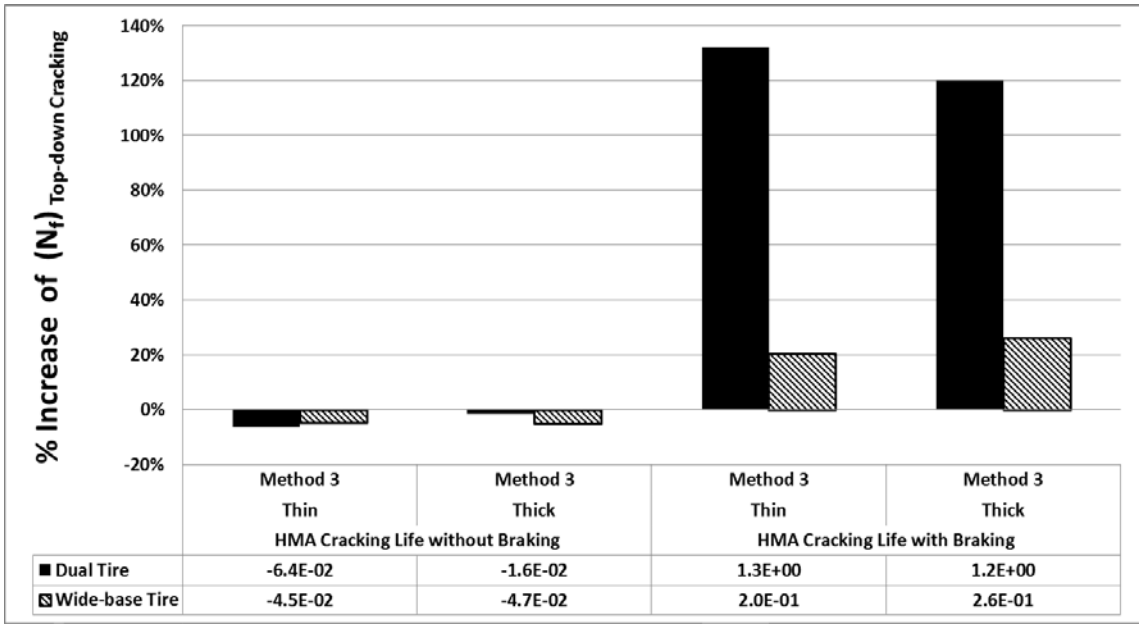

(c)

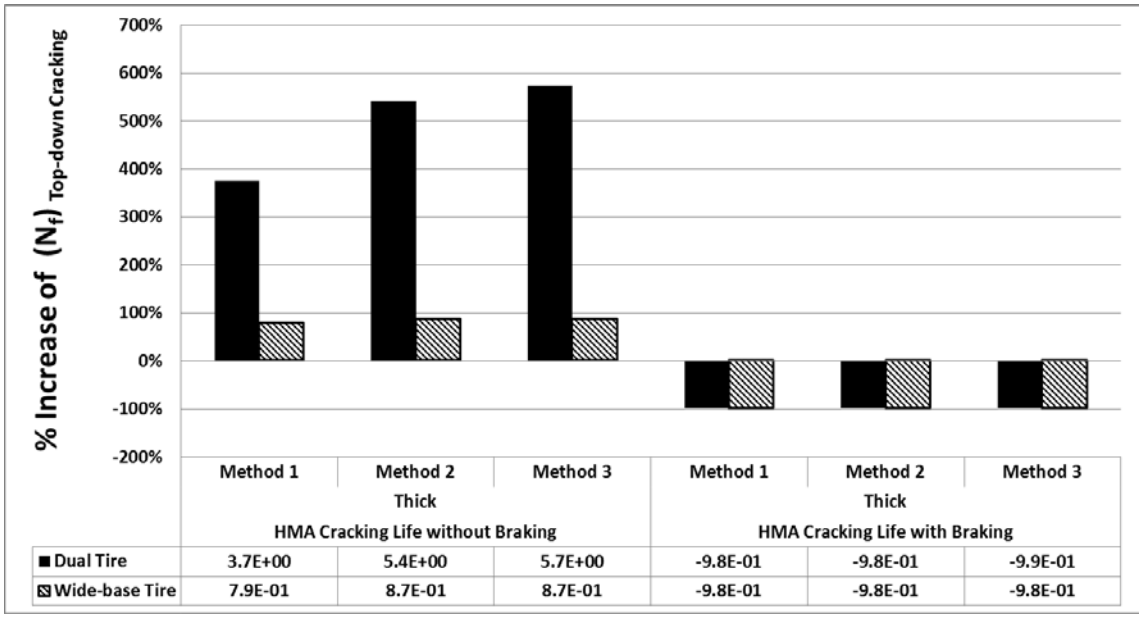

(d)

Fig. 4.11: PG64-28NV, 70°F, HMA top-down cracking life: (a) Predicted (b) Percentage of Increase of Predictions Using Method 2 and Method 3 Based on Method 1 (c) Percentage of Increase of Predictions Using Method 3 Based on Method 2 (d) Percentage of Increase of Predictions Using Thick Pavement Based on Thin Pavement

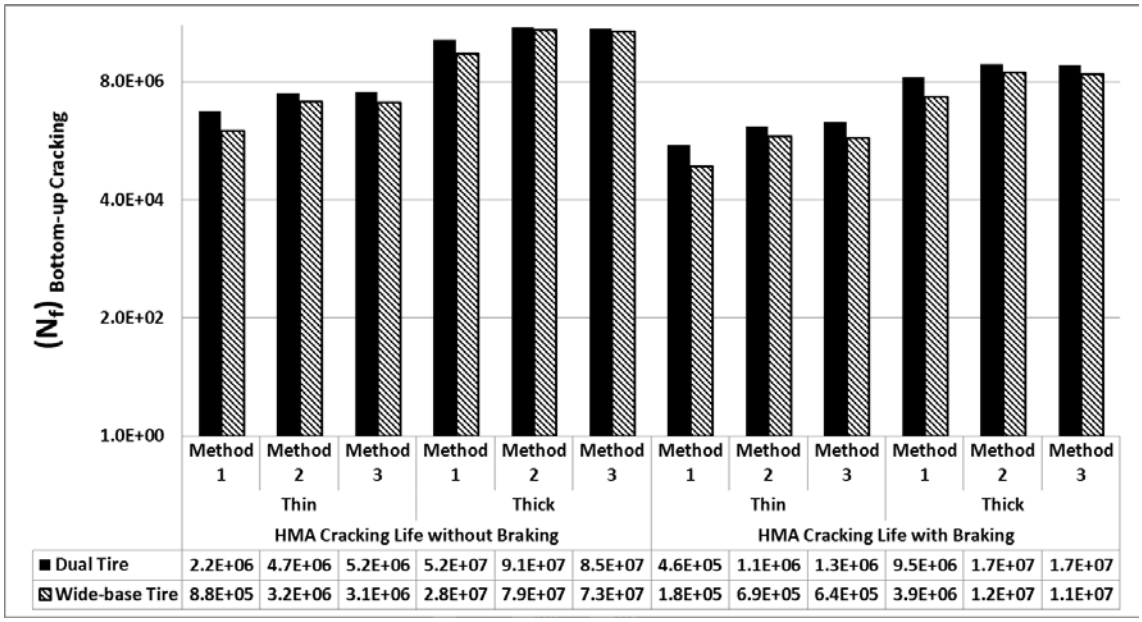

	HMA Cracking Life without Braking						HMA Cracking Life with Braking					
	Thin			Thick			Thin			Thick		
	Method 1	Method 2	Method 3	Method 1	Method 2	Method 3	Method 1	Method 2	Method 3	Method 1	Method 2	Method 3
Dual Tire	2.2E+06	4.7E+06	5.2E+06	5.2E+07	9.1E+07	8.5E+07	4.6E+05	1.1E+06	1.3E+06	9.5E+06	1.7E+07	1.7E+07
Wide-base Tire	8.8E+05	3.2E+06	3.1E+06	2.8E+07	7.9E+07	7.3E+07	1.8E+05	6.9E+05	6.4E+05	3.9E+06	1.2E+07	1.1E+07

(a)

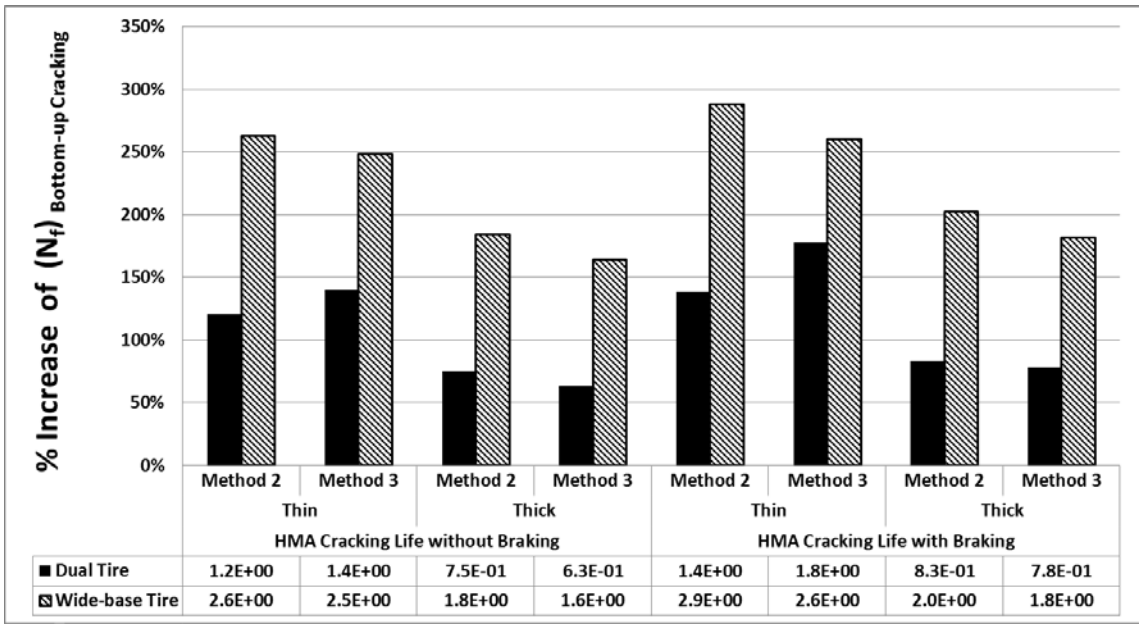

	HMA Cracking Life without Braking				HMA Cracking Life with Braking			
	Thin		Thick		Thin		Thick	
	Method 2	Method 3	Method 2	Method 3	Method 2	Method 3	Method 2	Method 3
Dual Tire	1.2E+00	1.4E+00	7.5E-01	6.3E-01	1.4E+00	1.8E+00	8.3E-01	7.8E-01
Wide-base Tire	2.6E+00	2.5E+00	1.8E+00	1.6E+00	2.9E+00	2.6E+00	2.0E+00	1.8E+00

(b)

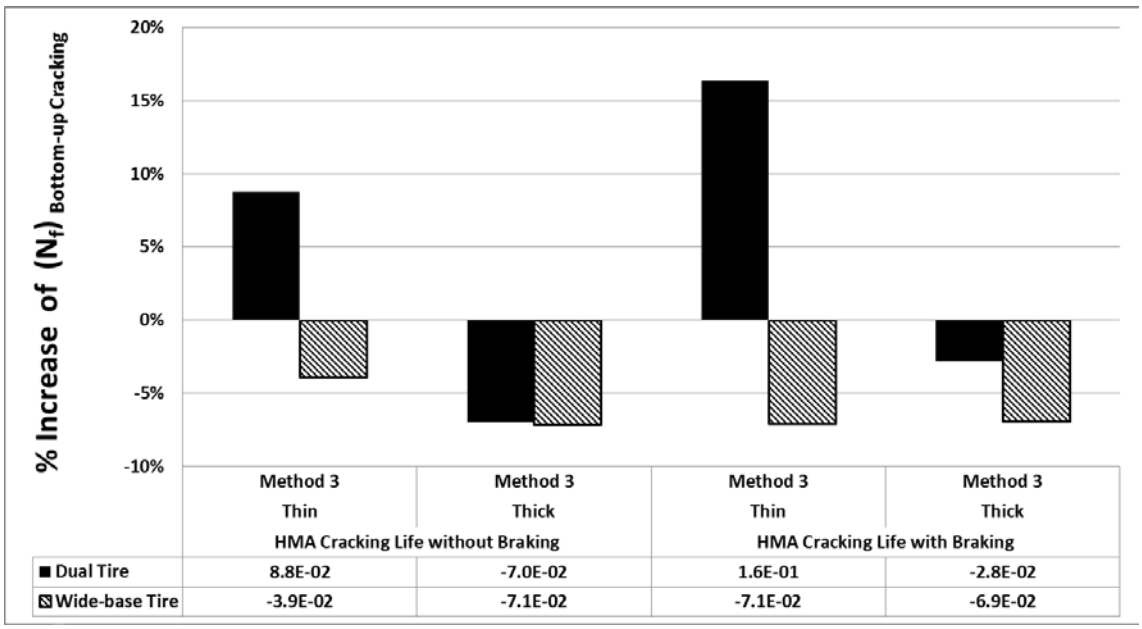

(c)

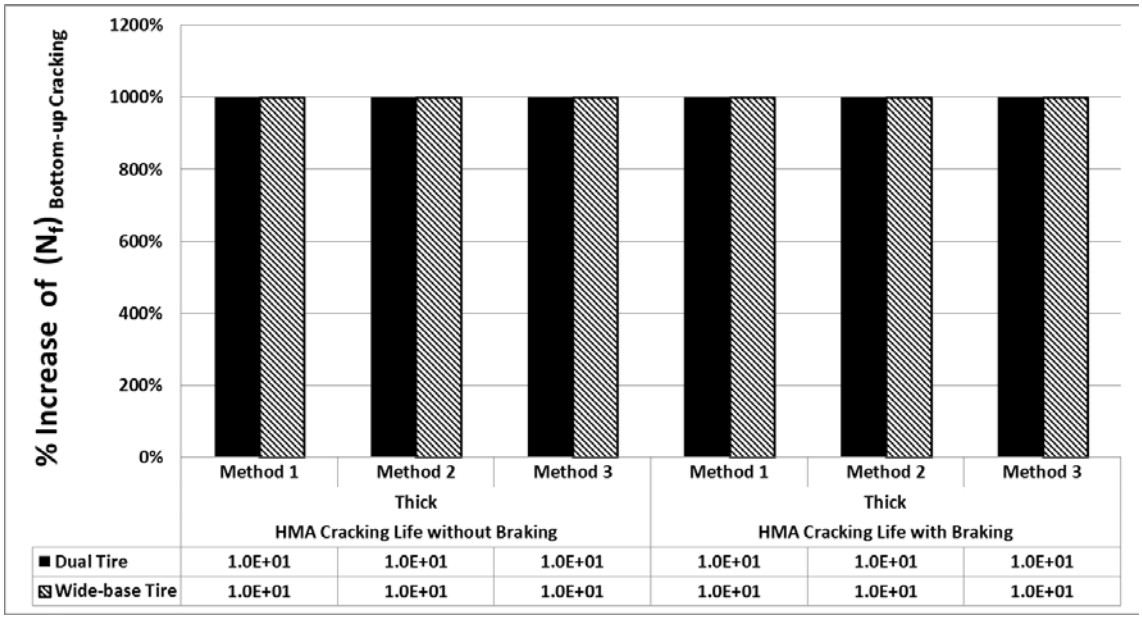

(d)

Fig. 4.12: PG64-28NV, 70°F, HMA bottom-up cracking life: (a) Predicted (b) Percentage of Increase of Predictions Using Method 2 and Method 3 Based on Method 1 (c) Percentage of Increase of Predictions Using Method 3 Based on Method 2 (d) Percentage of Increase of Predictions Using Thick Pavement Based on Thin Pavement

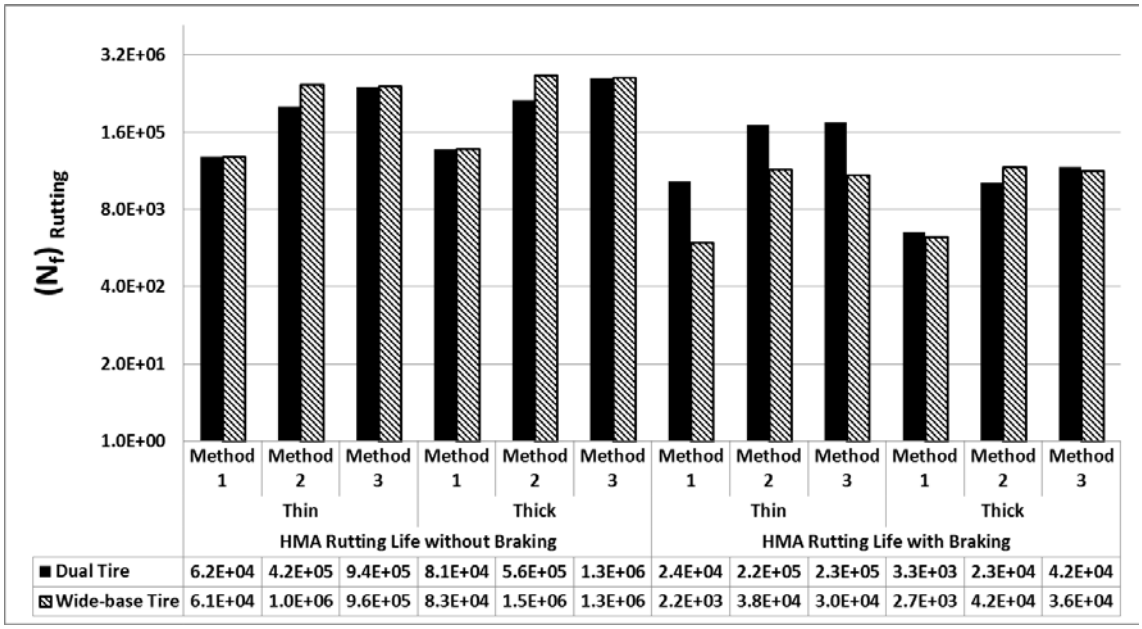

	Thin			Thick			Thin			Thick		
	Method 1	Method 2	Method 3	Method 1	Method 2	Method 3	Method 1	Method 2	Method 3	Method 1	Method 2	Method 3
	HMA Rutting Life without Braking						HMA Rutting Life with Braking					
Dual Tire	6.2E+04	4.2E+05	9.4E+05	8.1E+04	5.6E+05	1.3E+06	2.4E+04	2.2E+05	2.3E+05	3.3E+03	2.3E+04	4.2E+04
Wide-base Tire	6.1E+04	1.0E+06	9.6E+05	8.3E+04	1.5E+06	1.3E+06	2.2E+03	3.8E+04	3.0E+04	2.7E+03	4.2E+04	3.6E+04

(a)

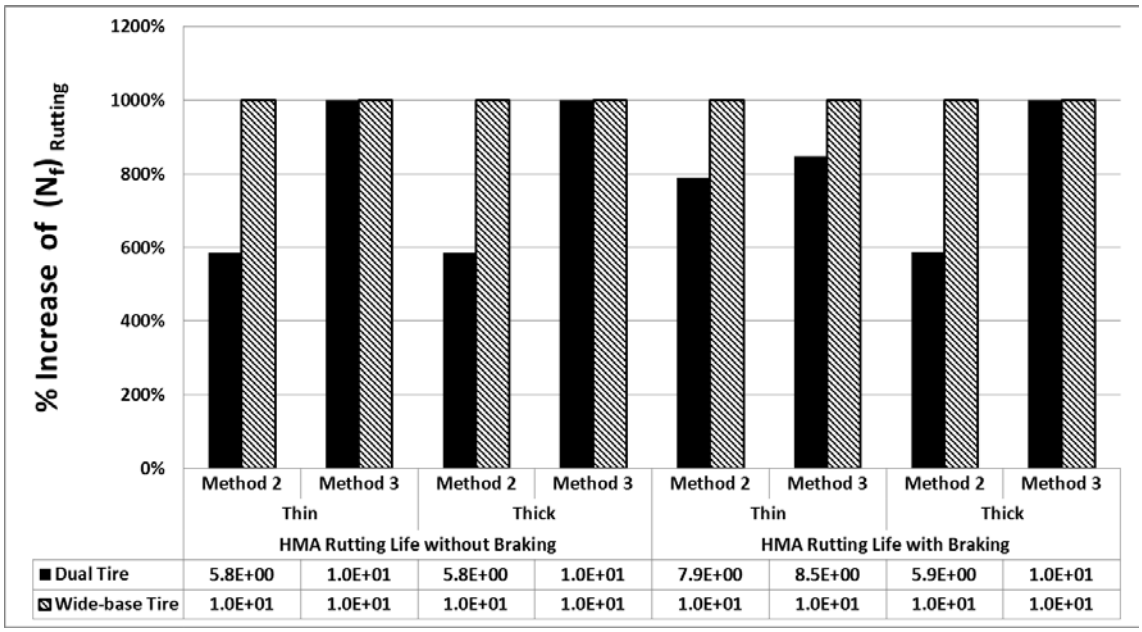

	Thin		Thick		Thin		Thick	
	Method 2	Method 3	Method 2	Method 3	Method 2	Method 3	Method 2	Method 3
	HMA Rutting Life without Braking				HMA Rutting Life with Braking			
Dual Tire	5.8E+00	1.0E+01	5.8E+00	1.0E+01	7.9E+00	8.5E+00	5.9E+00	1.0E+01
Wide-base Tire	1.0E+01	1.0E+01	1.0E+01	1.0E+01	1.0E+01	1.0E+01	1.0E+01	1.0E+01

(b)

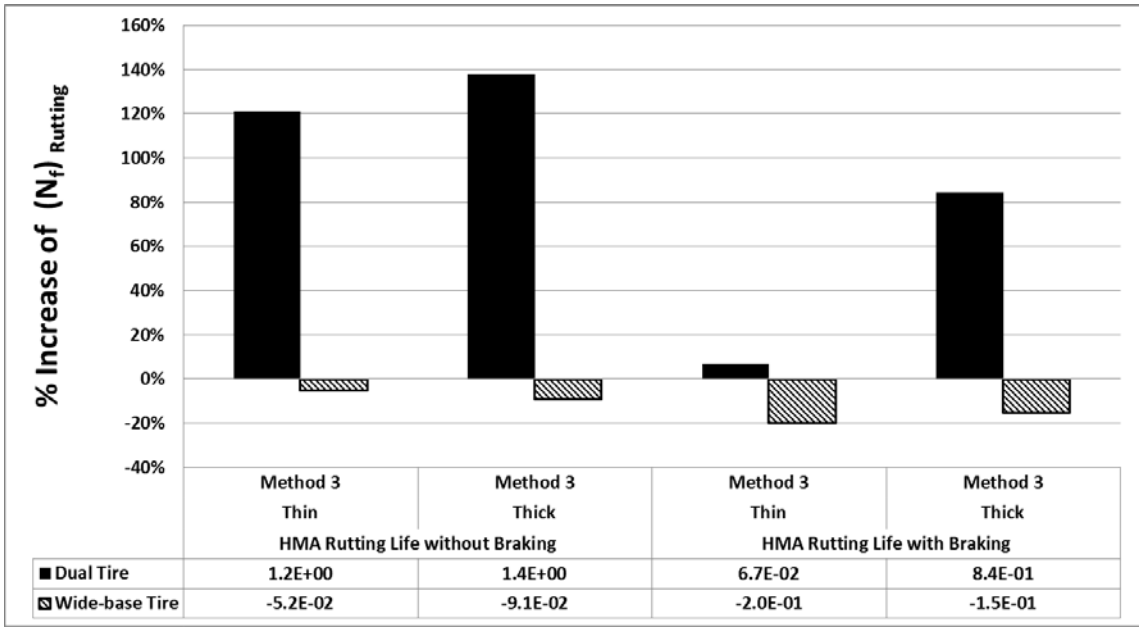

(c)

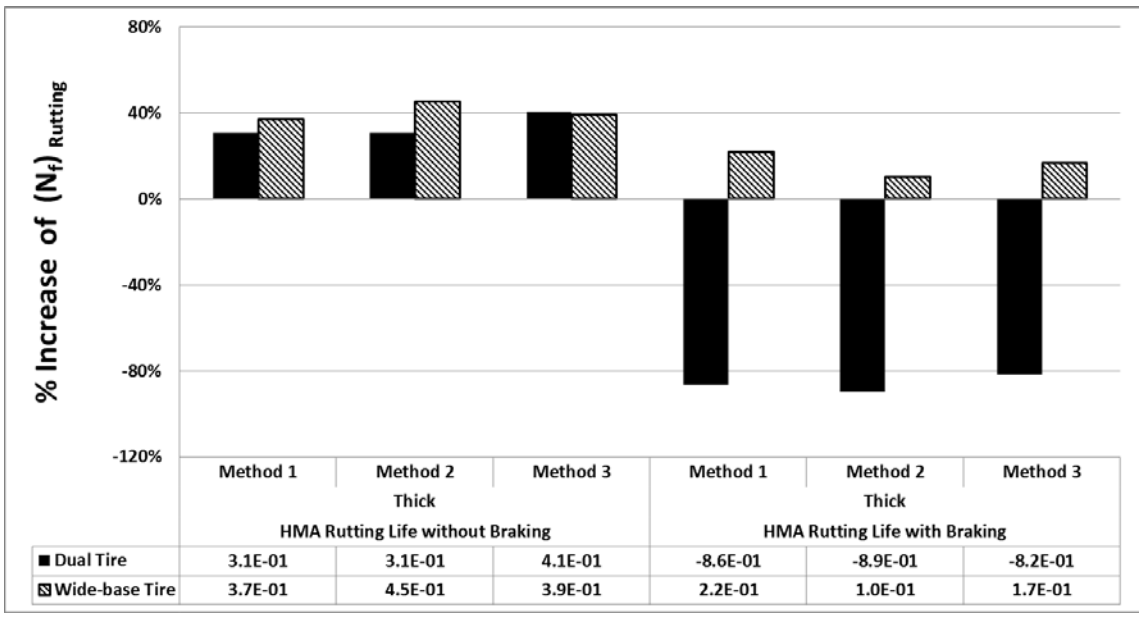

(d)

Fig. 4.13: PG64-28NV, 104°F, HMA Rutting Failure Cycle for 0.5 Inches Rut Depth: (a) Predicted (b) Percentage of Increase of Predictions Using Method 2 and Method 3 Based on Method 1 (c) Percentage of Increase of Predictions Using Method 3 Based on Method 2 (d) Percentage of Increase of Predictions Using Thick Pavement Based on Thin Pavement

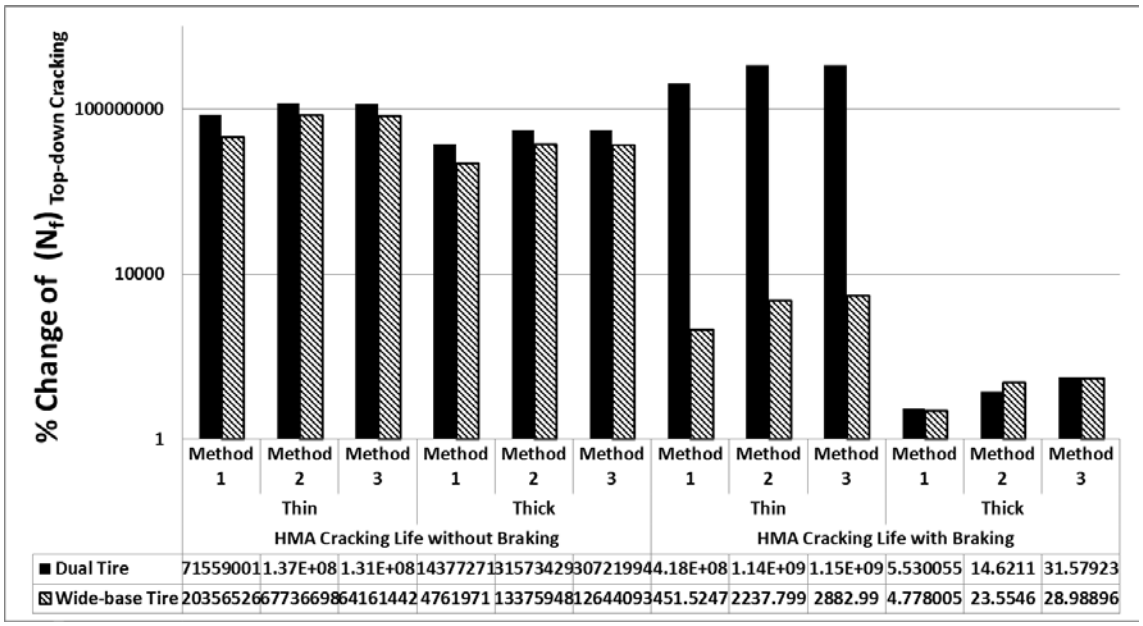

	Method 1	Method 2	Method 3	Method 1	Method 2	Method 3	Method 1	Method 2	Method 3	Method 1	Method 2	Method 3
	Thin			Thick			Thin			Thick		
	HMA Cracking Life without Braking						HMA Cracking Life with Braking					
Dual Tire	71559001	1.37E+08	1.31E+08	14377271	31573429	30721994	4.18E+08	1.14E+09	1.15E+09	5.530055	14.6211	31.57923
Wide-base Tire	20356526	67736698	64161442	4761971	13375948	12644093	451.5247	2237.799	2882.99	4.778005	23.5546	28.98896

(a)

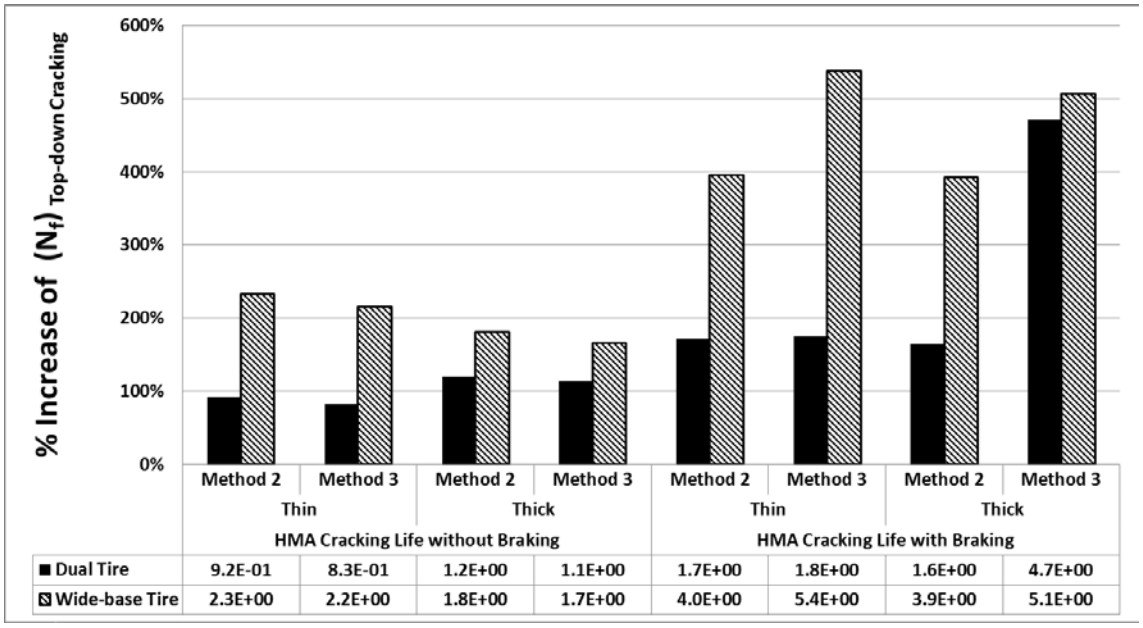

	Method 2	Method 3	Method 2	Method 3	Method 2	Method 3	Method 2	Method 3
	Thin		Thick		Thin		Thick	
	HMA Cracking Life without Braking				HMA Cracking Life with Braking			
Dual Tire	9.2E-01	8.3E-01	1.2E+00	1.1E+00	1.7E+00	1.8E+00	1.6E+00	4.7E+00
Wide-base Tire	2.3E+00	2.2E+00	1.8E+00	1.7E+00	4.0E+00	5.4E+00	3.9E+00	5.1E+00

(b)

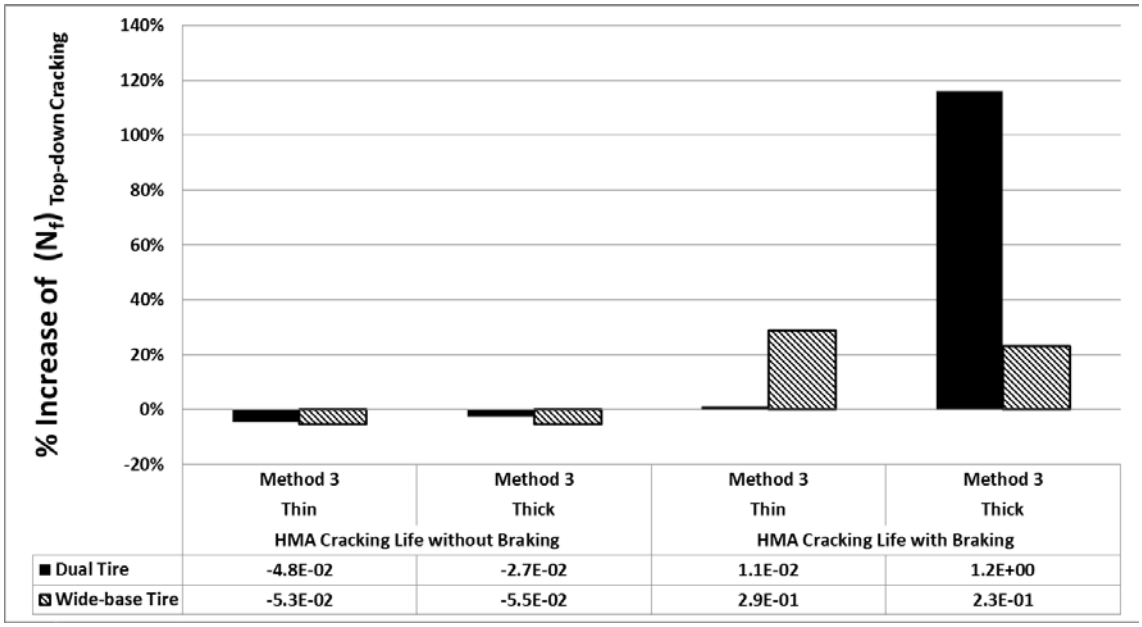

(c)

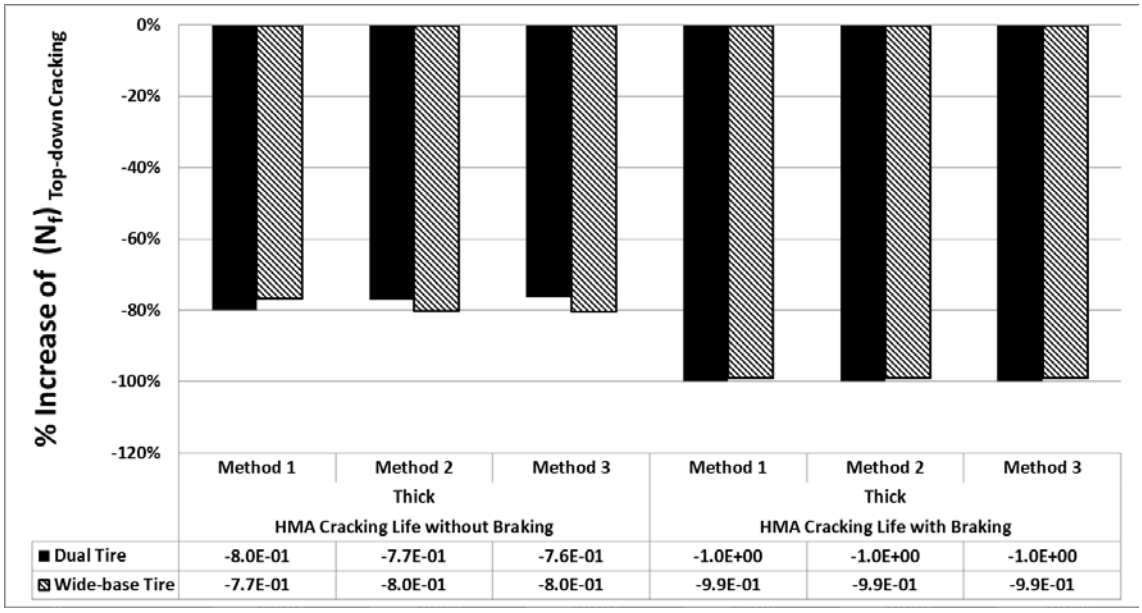

(d)

Fig. 4.14: PG64-28NV, 104°F, HMA top-down cracking life: (a) Predicted (b) Percentage of Increase of Predictions Using Method 2 and Method 3 Based on Method 1 (c) Percentage of Increase of Predictions Using Method 3 Based on Method 2 (d) Percentage of Increase of Predictions Using Thick Pavement Based on Thin Pavement

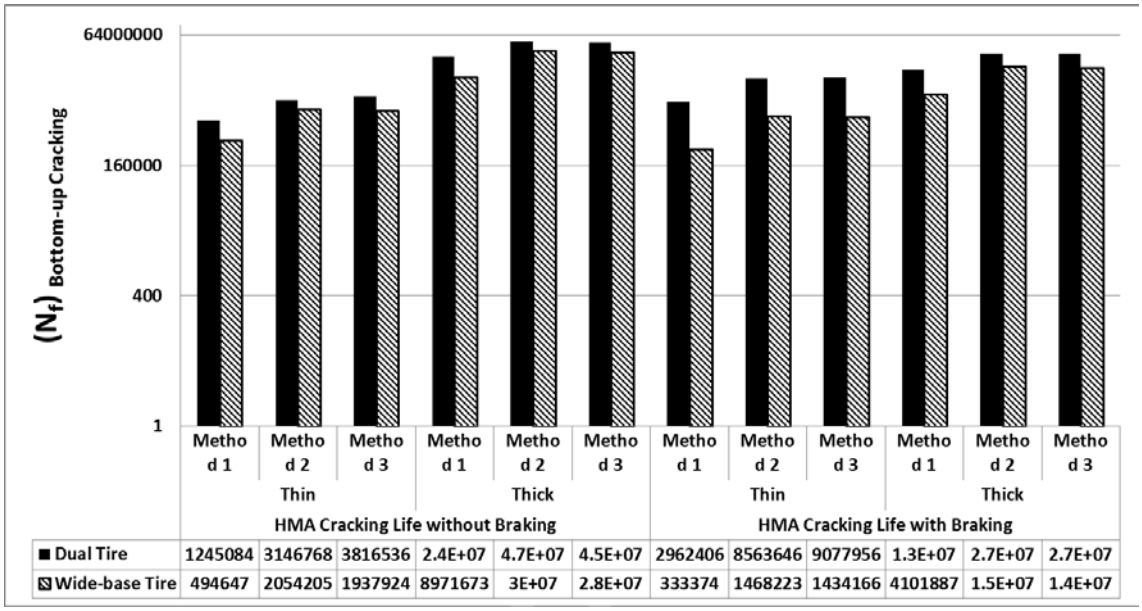

	Thin			Thick			Thin			Thick		
	Method 1	Method 2	Method 3	Method 1	Method 2	Method 3	Method 1	Method 2	Method 3	Method 1	Method 2	Method 3
	HMA Cracking Life without Braking						HMA Cracking Life with Braking					
Dual Tire	1245084	3146768	3816536	2.4E+07	4.7E+07	4.5E+07	2962406	8563646	9077956	1.3E+07	2.7E+07	2.7E+07
Wide-base Tire	494647	2054205	1937924	8971673	3E+07	2.8E+07	333374	1468223	1434166	4101887	1.5E+07	1.4E+07

(a)

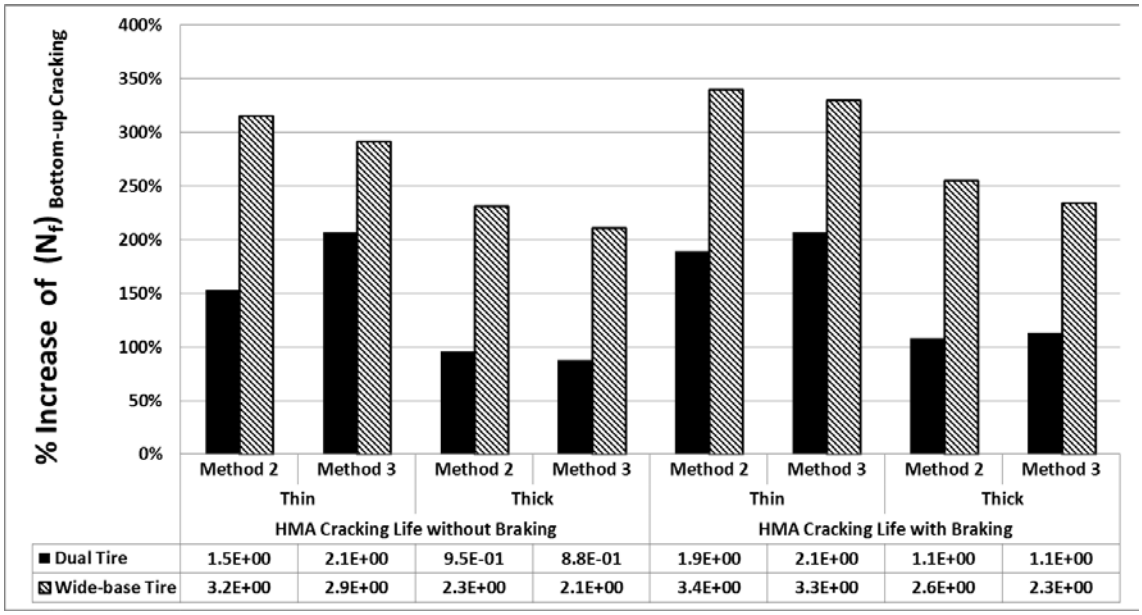

	Thin		Thick		Thin		Thick	
	Method 2	Method 3	Method 2	Method 3	Method 2	Method 3	Method 2	Method 3
	HMA Cracking Life without Braking				HMA Cracking Life with Braking			
Dual Tire	1.5E+00	2.1E+00	9.5E-01	8.8E-01	1.9E+00	2.1E+00	1.1E+00	1.1E+00
Wide-base Tire	3.2E+00	2.9E+00	2.3E+00	2.1E+00	3.4E+00	3.3E+00	2.6E+00	2.3E+00

(b)

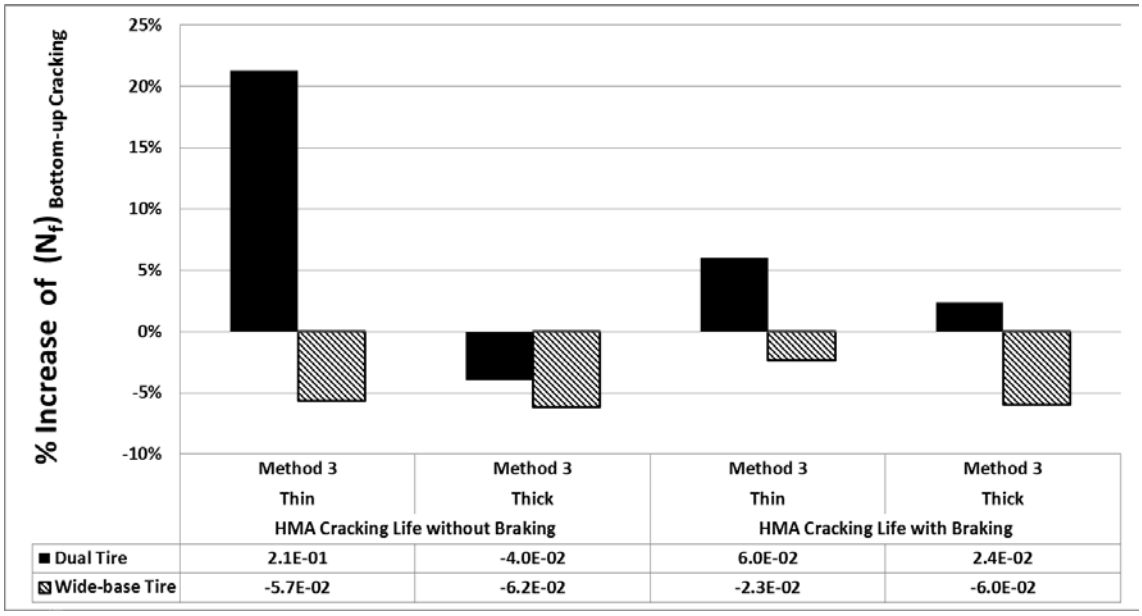

(c)

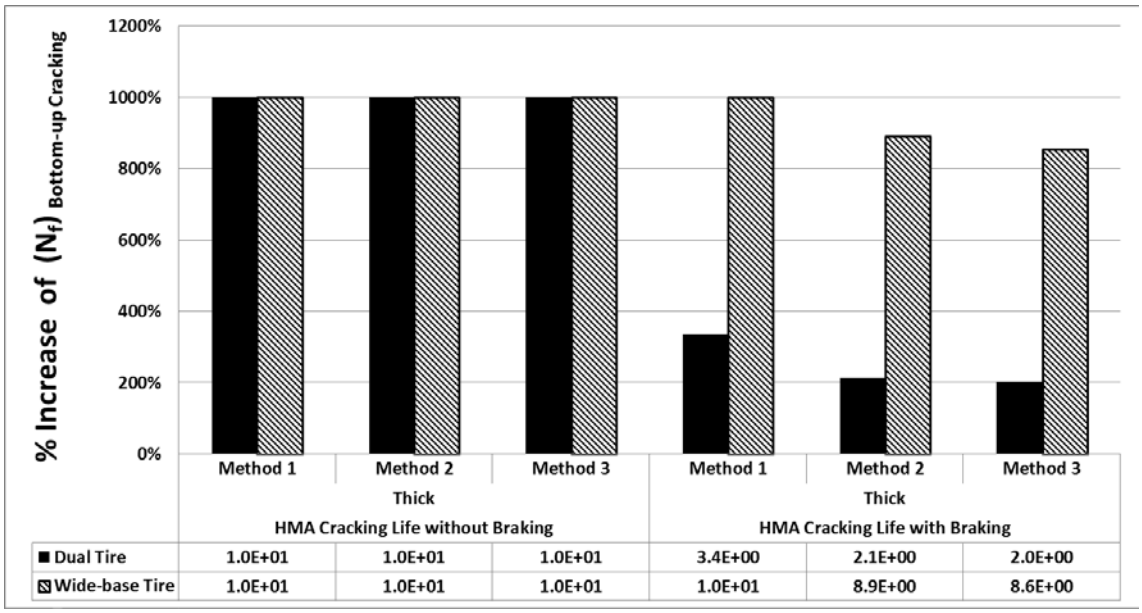

(d)

Fig. 4.15: PG64-28NV, 104°F, HMA bottom-up cracking life: (a) Predicted (b) Percentage of Increase of Predictions Using Method 2 and Method 3 Based on Method 1 (c) Percentage of Increase of Predictions Using Method 3 Based on Method 2 (d) Percentage of Increase of Predictions Using Thick Pavement Based on Thin Pavement